CSIC
Consejo Superior de Investigaciones Científicas

VNiVERSiDAD D SALAMANCA
CAMPUS DE EXCELENCIA INTERNACIONAL

ibfg

Characterization of the regulation of APC/C^{FZR-1} activity in the germline of *Caenorhabditis elegans*

David Puerta Martos

PhD thesis

Instituto de Biología Funcional y Genómica
CSIC-Universidad de Salamanca

Salamanca, 2022

Universidad de Salamanca

Instituto de Biología Funcional y Genómica (USAL-CSIC)

Characterization of the regulation of APC/C^{FZR-1} in the germline of *Caenorhabditis elegans*

David Puerta Martos

PhD thesis

Salamanca, 2022

Memoria presentada por David Puerta Martos para optar al título de Doctor por la Universidad de Salamanca.

Este trabajo ha sido realizado en el Instituto de Biología Funcional y Genómica (IBFG-CSIC) y en el Instituto de Biomedicina de Valencia (IBV-CSIC), bajo la supervisión del Profesor de Investigación y Doctor José Pérez Martín.

Acknowledgments/Agradecimientos

I would like to thank Judith Kimble for allowing me to stay in her lab, this thesis would not have been possible without the knowledge that you produced during your career. I want to thank Jane and her cats for hosting me in Madison! Thanks to all the members of Kimble's lab: Sarah, Peggy, Brian, Ahlan, and all the others for helping and welcoming me!

Me gustaría darle las gracias a mi director de tesis, Pepe, por darme la oportunidad y creer en mi desde el principio, creo que has hecho una muy buena labor como mentor. También me gustaría agradecer los miembros originales del laboratorio, Antonio y Adrián que me acogieron como a uno más desde el principio, me enseñaron e hicieron muy agradable el trabajo.

También me gustaría mencionar a los miembros de mi laboratorio de acogida durante los últimos meses: Alfonso, Rebeca, Alberto, Sabas y otros. Muchas gracias por facilitarme este último tramo de la tesis. Al igual que me gustaría mencionar en general a todas las personas que trabajan en el IBFG, por el buen ambiente de trabajo a diario. Especial mención a los servicios técnicos que nos facilitan todo, microscopia, administración, consejería, cocina…

También me gustaría agradecer a mi familia, y en especial a mis padres, que siempre me han apoyado en todo lo que he decidido y me han dado una educación invaluable. Y por supuesto me gustaría agradecer a Espe me ha aguantado a diario durante la tesis y ha actuado como mi motor día a día, especialmente en los días más complicados. ¡Pelusa tu tampoco te ibas a escapar! ¡Miau!

Tabla de contenido

Abstract

Cell cycle regulation in dividing and differentiating cells is usually studied *in vitro* or in unicellular organism models. However, the *C. elegans* germline represents an excellent *in vivo* model for studying stem cell dynamics and differentiation. The germline is composed of a pool of stem cells arranged spatiotemporally, supported by a niche cell called Distal Tip Cell (DTC). As the stem cells leave the vicinity of the niche, they enter meiosis. This unique physical organization enables its study by microscopy, which is enhanced by the easiness of genetic manipulations. The maintenance of the germline features requires the essential MES-3 and MES-4 chromatin regulators, which previous research in our group showed to be downregulated by the conserved E3 ubiquitin ligase APC/C^{FZR-1}. This cell cycle regulatory complex marks these proteins for degradation during the transition to meiosis. In this work, we showed that APC/C^{FZR-1} is tightly downregulated and upregulated at several different levels to allow the timely down-regulation of MES-3 and MES-4 proteins. It was intriguing how the niche could coordinate the signaling to inactivate APC/C^{FZR-1} in the mitotic zone. However, as cells differentiate into meiosis, the negative regulation was timely lifted, and the chromatin regulators were degraded.

In the mitotic zone, the Notch Pathway, through FBF RNA-binding proteins, represses *fzr-1* translation. Indirectly, FBF proteins also activate the translation of CYE-1 cyclin, resulting in high CDK levels that inhibit APC/C^{FZR-1} activity. In contrast, upon the cells differentiate to meiosis, APC/C^{FZR-1} activity is upregulated through two main pathways: polyA polymerase GLD-2 and another E3 ubiquitin ligase complex, SCF^{PROM-1}. SCF^{PROM-1} acts by initiating the degradation of CYE-1, while GLD-2 promotes new *fzr-1* translation and acts upstream of CKI-2, a conserved CDK inhibitor. We discovered that after upregulation, APC/C^{FZR-1} could also recognize and mark for degradation CYE-1, acting as a backup of SCF^{PROM-1}. It also recognizes CYA-1, a cyclin highly expressed at the end of the mitotic zone, and finally, can catalyze the degradation of its own coactivator, FZR-1.

.

Abbreviation list

APC/C: Anaphase Promoting Complex / Cyclosome

bp/kbp: Base pair / Kilo Base Pair

BSA: Bovine Serum Albumin

CDK: Cyclin Dependent Kinase

CKI: CDK inhibitor

CRISPR: Clustered regularly interspaced short palindromic repeats

crRNA: CRISPR RNA

CYA-1/CYE-1/CYD-1/CYB-1: Cyclin A-1/E-1/D-1/B-1

DNA: Deoxyribonucleic Acid

DTC: Distal Tip Cell

FBF: Fem-3 mRNA Binding Factor

FZR-1: Fizzy related

FZY-1: Fizzy

GFP: Green Fluorescent Protein

GLD-1/2/3: defective in **G**erm **L**ine **D**evelopment

GLP-1: Abnormal **G**erm **L**ine **P**roliferation

GSCs: Germline Stem Cells

MES-3/MES-4: Maternal Effect Sterile 3/4

MosSCI: Mos-1-mediated single copy insertion

mRNA: Messenger RNA

PBS/PBST: Phosphate-buffered saline + Tween-20.

PcG: Polycomb Group

PolyA: Polynucleotide Adenylyl transferase

pRB/LIN-35: Retinoblastoma Protein.

PROM-1: Promoter of meiosis

PUF: Pumilio and FBF

PZ: Progenitor Zone (Equivalent to Mitotic Zone)

RNA: Ribonucleic Acid

RNAi: RNA interference

SCF: Skp1, Cullin and F-box factor complex

ssDNA: single strand DNA

TracRNA: Trans-activating CRISPR RNA

TZ: Transition Zone

UTR: Untranslated Region

INTRODUCTION

1. INTRODUCTION

1.1 Introduction to the Thesis

Stem cells have the potential to proliferate and differentiate into multiple types of cells. Some, like germ stem cells (GSC), can differentiate into all types of cells, storing the potential to form an entirely new organism. One of the features of stem cells is that their chromatin acquires a relaxed and “open” conformation allowing proliferation and providing the potential to acquire different fates (pluripotency). Nevertheless, when stem cells differentiate, they reduce their pluripotency, partly achieved by modifying the chromatin landscape. The chromatin enters a more “closed” state, reducing the plasticity and preparing the cells for new transcriptional programs that allow the acquisition of new fates (Reviewed in Klein & Hainer, 2020; Ye et al., 2017).

The differentiation process of stem cells is tightly bound to the cell cycle. It is observed that when cells are about to differentiate, they enlarge the G1 phase (Liu et al., 2017). In addition, G1 enlargement correlated with chromatin restructuring (Singh et al., 2015). A considerable work, mostly *in vitro*, has been done studying the link between differentiation, cell cycle, and chromatin remodeling. However, *in vivo* studies, although more complex, may help to overcome the main caveat of in *vitro* studies, which is the ability to replicate ambient conditions such as the signaling provided by the niche surrounding the stem cells.

The gonad from the nematode *Caenorhabditis elegans* presents an excellent opportunity to study stem cell differentiation *in vivo*. It is composed of a pool of GSCs maintained by a single cell niche, the Distal Tip Cell (DTC). In addition, they are organized in a spatial-temporal way, allowing them to be studied easily by optical microscopy (reviewed in (Byrd & Kimble, 2009). These characteristics allow us to observe in *vivo* the interplay between niche signaling, cell cycle, and the differentiation process.

In the *C. elegans* germline, previous work from our lab showed that the chromatin regulators MES-4 (Rivera-Martín *PhD thesis*, 2018) and MES-3 (Fragoso *PhD thesis*, 2020) are promoted for degradation by the E3 ubiquitin

complex APC/C^{FZR-1}, a cell cycle regulator complex active during G1 phase in mitotic cell cycle and with proposed roles in the meiotic cell cycle. These chromatin regulators are degraded as the cells leave the mitotic region of the germline and start to differentiate into meiosis, providing striking new evidence of how this cell-cycle coupled complex directly affects chromatin regulators.

This thesis aims to study how the cell cycle and niche signaling coordinate to regulate the APC/C^{FZR-1} activity in the C. elegans germline: The presence of MES-3 and MES-4 essential chromatin regulators has to be allowed in the mitotic region, but as the cells differentiate and enter meiosis APC/C^{FZR-1} activity has to be promoted to ensure the timely degradation of the chromatin factors. MES-3 and MES-4 are chromatin regulators essential for the maintenance of the GSCs, and their presence is necessary to ensure fertility as knocking down these genes causes maternal sterility (Bender et al., 2006; Garvin et al., 1998; Tabuchi et al., 2014; Xu, Fong, et al., 2001). Accordingly, they are required in the mitotic region but down-regulated by APC/C^{FZR-1} complex as cells differentiate into meiosis. Due to this duality, the APC/C^{FZR-1} complex´s activity must be appropriately modulated.

1.2 The connection between cell cycle and differentiation

1.2.1 The cell cycle

The cell cycle is a repetitive and serial process tightly controlled, leading to cell division and multiplication. The canonical cycle consists of the synthesis (S) phase, in which cells duplicate the genetic material, followed by the mitosis (M), in which cells physically divide. These key steps are separated by gap phases, G1 and G2, whose length is variable. The processes that trigger the entry in each specific phase are highly regulated to ensure the irreversible progression of the cell cycle. This regulation enables the stability of the hereditary material through the different divisions. The main driver of the progression of the cell cycle is a protein complex called Cyclin-CDK, composed of a catalytic subunit (CDK, Cyclin-Dependent Kinase) and a regulatory subunit (Cyclin) (Nurse et al., 1976). The phosphorylation of different substrates by CDKs triggers the different key events promoting the cell cycle progression until cell division is achieved and a new cycle starts. One main characteristic of this cycle is that it is irreversible, moving forward in a single direction (Swaffer et al., 2016).

Cell cycle and division are strongly linked to differentiation processes in multicellular organisms. Stem cells are a key example; they need to divide to maintain the population and differentiate to give birth to new cell types (Reviewed in (Gao & Liu, 2019).

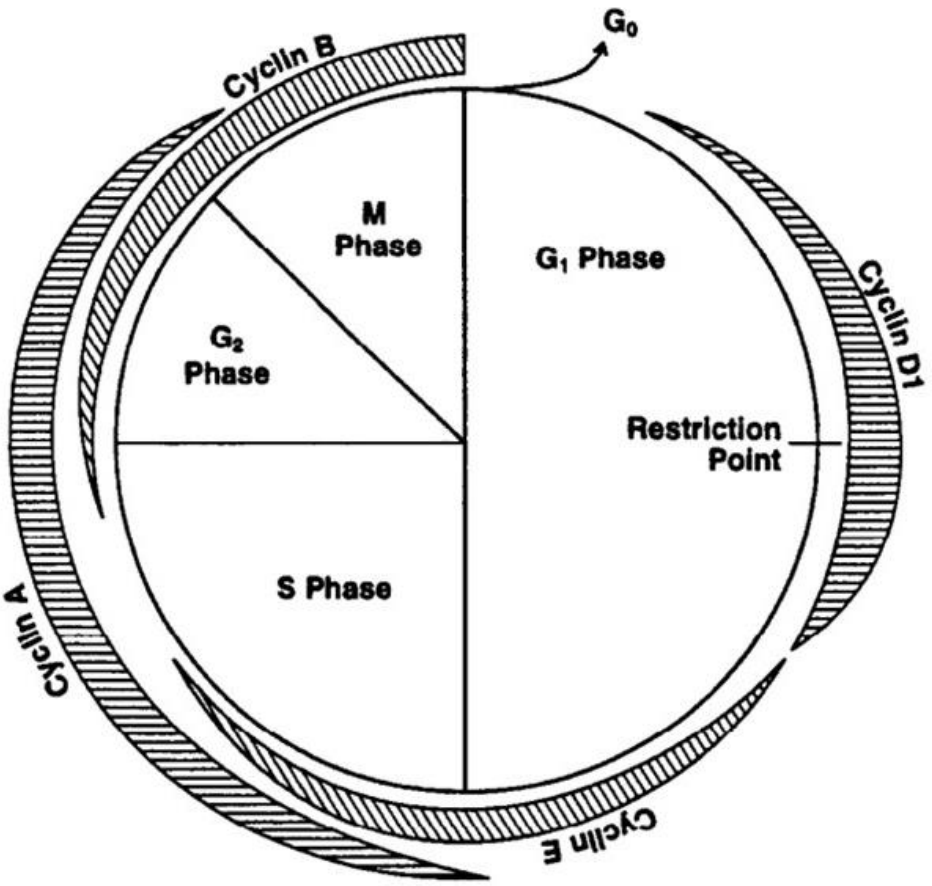

Figure 1.1: The cell cycle is driven by different cyclins-CDKs. Extracted from (Schafer, 1998)**.**

Different cyclins partner with different CDKs through the cell cycle, they drive the progression of the cycle through the phosphorylation of a variety of proteins. The cell replicates the hereditary material in the S phase, followed by a G2 interphase. After the physical division of the cell and distribution of the chromosomes (Mitotic or M phase), another interphase takes place, the G1.

1.2.2 Cell cycle exit and differentiation: G1 phase

In G1, the cell is presented with three choices: to continue dividing, to enter a dormancy state (called G0), or to differentiate. The final decision depends on integrating extracellular and intracellular signals, converging in CDK activity. Cells are committed to another division when CDK activity increases, reaching a determined threshold (Schwarz et al., 2018). Consequently, G1 phase length opens an “opportunity window” for the cells to enter differentiation or not (Reviewed in (ter Huurne & Stunnenberg, 2021).

The G1 phase representing a switch in cell commitment is logical as this phase occurs just after the cell has completed physical division, during the M phase. The transition of the M phase to G1 involves reforming the nuclear envelope, chromosome decondensation, and chromosome repositioning. These events could change the transcriptional programs and predispose the cells to change their fate (Reddy et al., 2008). Furthermore, in the G1 phase, the epigenetic labels on chromatin are remodeled and developmental genes acquire positive marks promoting their transcription. (Singh et al., 2013, 2015). These events could trigger the cell to enter an “open and ready” state to receive differentiation cues. Nevertheless, if the G1 phase is very short, as happens in dividing stem cells (Gao & Liu, 2019), the cells cannot have the opportunity to differentiate. This way, G1 length regulation would influence the wiliness of a cell to enter a differentiation process: Cells with shorter G1 phases would not be sensitized to differentiate, but cells with longer G1 phases could be more prone to restructure the transcriptional program and acquire a new fate.

1.2.3 G1 length regulation

Cell cycle inhibitors act as “brakes,” enabling the lengthening of the G1 phase. These brakes converge in reducing CDK activity (**Figure 1.2**). The main CDK complex believed to drive the G1/S transition is the Cyclin E-Cdk2 complex. Cyclin E accumulates along the G1 phase, and the activity of the corresponding

CDK complex determines the “point of no return” that causes cells to enter a new division cycle (Reviewed in (Möröy & Geisen, 2004).

The first one of the “brakes” reducing CDK activity and promoting cell cycle exit is the Retinoblastoma protein (Rb), LIN-35 in *C. elegans*. Rb acts by targeting the transcription factor E2F-DP, which promotes the transcription of genes driving G1/S transition, including Cyclin E (Lavia & Jansen-Dürr, 1999; Lukas et al., 1997; Pajalunga & Crescenzi, 2004). In the canonical pathway, proteins from the Retinoblastoma family bind to E2F-DP, inhibiting the transcription of genes that promote G1/S transition (Reviewed in(Trimarchi & Lees, 2002). In *C. elegans*, LIN-35 interacts with EFL-1/DPL-1 (E2F-DP ortholog) (Ceol & Horvitz, 2001). Furthermore, it has been demonstrated that LIN-35 interaction with EFL-1/DPL-1 causes transcriptional repression of cell cycle-promoting genes, favoring cell cycle exit (Goetsch et al., 2017). Retinoblastoma activity is downregulated in mammalian cells via phosphorylation by the Cyclin D-Cdk4/6 complex (Schade et al., 2019). Analogously, in *C. elegans,* LIN-35 is phosphorylated by CYD-1/CDK-4 (The et al., 2015). Therefore, Cyclin D-CDK4 inhibition of pRb reduces transcriptional repression of factors such as Cyclin E, promoting the irreversible trigger of S-phase entry.

The second group of “brakes” are CDK inhibitors (CKIs). These proteins bind to cyclin-CDK complexes inhibiting their activity. These proteins are grouped into two families: the INK family, which inhibits Cyclin D-CDK4/6 complex activity and indirectly promotes pRb activity (Lukas et al., 1995); and the CIP/KIP family members p21/p27/p57 (in mammals) that inhibits Cyclin E-CDK2 activity (Harper et al., 1993, Polyak et al., 1994; Reynaud et al., 1999;). In *C. elegans*, only two CIP/KIP members have been described, CKI-1 and CKI-2, whose expression promotes cell cycle arrest (Buck et al., 2009). CKI-1 is essential and is required for the proper timing of cell-cycle exit (Fujita et al., 2007; Yang Hong et al., 1998). CKI-2 is not essential (Buck et al., 2009), although it is the predominant CKI expressed in the adult *C. elegans* germline, mainly in cells entering meiosis (Kalchhauser et al., 2011).

The third group of cell cycle inhibitors acting in G1 is the E3 ubiquitin ligase complexes. These complexes incorporate ubiquitin subunits into their substrates, marking them for proteasomal degradation. The first E3 ubiquitin ligase complex

involved in G1/S is the SCF complex (Skp1, Cullin, and F-box factor) that, in some instances, promotes and, in others, inhibits G1/transition, depending on the F-box factor interacting. For instance, In the case of SCF acting with Skp2 and Csk1, it causes CKI degradation, promoting cell cycle progression (Hao et al., 2005; W. Wang et al., 2005). Conversely, SCF acting with Fbw7 causes Cyclin E degradation, promoting cell cycle exit (Koepp et al., 2001). In *C. elegans* SCF acting with the F-box protein PROM-1 causes Cyclin E degradation in the germline (Mohammad et al., 2018). The second E3 ubiquitin ligase complex involved in G1/S is the Anaphase Promoting Complex/Cyclosome in collaboration with Cdh1, reviewed in more detail below. One of the targets of APC/C^{Cdh1} is the F-box protein Skp2, which degradation resulted in CKIs stabilization and elongation of the G1 phase (Bashir et al., 2004).

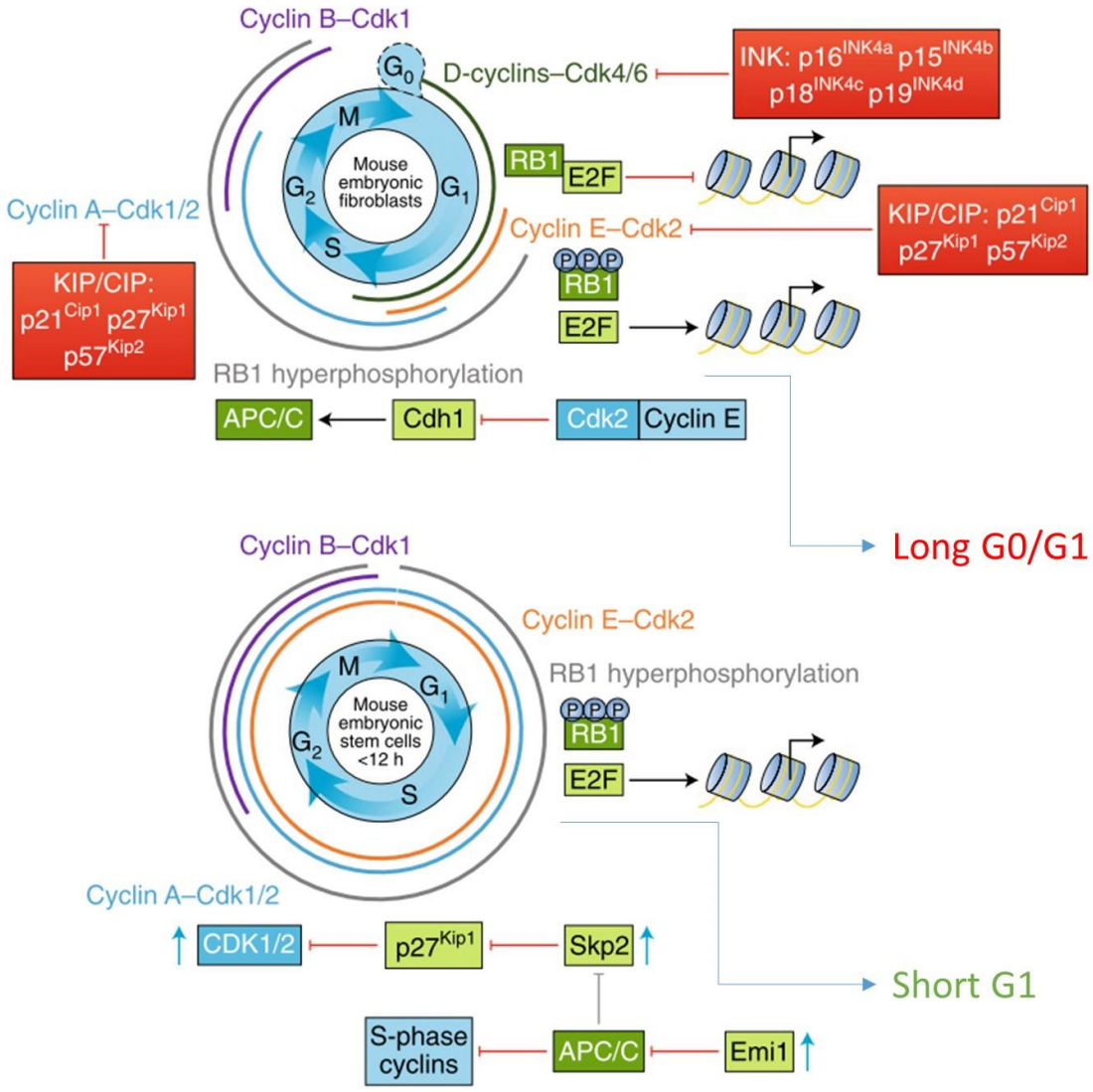

Figure 1.2: G1 length is shorter in dividing stem cells. Figure from (Liu et al., 2017)**.**

In mouse embryonic stem cells (mESCs), shown on the lower side, G1 is short. Cyclin E-CDK activity is high through the cycle, Retinoblastoma is permanently hyper-phosphorylated, CDK inhibitors are inhibited and APC/C^{Cdh1} is phosphorylated and additionally suppressed by Emi1. However, in the mouse embrionary fibroblasts (MEFs), a more differentiated cell type shown on the upper side, the cell cycle has periods of activation of CDK inhibitors (INK and KIP/CIP families), Retinoblastoma protein and APC/C^{Cdh1} that cause G1 lengthening.

1.2.4 APC/C$^{CDH1/FZR-1}$ roles in cell cycle and differentiation

APC/C is an evolutionarily conserved complex with more than 15 subunits. This E3 ubiquitin ligase can promote the degradation of various substrates during different phases of the cell cycle in collaboration with two main coactivators, Cdh1 and Cdc20 (Reviewed in (Kimata, 2019). CDC20/FZY-1 coactivator binds and activates APC/C in the M phase triggering chromatid separation and promoting mitotic progression. Afterward, when CDK activity is low, CDH1 is dephosphorylated and binds APC/C, which causes CDC20 degradation, and retains the cells in G1/G0 phase.

It is believed that APC/C^{Cdh1} is one of the key regulators of the G1/S transition (Reviewed in (Kernan et al., 2018). There is evidence in cultured mammalian cells and yeast: When *cdh1* was silenced in human cell lines or knocked down in mouse embryonic fibroblasts, cells could exit mitosis, but the G1 phase was shortened, and the S phase was more extended (Sigi et al., 2009). Cdh1 is also required for yeast cells deprived of nutrients to stay in the G0 phase (Kitamura et al., 1998). In multicellular organisms, APC/C^{Cdh1} also has a crucial role in G1/G0 arrest (Sigi et al., 2009; Sigrist & Lehner, 1997).

The role of APC/C^{Cdh1} as only a canonical cell cycle regulator has changed in the last few years. As mentioned before, G1 length prolongation is correlated with differentiation. It is believed that a longer G1 gives time for the cell to be exposed to differentiation determinants. This “cell cycle length hypothesis” has been supported by studies in neuronal progenitors (Reviewed in (Salomoni & Calegari, 2010): In an *in vitro* model of neuron differentiation, CDH1 knockout inhibited G1 elongation and the expression of neuronal markers. Coherently, an overactivated allele of CDH1 caused G1 elongation and augmented neuronal differentiation. Furthermore, *in vivo* CDH1 knockdown in neural progenitors prevented G1 elongation and the differentiation of neurons, causing a phenotype similar to microcephaly (Delgado-Esteban et al., 2013; Eguren et al., 2013).

Nevertheless, the role of APC/C^{Cdh1} in differentiation goes beyond cell cycle regulation, having substrates unrelated that process, which are highly expressed in neuronal progenitors and not expressed in the differentiated cells (Liu et al., 2017b; Penas et al., 2015). In an *in vitro* mouse myogenesis model, APC/C^{CDH1} promotes the degradation of the transcription factor Myf5. APC/C^{CDH1} can also influence key signaling pathways. For example, it targets SnoN, a protein that inhibits TGF -β signaling pathway (Djabrayan & Casanova, 2016; Stegmüller et al., 2006; Y. Wan et al., 2001). In *Drosophila,* APC/C$^{CDH1/FZR-1}$ regulates the Wnt pathway by triggering the degradation of a conserved kinase, Nek2 (Martins et al., 2017; Weber & Mlodzik, 2017). In our group we have found that *C. elegans fzr-1* knockout resulted in defects in the formation of the Distal Tip Cell (DTC), a cell that provides Notch signaling to the germline (Fragoso *PhD thesis*, 2020). Furthermore, APC/C binding of chromatin modulators has also been studied *in silico* and *in vitro* (Franks et al., 2020).

1.2.5 APC/C$^{CDH1/FZR-1}$ role in meiotic cycle

APC/C role has also been studied in meiosis, as this complex also plays an important role in this process in all organisms tested (Reviewed in(Pesin and Orr-Weaver, 2010). Meiosis is a modified cell division in which a single diploid cell generates four daughter haploid cells forming male and feminine gametes. In meiosis, there is a starting S-phase and two successive divisions without an intermediate S-phase. General cell cycle regulators and meiosis-specific factors control the whole process.

In the yeast *Saccharomyces cerevisiae,* a specific APC/C meiotic coactivator, Ama1, is required for spore formation (Cooper et al., 2000). However, this seems to be a particular case in fungi because, in the yeast *Schizosaccharomyces pombe,* the corresponding Cdh1 ortholog (Ste9/Swr9) associates with APC/C during meiosis (Blanco et al., 2001). In *Drosophila*, there are two members of the Cdc20/FZY family with specific roles in meiosis: *cort,* in which null mutants are viable but female sterile as they lay eggs that never complete meiosis (Chu et al., 2001), and *fzr2*, which is expressed only in male meiosis (Jacobs et al., 2002). In *C. elegans* and vertebrates, there are no specific

meiotic APC/C coactivators described, suggesting that either Cdc20/Fzy-1, Cdh1/Fzr-1, or both could be involved.

Despite the presence of additional APC/C coactivators with specific roles in meiosis, Cdh1/Fzr-1 seems to be important for meiosis, although his role still need to be better understood. In *S. cerevisiae*, *cdh1* mutants show incomplete synapsis of bivalents in prophase I (Penkner et al., 2005). However, it is unclear whether this is due to the role of Cdh1 in meiosis or the previous mitosis. APC/C^{CDH1} seems to be required for correct oogenesis and spermatogenesis in mammals by maintaining prophase I arrest (Marangos et al., 2007). Moreover, *cdh1* knock-down in mouse oocytes accelerates progression through meiosis I, resulting in premature anaphase and nondisjunctions (Reis et al., 2007). On the other hand, in *Xenopus laevis* oocytes, *cdh1* knock-down produces the opposite effect, inhibiting the maturation of the oocyte (Papin et al., 2004).

In the mitotic cycle, CDH1 activates APC/C during G1. Strikingly, in meiosis, APC/C$^{CDH1/FZR-1}$ is active in prophase I, which is equivalent to the G2 interphase. During meiosis, APC/C^{Cdh1} activity (G2) acts **before** APC/C^{Cdc20} activity (M phase, triggering homolog disjunction) in clear opposition to what happens during the mitotic cycle in which CDH1 activity (G1) acts **after** CDC20 activity (M). Most likely, during the prophase I/G2 arrest, APC/C^{CDH1} enables the downregulation of CDK1 activity, impeding in this way a premature CDC20 activation that may result in an unscheduled M-phase triggering (Reviewed in (Homer, 2013).

In summary, APC/C$^{CDH1/FZR-1}$ has critical roles in regulating the mitotic and meiotic cell cycle. It is also involved in cell differentiation in various cell types and organisms. However, an important question still open is how these multiple functions are regulated.

1.2.6 APC/C$^{CDH1/FZR-1}$ regulation

APC/C's first layer of regulation is the recognition of specific substrates. In contrast to SCF E3 ubiquitin ligases, which usually recognize their substrates upon phosphorylation, APC/C is not dependent on substrate modifications. (Rape et al., 2006). APC/C binds the substrates through the coactivators Cdc20/Fzy-1

and Cdh1/Fzr-1. The coactivators work as adaptors to provide specificity and affinity to recruit and ubiquitinate substrates. Recognition and binding of substrates occur through highly conserved sequences of amino acids: The KEN-box (xx**KEN**xx) and the D-box (**R**xx**L**xxxx**N)**, although there are other non-frequent motifs such as A-box, GxEN-box, O-box or TEK-box (He et al., 2013; Reviewed in (Song & Rape, 2011). The determination of the molecular structure of the APC/C complex indicated that coactivators are involved in the KEN-box recognition (Chao et al., 2012), while they partner with the Apc10 subunit to interact with the D-box motif (Da Fonseca et al., 2011). Strikingly the conformation changes occurring in the APC/C complex upon recognition of the D-boxes is a requirement to process all of the substrates, although many of them lack canonical D-boxes (Qin et al., 2017). Although it is not general, in some cases, APC/C substrates are regulated by phosphorylation of recognition motifs, resulting in the absence of APC/C recognition. Cdk-1 phosphorylates securin near D-box to inhibit ubiquitination by APC/C (Holt et al., 2008), and Aurora A phosphorylation near A-box also inhibits ubiquitination by APC/C (Crane et al., 2004). The union of a facilitator can also promote APC/C degradation of specific: Cks1 and Cks2 bind to Cyclin A/Cdk1 and Cyclin B/Cdk1 complexes facilitating the APC/C mediated degradation of Cyclin A and B but not the degradation of other APC/C substrates.

The second layer of regulation of the APC/C complex is linked to cell cycle progression and is mediated by the phosphorylation by CDK, by which interaction of the core complex to its respective coactivators can be promoted or inhibited (Kraft et al., 2003). During a mitotic cell cycle, CDK activity promotes the binding and activity of APC/C^{Cdc20} by phosphorylation of core APC/C subunits (Kraft et al., 2003) by Cyclin B/CDK1, which enables the binding of Cdc20. In contrast, CDK activity phosphorylates Cdh1 inhibiting its binding with APC/C during S, G2, and M phases (Kramer et al., 2000; Zachariae et al., 1998). Only in late mitosis does APC/C^{Cdc20} degrades the mitotic cyclins resulting in a decrease in CDK activity, which allows the presence of unphosphorylated Cdh1 subunits. The dephosphorylation of pre-existing Cdh1 subunits by some specific phosphatases (not fully characterized) reinforces this step. As a result, unphosphorylated Cdh1

replaces Cdc20 and orchestrates mitotic exit (Wurzenberger & Gerlich, 2011). Interestingly, APC/C^{Cdh1} degrades the former coactivator Cdc20 and can also target the remains of mitotic cyclins, further reducing CDK activity (Thornton & Toczyski, 2003). All these steps resulted in the directionality and irreversibility of the coactivator switch, enabling total activity of APC/C^{Cdh1} during the early G1 phase. If the cell enters a new cell cycle, the Cyclin D-CDK4/CDK6 complex, which accumulates along the G1 phase and is not targeted by APC/C, phosphorylates and inhibits APC/C^{Cdh1} in mammals and worms (The et al., 2015; Wan et al., 2017). This inhibitory phosphorylation is later on promoted by Cyclin E-CDK2, involved in S-phase in mammals (Keck et al., 2007). In some organisms, such as *Drosophila* Cyclin A-CDK1/CDK2, a complex involved in S and G2 phases, has also been found able to phosphorylate and inhibit Cdh1 activity (Reber et al., 2006a). Strikingly, the temporal regulation of APC/C is slightly different during the meiotic cycle. CDH1 is activated in prophase I (equivalent to G2) because of the down-regulation of CDK activity promoted by BubR and is responsible for the prophase I arrest , which is necessary for correct oogenesis (Homer et al., 2009). Once this arrest is released, the increase in CDK activity inhibits Cdh1 and promotes APC/C^{CDC20} activity in metaphase I.

It is also believed that the regulation of the subcellular localization of Cdh1 could also control the cell cycle-dependent activity of the APC/C^{Cdh1} complex: Cdh1 has nuclear localization during G1 but cytoplasmic localization during S-G2-M phases. CDK phosphorylation promotes nuclear export (Jaquenoud et al., 2002; Maestre et al., 2008).

In addition to CDK phosphorylation, there are a variety of APC/C inhibitors like Emi1 or Acm1 (Cappell et al., 2018; He et al., 2013) (Reviewed in (Pesin & Orr-Weaver, 2008), acting as pseudosubstrates and inhibiting APC/C activity. Also targeted degradation of APC/C elements regulates the activity of the distinct complexes. For instance, targeted degradation of specific E2s like UbcH10 negatively affects APC/C activity (Rape & Kirschner, 2004). Phosphorylated Cdh1 can be targeted for degradation by SCF E3 ubiquitin ligase complex during the S phase (Benmaamar & Pagano, 2005; Fukushima et al., 2013; Pal et al., 2020). Even the coactivators are targeted by the APC/C^{Cdh1} complex. In the first

place, Cdc20 and later Cdh1 can catalyze its own destruction through the APC/C activity in mammals (Listovsky et al., 2004).

Finally, the protein abundance of the coactivator Cdh1 is also a possible manner to control the activity of APC/C^{Cdh1} complex. Cdh1 levels could be regulated spatially or temporally inside the cell and in coordination with the cell cycle, but the protein abundance can also be different depending on the cell or tissue, adding complexity to the model. This possibility is especially relevant in multicellular organisms. Interestingly, a study searching for Pumilio interactors in the murine brain revealed APC/C complex subunits as the main functional category (Botta et al., 2022). Pumilio is a family of RNA-binding proteins that act upstream of developmental processes modulating protein expression in different cells.

1.3 *Caenorhabditis elegans* germline as a model to study cell cycle and differentiation

1.3.1 The nematode *Caenorhabditis elegans*

Caenorhabditis elegans is a free-living, transparent nematode used as a model organism for over 50 years. One of this model's main advantages is its ease of maintenance in the laboratory: the nematodes can grow in lab plates as they are fed with bacteria on top of the plates (Brenner, 1974). The life cycle of *C. elegans* is very convenient for lab work. In conditions of controlled temperature, the timing of the life cycle is very stable: At 20ºC the life cycle last 78h (3.5d approximately); at 15ºC the life extends to 125h (~5d) and at 25ºC the life cycle last 60h (~2.5d). Upon hatching from the egg in appropriate environmental conditions, the post-embryonic development proceeds through four larval stages (L1, L2, L3, and L4). A molting phase, in which a new cuticle is produced and the old one is released (Raizen et al., 2008), precedes the transition between every larval stage. However, during harsh environments, like, for instance, starving conditions or overcrowded population, the worms can enter several kinds of programmed developmental arrests: The first one can happen

after embryo hatching; L1 larvae can arrest development if food is scarce (Reviewed in (Baugh, 2013); The second one happens later, instead of reaching normal L2 and L3 stages, worms can enter an alternative developmental program becoming a particular resistant larval stage called “dauer” (Reviewed in (Fielenbach & Antebi, 2008). Finally, in adult worms, in response to food limitation or other stresses, the germline stops producing more progeny until the conditions are good enough again (Seidel & Kimble, 2011, 2015).

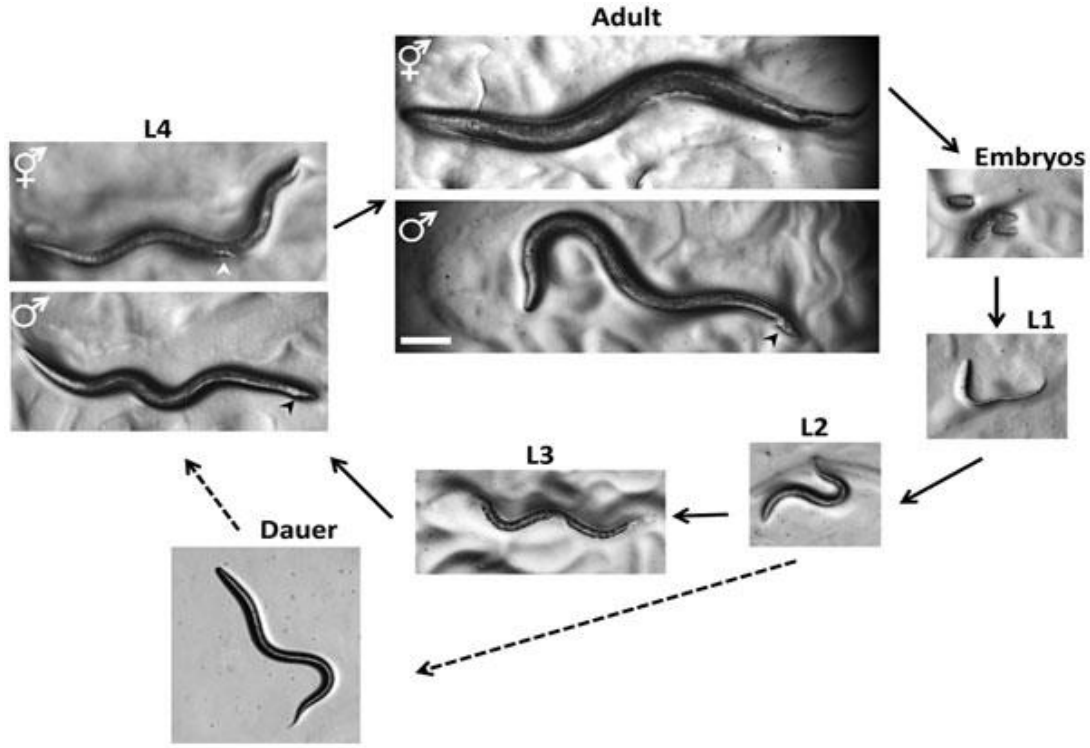

Figure 1.3: *Caenorhabditis elegans* larval stages and life cycle. Figure from Wormbook introduction (Corsi et al., 2015)**.**

“Life Cycle of *C. elegans*. Animals increase in size throughout the four larval stages, but individual sexes are not easily distinguished until the L4 stage. At the L4 stage, hermaphrodites have a tapered tail and the developing vulva (white arrowhead) can be seen as a clear half circle in the center of the ventral side. The males have a wider tail (black arrowhead) but no discernable fan at this stage. In adults, the two sexes can be distinguished by the wider girth and tapered tail of the hermaphrodite and slimmer girth and fan-shaped tail (black arrowhead) of the male. Oocytes can be fertilized by sperm from the hermaphrodite or sperm obtained from males through mating. The dauer larvae are skinnier than all of the other larval stages. Photographs were taken on Petri dishes (note the bacterial lawns in all but the dauer images)” (Corsi et al., 2015).

Another significant advantage is the suitability for genetics analyses. Forward genetic screenings can be easily performed due to efficient RNA interference mechanisms that allow the silencing of genes by feeding the worm with transformed *Escherichia coli* bacteria (Timmons & Fire, 1998). Whole genome sequencing is available as any other kind of omic analysis. Regarding sexes, males are rarely present in lab populations (<0.2%), and most worms are hermaphrodites, so the population is primarily clonal once homozygosity is reached.

This nematode is also an excellent tool for cell biology and development. The worm has an invariant cell lineage with a predetermined somatic cell number, 959 in hermaphrodites and 1031 in males (Sulston & Horvitz, 1977), and all of those cells have been characterized and categorized. Furthermore, as the worm is transparent, the organs can be distinguished by dissecting microscopes, and high-resolution microscopy analysis can be done by mounting the whole worm. The germline, a lineage of cells that give rise to the progeny, is a fascinating tissue. In the adult worm, the germline harbors most of the worm's cells; interestingly, they are organized spatiotemporally from stem cells to differentiated oocytes and sperm. Efficient dissection of the germline can be performed to isolate it, increasing the resolution of the microscopy and allowing immunostaining over it. For that, the germline of *C. elegans* is excellent *in vivo* model to study stem cells and their differentiation.

1.3.2 *C. elegans* germline and the niche signaling

In *C. elegans* adult hermaphrodites, the reproductive system has two gonads with a U-shape that bind to the uterus through the spermatheca. Initially, each gonad produces around 150 sperm cells stored in the spermatheca. After the L4 stage, gonads stop sperm production and produce oocytes that become fertilized as they pass the spermatheca to reach the uterus and, finally, are deposited through the vulva. A single hermaphrodite worm can produce around 300 self-fertilized eggs and nearly 1000 when fertilized by a male (Hodgkin et al., 1979). The gonad can be divided into the germline, the group of cells that give rise to the gametes, and the somatic gonad, the rest of the tissues that aid the germline. The somatic gonad is formed by the Distal Tip Cell (DTC); the gonadal sheath that physically covers the germline; the spermatheca that stores the sperm; the uterus that stores fertilized early embryos, and the vulva (Judith Kimble & Hirsh, 1979).

The adult germline maintains a Distal-to-Proximal (D-P) polarity. The distal end is defined as the mitotic zone, and some authors also refer to it as the “progenitor zone” (Haupt et al., 2020; Seidel & Kimble, 2015; Shin et al., 2017). The mitotic zone is composed of two distinct cell populations. The first is the pool of mitotically dividing **Germline Stem Cells (GSCs**). The GSC pool is followed by dividing cells completing their last mitotic cycle before meiosis that are primed or **launched for differentiation** (Cinquin et al., 2010). Some authors name this region “transit-amplifying cells” (Crittenden et al., 2017).

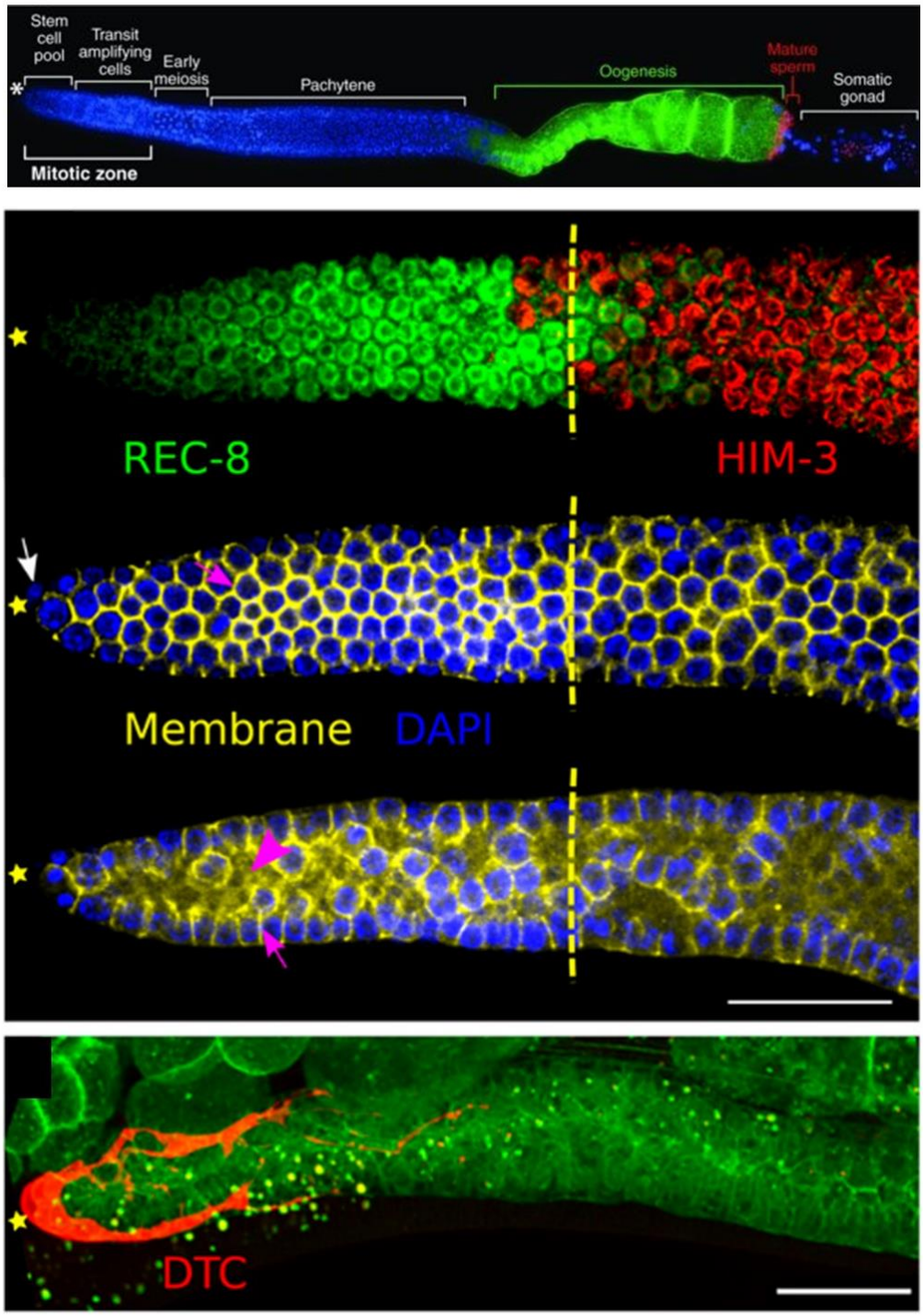

Figure 1.4: *Caenorhabditis elegans* germline (top), from (Kimble & Seidel, 2008)**. Amplification of mitotic and early meiotic zones of the germline (bottom), from** (Hubbard & Schedl, 2019)

The germline has a mitotic zone with a stem cell pool (GSCs) and cells primed to differentiate (transit amplifying cells). After that, we can find the transition zone (early meiosis), followed by pachytene and oogenesis region. The transition zone start is represented with yellow dashed lines, determined by the crescent-shaped nuclei.

After the last round of mitotic cells primed to differentiate, the **transition zone** is characterized by crescent-shaped nuclei. This zone harbors cells entering the early stages of meiosis (leptotene-zygotene). More proximally to the transition zone, we can find cells in early and late **pachytene** stages of meiosis, then **diplotene,** and finally **diakinesis** (unfertilized oocytes). The stem cell pool is maintained by the Distal Tip Cell (DTC), a cell that establishes the niche and physically surrounds the distal end of the germline, extending its processes until the transition zone (Byrd et al., 2014; Kimble & White, 1981). The niche signal is mediated through the highly conserved Notch pathway, promoting the polarity in the germline (Austin & Kimble, 1987). The plasma membrane of the DTC expresses a Notch ligand, LAG-2, that activates the Notch Receptor, GLP-1, on the surface of the germ cells (Henderson et al., 1994; Kimble & Simpson, 1997). Once activated, the receptor, GLP-1, self-cleaves and translocates to the nucleus, forming a complex with LAG-1 DNA binding protein and LAG-3 transcription co-activator (Chen et al., 2020; Kimble & Petcherski, 2000). This cascade acts upstream of a regulatory hub, named as PUF (Pumilio and FBF) hub. The PUF hub comprises RNA binding proteins necessary for maintaining the GSCs pool, mainly FBF-1 and FBF-2 (Haupt et al., 2020). Recently, it has been proposed that the Notch pathway acts only transcriptionally upstream of proteins LST-1 and SYGL-1 (Chen et al., 2020). The link Notch-PUF is then established as LST1, and SYGL-1 can physically interact with PUF RNA binding proteins, modulating their activity (Shin et al., 2017). In summary, the Notch Pathway establishes spatial regulation of pro-mitotic and anti-meiotic proteins in the progenitor zone, mainly through RNA interaction mediated by the PUF regulatory hub.

As stem cells proliferate, they physically push themselves, moving and distancing from the DTC at the same time that they start to get ready for differentiation. When cells are primed for differentiation, SYGL-1 and LST-1 drop, changing the activity of the PUF hub, although how this exactly happens is still under study (*Kimble lab communications*). Finally, the entry into meiosis, noted by the crescent-shaped nuclei (transition zone), concurs with the fading away of the Notch pathway and the PUF hub and the upregulation of meiotic driving proteins.

1.3.3 *C. elegans* germline differentiation: The entry into meiosis

A key process for worm biology is the production of gametes from the germline stem cells. This is achieved by transitioning from a proliferating mitotic cycle to a differentiated meiotic cycle. Both masculine and feminine gametes have to become haploid (n) to maintain the ploidy (2n) of the next generation when they combine. For this, the meiotic cycle is essential. During the *C. elegans* meiosis program, sperm and oocyte differentiation occurs. The future gametes, especially the oocyte, are loaded with maternal mRNAs, proteins, and other factors necessary for embryo development. The transition from mitosis to meiosis involves the downregulation of mitotic factors and activities and simultaneously the upregulation of early meiotic factors.

Meiotic entry can occur in a variable and non-synchronous region of approximately 8 cell diameters. The variability is a consequence of the asynchronous cycling of the cells completing the mitotic cycle and starting the meiotic S-phase (Fox et al., 2011). The meiotic S-phase precedes the denominated transition zone of the germline, but it is hard to differentiate from cells finalizing the last round of mitosis. The transition zone can be easily observed because of the crescent-shaped nuclei and marks the leptotene-zygotene phases of meiosis. To distinguish the mitotic cycle from the meiotic cycle, various proteins have been used: WAPL-1 and REC-8 are examples of proteins that accumulate in the mitotic cells and are downregulated in the meiotic cycle. For meiotic entry, proteins such as phospho-SUN-1 nuclear envelope protein, phospho-HIM-8, and phospho-HIM-3 have been used.

As previously mentioned, GLP-1 Notch receptor signaling promotes the maintenance of stem cells generating the polarity of the germline. In addition, Notch signaling inhibits two parallel pathways that promote meiotic entry, GLD-1, and GLD-2 pathways, through the SYGL-1, LST-1, and PUF cascade of signals (Brenner & Schedl, 2016; Kershner & Kimble, 2010). GLD-1 pathway involves GLD-1 and NOS-3, RNA-binding proteins that inhibit the translation of mitotic genes and therefore promote meiotic entry (Hansen et al., 2004). GLD-2 pathway is formed by a noncanonical poly-A polymerase GLD-2 (Suh et al., 2006; Wang

et al., 2002) and the Bicaudal-C-type RNA-binding protein, GLD-3 (Eckmann et al., 2004), which are believed to promote translation of gene products that promote meiotic entry.

In GLD-1-pathway mutants, cells enter meiosis but cannot complete the differentiation program and abruptly return to mitosis. In GLD-2-pathway mutants, cells enter meiosis, although they form non-functional gametes. Nevertheless, cells cannot enter meiosis in double mutants of both GLD-1 and GLD-2 pathways. The third component of this regulatory hub is the E3 ubiquitin-ligase SCF^{PROM-1} (Mohammad et al., 2018), which is also a promoter of meiotic entry, acting in parallel with the GLD-1 pathway and GLD-2 pathway. SCF^{PROM-1} can upregulate CHK-2 kinase - a master regulator directing homologous chromosome pairing - by promoting the degradation of PPM-1.D (Baudrimont et al., 2022) and also contributes to anti-mitotic activity by degrading CYE-1 (Fox et al., 2011; Mohammad et al., 2018). In summary, *C. elegans* has three post-transcriptional pathways promoting meiotic entry and mitotic exit: SCF^{PROM-1} specific protein degradation, GLD-1 by mediating translational repression, and GLD-2 by mediating translational activation.

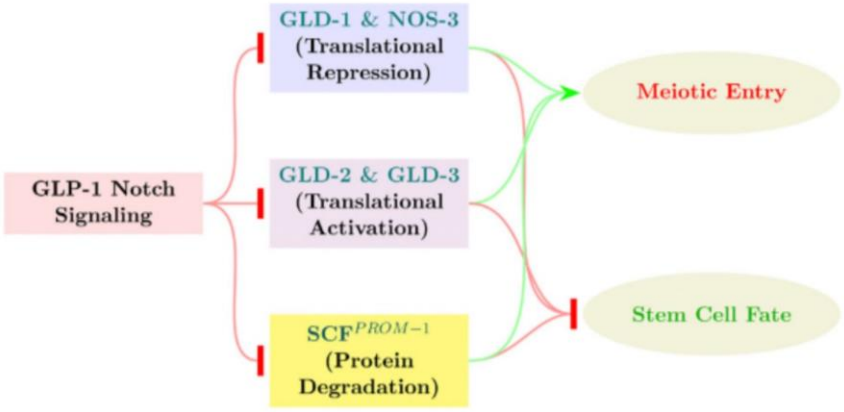

Figure 1.5: Notch pathway maintains the stem cell pool and opposes the meiotic entry pathways. Figure extracted from (Mohammad et al., 2018)
Notch signaling is active in the germline stem cells and represses the three main known pathways that promote meiotic entry due to post-transcriptional regulation: GLD-1-pathway represses mitotic mRNAs translation, GLD-2-pathway promotes mRNA translation of factors that promote entry into meiosis and SCF^{PROM-1} is an E3 ubiquitin ligase complex that promotes degradation of the mitotic cyclin E and PPM-1.D, releasing CHK-2 activity. As cells move further away from the niche, Notch signaling fades away and cells enter meiosis.

1.3.4 Cell cycle in *C. elegans* germline

In the proliferation zone of *C. elegans* adult germline, cells are rapidly and continuously dividing. Human and mouse stem cells were described as having a short G1 phase (Liu et al., 2019; ter Huurne & Stunnenberg, 2021). Similarly, in C. elegans, germline stem cells (GSCs) have a rapid cell cycle with alternating S and M phases and with short G1 (Fox et al., 2011; Kocsisova et al., 2018). These rapid divisions result from high levels of the S-phase cyclin E/CDK-2 complex. *cye-1* knock-down causes all cells in the proliferation zone to arrest the cycle and show a characteristic enlarged nuclei (Fox et al., 2011; Jeong et al., 2011). In the progenitor zone, the levels of this cyclin are not downregulated along different phases of the cycle; therefore, CYE-1 is present through all the proliferation zone. Inhibitors of CYE-1/CDK-2 activity are not active in the *C. elegans* proliferating zone. For instance, *lin-35* (Retinoblastoma protein) mutants have fertility defects, but no role in the proliferation zone has been reported for the protein (Fay et al., 2002). CKI-1 is not expressed in the *C. elegans* germline, and CKI-2 is expressed after the mitotic zone but downregulated in the proliferation zone (Kalchhauser et al., 2011). SCF^{PROM-1} , the E3 ubiquitin ligase complex in charge of initiating the degradation of CYE-1, is only active after meiosis S-phase and not in the proliferation zone (Mohammad et al., 2018). GLD-1 protein also represses mRNA translation of CYE-1 but only in meiosis (Biedermann et al., 2009), this happens because GLD-1 is repressed in the proliferation zone by multiple pathways, one of which is the phosphorylation by CYE-1/CDK-2 activity (Jeong et al., 2011). Furthermore, Cyclin D/CDK-4 does not play an important role in the germline (Fox et al., 2011). This is consistent as one of the roles of Cyclin D is to allow exit from G1, and this could not be necessary if inhibitors of S-phase Cyclin E are inactive, and G1 is almost inexistent.

Due to continuous high CYE-1/CDK-2 activity, interphases are short during proliferation, only 2% of cells are in G1, and most are in S-phase (Fox et al., 2011). However, as cells move to the transit-amplifying region, the cell cycle changes and G2 enlarges (Roy et al., 2016). In addition, CYE-1 protein is degraded due to SCF^{PROM-1} activity just after the meiotic S phase (Fox et al., 2011; Mohammad et al., 2018), corroborating a change in the pace of the cycle in the

differentiation from mitosis to meiosis. GLD-1 activity also inhibits new CYE-1 translation as cells enter meiosis. The increase in GLD-1 activity is triggered by two redundant mechanisms: the decrease in Notch signal that down-regulates GLD-1 translation and the decrease in CYE-1-CDK2 activity that phosphorylate GLD-1. Furthermore, GLD-2 pathway activity also upregulates GLD-1. GLD-2 upregulated downstream targets include multiple cell cycle factors that could also trigger a switch of cell cycle regulation (Kadyk & Kimble, 1998).

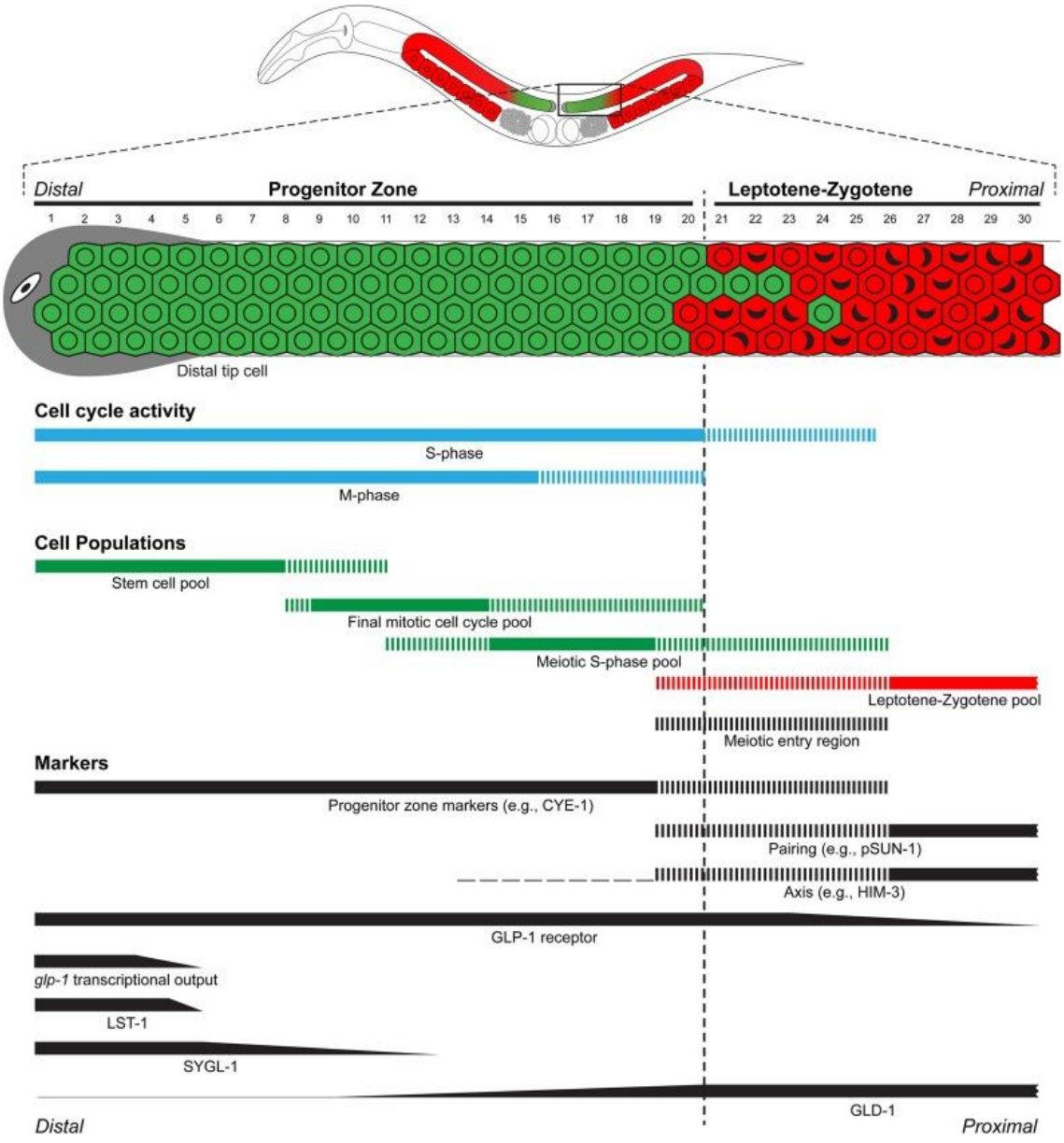

Figure 1.6: Organization and markers in the germline stem cell system. Figure extracted from (Hubbard & Schedl, 2019)**.**

(Figure 1.6 continuation)

"Schematic diagram of the distal germ line and the approximate extent of cell pools and marker accumulation as observed in the "day 1" adult hermaphrodite (24h past the mid-L4)). Distal tip cell (gray), PZ cells (green), and leptotene-zygotene cells (red). The extent of M phase and S phase cell cycle activity is shown in blue horizontal bar, based on EdU incorporation and phospho-H3 staining, respectively. Cell populations in the progenitor zone (PZ; green bars): the stem cell pool, final mitotic cell cycle pool, and meiotic S phase. The leptotene-zygotene pool (red bar) is based on staining of meiotic chromosome pairing or axis. For categorical markers and activities that show nuclear staining (PZ markers, etc.), the solid bar indicates region where all cells stain, while vertical hatching indicates region where only a subset of cells have nuclear staining" (Hubbard & Schedl, 2019).

1.3.5 APC/C^{FZR-1} degrades chromatin regulators MES-3 and MES-4 in the transition from mitosis to meiosis

The proliferative zone of *C. elegans* is characterized by a specific chromatin landscape. Chromatin regulation is a master key to maintaining pluripotency. In C. elegans, the histone methylation complexes Polycomb Repressive Complex 2 (PRC2) and MES-4 are essential in maintaining the chromatin landscape and the correct expression pattern. PRC2 and MES-4 protect germline development by regulating several transcription factors, like LIN-15B (Cockrum & Strome, 2022) (Gaydos et al., 2012). Because of this protective role, *mes* mutants are prone to transdifferentiation of the germ cells into somatic cells when combined with the ectopic expression of terminal transcription factors (Patel et al., 2012).

MES-4 (Maternal Effect Sterile 4) is an H3K36me2-3 type histone methyltransferase that modulates the differences between germline and soma chromatin status and is also essential for the maintenance of germline stem cells and, therefore, for the maintenance of fertility through generations (Rechtsteiner et al., 2010). This protein, which contains a SET domain, is the ortholog of NSD proteins conserved in vertebrates. MES-4 is linked to transcriptionally active germline genes (Rechtsteiner et al., 2010)

MES-2, MES-3, and MES-6 are part of the *C. elegans* Polycomb Repressive Complex 2 (PRC2), a conserved complex with H3K27me3 type of histone methyltransferase activity. This complex generates repressive methylation and opposes the transcription of somatic genes in the germline (Bender et al. 2004). While MES-2 and MES-6 are orthologs of Drosophila Enhancer of Zeste, E(Z), and Extra Sex Combs (ESC), the MES-3 subunit is exclusive of *C. elegans*, with no homologs found in other organisms (Holdeman et al., 1998; Ketel et al., 2005; Xu, Paulsen, et al., 2001)

Previous work from our lab indicated that MES-4 (Rivera-Martín *PhD thesis*, 2018) and MES-3 (Fragoso-Luna *PhD thesis*, 2020) are recognized and primed for degradation by APC/C^{FZR-1}. To carry out these studies, CRISPR-tagged endogenous alleles of MES-3 and MES-4 with GFP were generated and analyzed under confocal microscopy. MES-3 and MES-4 showed high levels of expression in the proliferation zone of the germline, decaying abruptly in early pachytene and were maintained low until late pachytene. However, when FZR-1 activity is impaired, either by using a strain carrying a hypomorphic allele, *fzr-1(ku298)* (Fay et al., 2002) or *fzr-1* RNAi silencing, MES-3 and MES-4 protein levels were maintained high throughout the germline. These results were not replicated with RNAi silencing of *fzy-1/cdc20*, the other APC/C coactivator. Furthermore, the “KEN-box” APC/C^{FZR-1} recognition motifs of MES-3 and MES-4 were mutated, and it also caused the stabilization of both proteins throughout the germline (**Figure 1.7**). All these results strongly indicated that MES-4 and MES-3 were targets of the APC/C^{FZR-1} complex in the germline of *C. elegans*.

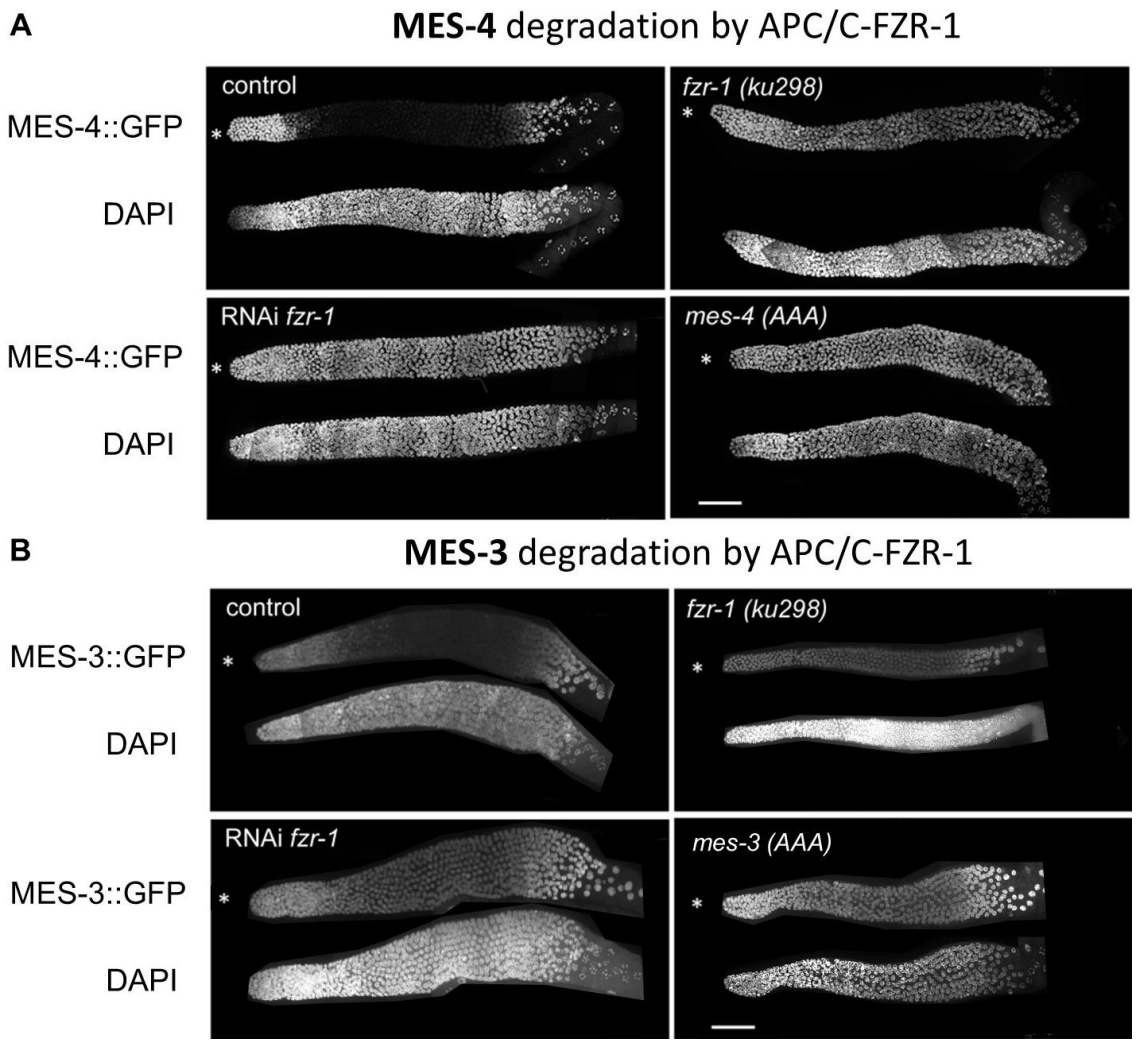

Figure 1.7: MES-3 and MES-4 chromatin regulators are marked for degradation by APC/C^{FZR-1} in the *C. elegans* germline. Results and images are extracted from (Fragoso *PhD thesis*, 2020; Rivera-Martín *PhD thesis*, 2018).

The MES-4::GFP (A) and MES-3::GFP (B) tagged proteins are present in the mitotic region and degraded in the transition zone to meiosis, in late pachytene they're present again. Nevertheless, when *fzr-1* is silenced or when *fzr-1* is mutated *(ku298)* both MES-3 and MES-4 degradation are impaired. Furthermore, if the KEN-box (their APC/C^{FZR-1} recognition motif) is mutated their degradation is also impaired, as we can observe the proteins in early and mid-pachytene. These results showed that MES-4 and MES-3 are recognized and marked for degradation by APC/C^{FZR-1} through the KEN-box motifs.

1.4 Objectives

APC/C^{FZR-1} has been classically linked to cell cycle control, although increasing evidence suggests additional roles in differentiation further than cell cycle regulation. The work presented here aims to understand better how germline stem cells decide between self-renewal and differentiation. This Thesis is supported by previous work from our lab revealing that MES-4 (Rivera-Martín *PhD thesis*, 2018) and polycomb subunit MES-3 (Fragoso *PhD thesis*, 2020) are recognized and primed for degradation by APC/C^{FZR-1} in *C. elegans* germline. MES-3 and MES-4 are essential chromatin regulators for a functional germline and cause maternal sterility when impaired. They are expressed in the mitotic region of the germline and disappear in early meiosis because of APC/C^{FZR-1}activity.

It is necessary to understand **how is APC/C^{FZR-1} regulated** to allow initially the presence of MES-3/MES-4 in the mitotic region and, lately the degradation in the meiotic cells. The main objective of this thesis is to understand the processes that cause that in dividing and undifferentiated cells, APC/C^{FZR-1} is not active but activates when cells are differentiating into meiosis in the *C. elegans* germline.

MATERIAL AND METHODS

2. MATERIALS AND METHODS

2.1 Molecular biology

2.1.1 DNA extraction and PCR amplification

For DNA extraction, we used standard protocol, which can be found in the last Wormbook version and can also be found in (Barstead et al., 1991). One single worm was picked and submerged in 10µl of Lysis Buffer with 0.1 µg/µl of proteinase K. Afterwards, samples were frozen (-80ºC) for a minimum of 5 minutes. Finally, samples were heated in a thermocycler reaction: 60ºC for 1h, then 95ºC for 15min.

DNA was amplified with Taq DNA polymerase when the PCR reaction was used for genotyping. For cloning or sequencing, DNA was amplified with high fidelity DNA polymerase Q5 (Biolabs). Reaction mixes (**Table 1**) and PCR programs (**Table 2**) are listed below.

Table 1. PCR reaction mixes for Taq and Q5 DNA Polymerases.

Taq		**Q5**	
Reactive	**Volume(µl)/Tube**	**Reactive**	**Volume(µl)/Tube**
MilliQ water	19,5	MilliQ water	35
Buffer 10x	2,5	Buffer 10x	10
dNTPs (10mM)	0,5	dNTPs (10mM)	1
Primer 1 (100µM)	0,125	Primer 1 (100µM)	0,5
Primer 2 (100µM)	0,125	Primer 2 (100µM)	0,5
Taq	0,25	Q5 (2u/µl)	1
DNA	2	DNA	2
Total	25	**Total**	50

Table 2. PCR reaction programs for Taq and Q5 DNA Polymerases.

Cycles	Step	Taq	Q5
1	Denaturation	94ºC 5min	98ºC 30s
30	Denaturation	94ºC 30s	98ºC 10s
	Annealing	60ºC 30s	55ºC 20s
	Elongation	68ºC 4min	72ºC 4min
1	Elongation	68ºC 7min	72ºC 2min

2.1.2 Plasmid cloning

For *in silico* design, we used Serial Cloner 2.6.1. Standard cloning protocols were used to cut and ligate plasmids (Maniatis et al.,1989). Transforming was done using competent bacteria *Escherichia coli* DH5α by heat shocking (Hanahan, 1983). Plasmid pJET1.2 (Thermo Fisher) was used to clone PCR products and sequence them to verify correct sequence amplification. PCR products were purified from the gel with QIAquick Gel Extraction Kit.

Plasmids were purified by alkaline lysis method and checked with restriction enzymes. If the plasmids were used for microinjection, they were purified instead with QIAprep Spin Miniprep Kit to ensure purity.

2.1.3 CRISPR-Cas9 and MosSCI integration

Guide crRNA was manually designed, checked using the IDT webpage, and then commercially produced by IDT. To check the efficiency of the designed crRNA, we carried out *in vitro* CRISPR-Cas9 reaction (**Table 3**). The product of the *in vitro* reaction was analyzed in a 1% agarose gel by electrophoresis, stained with ethidium bromide, and then the percentage of digested PCR product was quantified. This allowed us to assay the designed guide crRNA quality.

Table 3. *In vitro* CRISPR-Cas9 reaction for crRNA cutting assay.

Reactive	Negative control	crRNA assay	Concentration
PCR product	5.5µL	5.5µL	
Bovine Serum Albumin	1 µL	1 µL	1mg/mL
Nes3 Buffer	1 µL	1 µL	10x
tracRNA	1 µL	1 µL	300µM
crRNA	0 µL	1 µL	100µM
RNAse free water	1 µL	0 µL	
Cas9	0.5	0.5 µL	1 µg/µl
1 h 37ºC			
Proteinase K	1µl		0.1 µg/µl
10 min 55ºC			

Table 4. *In vitro* CRISPR-Cas9 assembly for microinjection and worm mutation.

Reactive	Volume(µl)/Tube	Concentration
tracDNA	1	300µM
crRNA *dpy-10*	0.5	100µM
crRNA designed	2.5	100µM
4 min 95ºC		
Cas9 (IDT)	1	1 µg/µl
15 min 37ºC		

Table 5. Templates were added after table 4 CRISPR-Cas9 assembly and before microinjection.

Reactive	Single-strain	Single strain DNA template
Plasmid template	2µg diluted in 15 µl IDT buffer	
dpy-10 template		1µl 1µg/µl
designed template		4µl 1µg/µl
IDT buffer		10µl
Centrifugation 10min max speed 25ºC		

To obtain mutated strains, we assembled *in vitro* the CRISPR-Cas9 reaction (**Table 4**), added the template (**Table 5**), and then microinjected the mix into worm gonads. To tag a gene with fluorescent proteins or insert big-size sequences, we used a plasmid as a DNA template for the homologous repair. For deletions or point mutations, we used commercially produced DNA monomers (IDT) and *dpy-10* mutation as a selection marker.

For MosSCI transgene integration, we have used MosSCI universal system described on the Jorgensen webpage (https://wormbuilder.org/old).

2.2 Worm procedures

2.2.1 Worm maintenance

All *C. elegans* strains used were derived from the wild-type strain Bristol N2. They were maintained with classical nematode maintenance methods (Brenner, 1974). Worms were maintained between 15-25º C on nematode growth media (NGM) plates seeded with *Escherichia coli* OP50. NGM was composed of 3g/L NaCl, 2.5g/L peptone, and 25g/L agar. After autoclaving, NGM was amended with 25ml/L 1M potassium phosphate buffer (1M K_2HPO_4 mixed with 1M KH_2PO_4 to obtain pH 6.0), 1 mM $CaCl_2$, 1mM $MgSO_4$, and 5 mg/L cholesterol dissolved in EtOH). OP50 bacteria were grown in LB-liquid medium overnight, 10-fold concentrated, and deposited on the NGM plates.

2.2.2 Strain generation by crossing

To cross worms, males were obtained by heat shock for 6h at 32ºC. 5-10 males were crossed to 2-4 hermaphrodites (ratio 5 ♂ : 2 ♀). After 3-4 days at 20ºC, F1 L4 hermaphrodites were isolated and allowed to have self-progeny. F1 worms were genotyped either by PCR, phenotype screening or tracking of fluorescence markers. After selecting positive F1 candidates, alleles were established as homozygous in successive generations by letting the F1 progeny self-fecundate and, afterwards, by selecting homozygous F2.

2.2.3 Worm synchronization

To reduce variability in experiments, worms were synchronized. Adult hermaphrodites were submerged in a bleaching solution, disrupted in the vortex for 3 minutes, and then washed three times with M9. Bleached embryos were allowed to hatch overnight at 20º C, obtaining synchronized L1 larvae. After feeding at 20º C, the L1 larvae became L2-L3 in 24h, L4 in 48H and young adults

in 72H. Using this protocol, worms in all stages of development were reliably obtained (Porta-de-la-Riva et al., 2012).

The recipe for 50 mL of bleaching solution is 12.5mL bleach, 6mL 4M NaOH, 31.5mL M9.

2.2.4 RNA interference for silencing genes

The RNA interference (RNAi) method was used to silence genes (Timmons & Fire, 1998). RNAi was introduced into worms by feeding them *E. coli* bacteria of the strain HT115 with different RNAi-producing plasmids. HT115 strains with different plasmids were either obtained from Ahringer's library (Kamath & Ahringer, 2003) or constructed by cloning 0.5-1kb gene fragments into pL4440 and then transforming the constructed plasmid into HT115. To silence multiple genes, up to three gene fragments of 0.5-1kb were cloned in tandem into the multi-cloning site in pL4440 (Gouda et al., 2010).

HT115 with different pL4440 were grown overnight at 37º C in Luria-Broth (LB) medium with ampicillin (200 mg/L). The culture was concentrated ten times and placed onto NGM plates with IPTG (50mg/L) and ampicillin (200mg/L). Furthermore, the RNAi plates were incubated at room temperature to allow double-strand RNA production.

Synchronized worms were placed at 20ºC on RNAi plates with appropriate HT115 strain with correct pL4440 to knock down selected genes (Kamath et al., 2001). To ensure efficient knockdown, worms were fed RNAi bacteria for a minimum of two days before microscopy imaging. For multiple gene knockdowns, worms were fed RNAi bacteria for a minimum of three days. Dissection and imaging of the germline of RNAi-fed worms were always carried out 48h after the L4 stage.

2.2.5 Microinjection of worm gonads

We injected CRISPR or MosSCI mixes (Described in **2.1.3**) into germlines of young adults (24h after L4) grown at 20ºC. The microscope used was Nikon ECLIPSE Ti, and the microinjection equipment was from Eppendorf company: FemtoJet Microinjector, PatchMan NP2 micromanipulator, and Femtotips II capillaries.

2% agarose pads were dried at 37ºC for 1-2 nights and covered with Halocarbon oil moments before the microinjection procedure. Worms were cleaned of bacteria and were gently placed on the pad until immobilized. Then they were put under the microscope and were microinjected into one or both gonads with a pressure of 2500hPa for 0.2 seconds.

2.3 Confocal microscopy

2.3.1 Dissection of germlines

Synchronized adult worms were picked and placed in a tube with 50µl of M9 with 0.1% Levamisole and 0.1% Tween-20, which allowed partial immobilization of the worms. After 5-10 minutes, they were transferred to a Petri dish filled with PBS + 0.1% Tween-20 (PBST) and were dissected by cutting the head at pharynx level with a scalpel, causing germlines to be expelled from the interior of the worms. Germlines were collected and transferred to a new tube for different protocols.

2.3.2 Fast fixation for direct protein observation in the germline

This protocol was used for the direct observation of fluorescent proteins. Collected germlines were partially fixated with methanol at --20ºC for 5 minutes.

Germlines were centrifuged in a tabletop centrifuge (2000rpm 30'') and washed with PBST three times. Afterward, germlines were stained in DAPI (0.5µg/ml) diluted in PBST for 5 minutes. Germlines were centrifuged, and most of the liquid was removed from the tube, allowing germlines to be transferred to a 2% agarose pad on top of a slide. A mounting agent (Vectashield) was added to each corner of the agarose pad, and a cover slip was gently placed on top of the sample. In the end, the sample was sealed with a nail polish placed on the coverslip edges.

2.3.3 Immunostaining of germlines

Collected germlines using the **2.3.1** protocol were fixated in paraformaldehyde 2% for 10 minutes. After centrifugation (4400rpm for 1 minute), they were placed in methanol at -20ºC. After 5 minutes, they were centrifuged, and the methanol was removed. Germlines were then incubated with blocking solution (PBST + 0.5% BSA (Bovine serum albumin)) for 1h. After blocking, germlines were incubated overnight at 4ºC with the primary antibody mix diluted in blocking solution. Each specific primary antibody was used at the concentration recommended by the commercial house or previous assays.

The following day germlines were centrifuged, the primary antibody mix was removed and then they were washed 3 times with PBST during 3-5 minutes. Germlines were incubated in the dark for 1h with the secondary antibody mix (PBST + 0.5% BSA + DAPI + secondary antibodies). Secondary antibodies were used at the concentration recommended by the commercial house. Germlines were centrifuged, secondary antibody mix was removed, and then washed 4 times with PBST for 3-5min.

After the final wash, germlines were left in only 10 µl of PBST and a drop of ProLong Gold antifade mounting oil was added and gently mixed. Germlines mixed with mounting oil were placed in a slide, bubbles and excessive liquid were removed and a cover was gently placed on top. Samples were left to cure for a least 1 day.

2.3.4 Microscope images

Germlines were imaged using Olympus IX81 confocal spinning disk (Yokogawa CSU-X1 disk unit and equipped with a Photometrics Evolve EM-CCD camera) with Metamorph software. Immunostained germlines were imaged using a Leica SP8 confocal scanning laser with LAS X software.

Z-stack images were converted into a Z-max projection using FIJI software. Olympus spinning disk images required stitching to observe the full germline in a single image. The stitching was carried out using Grid/Collection stitching plugin included in FIJI. On occasions that the characteristics of the images precluded automated stitching, manual stitching using Adobe Photoshop was carried out. Leica SP8 images required no stitching because the field of vision and zoom was appropriate to capture full germlines in a single image.

2.4 Computational analysis and statistics

2.4.1 Protein quantification: data acquisition

The open-source FIJI software was used to measure fluorescence intensity. This can be downloaded at https://imagej.net/software/fiji/downloads. To mark the germlines, we followed the shape of each germline with a segmented line with a width ranging from 30-50, the width was selected to adapt the germline width. Full germline images (converted to 8-bit) were marked from the most distal tip to the first single-row cell in diplotene, after late Pachytene. Afterward, the “Analyze” -> “Plot profile” option was selected, and the fluorescence intensity profile of the germline was saved as a .csv file (Figure 2.1).

The data obtained was an absolute measure of color (Gray Value), ranging from absolute black (0) to white (255). Higher meant more fluorescence signal. The fluorescence signal can directly correlate to more protein quantity in direct fluorescent protein observation and immunostaining.

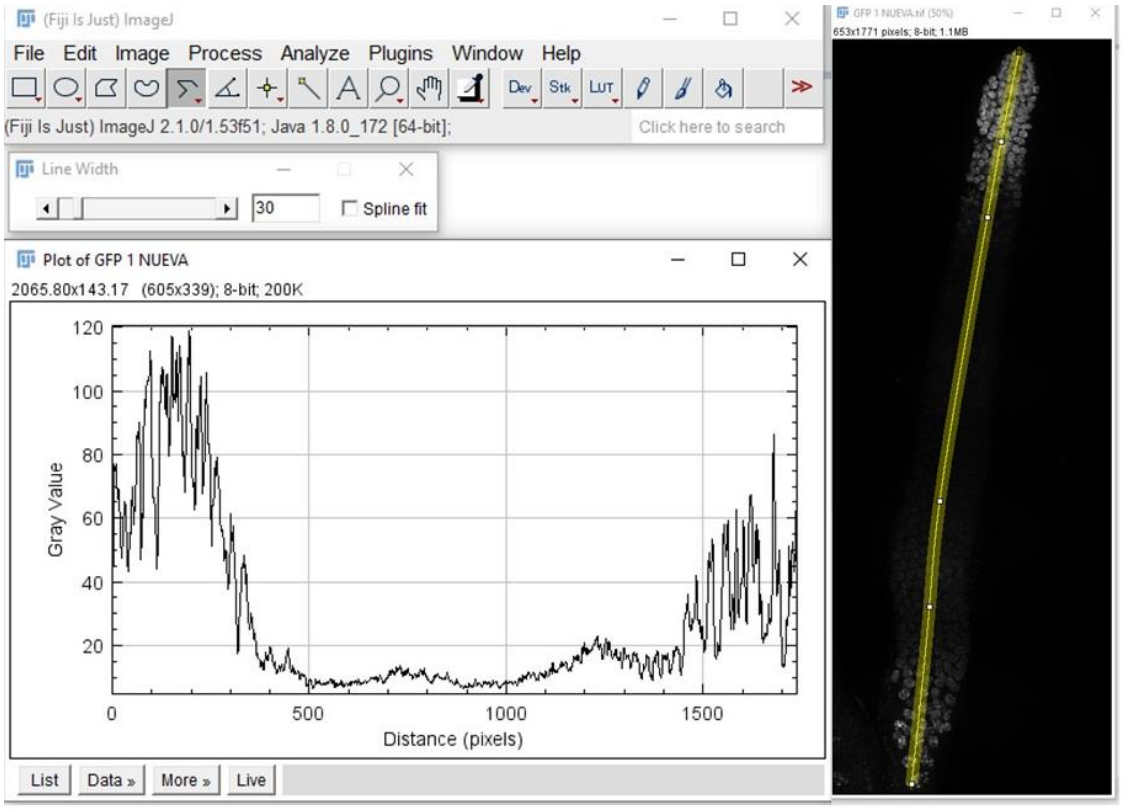

Figure 2.1: Gray value (from 0 to 255) graph obtained with FIJI/ImageJ.
The profile was selected with a segmented line from the distal end of the germline to the first single-row cell in diplotene.

2.4.2 Protein quantification: statistics and representation

To quantify fluorescence intensity and extrapolate protein quantity, multiple germlines were analyzed per sample. We always followed the same procedure to make a statistical representation of the sample.

The length of each germline was either used in absolute manner (pixels, microns or germline cell diameters, 3.5microns = 1 germline cell diameter) or more frequently, relativized. To relativize, we transformed absolute units (pixels or microns) to relative units (%): The most distal part was the 0% – the first single-row cell in diplotene was the 100%. This allowed the aggregation of germlines with variable lengths. Afterwards, germlines were split into a selected amount of intervals (usually ranging from 20-50), this allowed efficient averaging of the intervals of different germlines of the same sample.

Depending on the experiment, the average fluorescence intensity of the sample was transformed and displayed in different ways:

- In some of them, the **absolute intensity** was averaged and displayed (scale from 0 to 255). This was the preferred method to compare absolute protein quantity between samples or RNAi treatments.

- In some other cases, before averaging, each fluorescence interval was divided by the maximum intensity interval of that germline. In this case, the **relative intensity** value was displayed (scale from 0% to 100%). This was used when we were interested in the pattern of expression of a protein by itself or compared to others.

- Finally, in other cases, each interval was divided by the intensity of a previously decided interval (**fold-increase** compared to that region). For example, we could decide to display fluorescence intensity throughout the germline compared to the fluorescence in the distal part (interval 0-10%) of the germline. This was ideal for comparing how a protein expression increased compared to a specific region of the germline (Example: 5 times more protein in pachytene than in mitotic region).

The average intensity of each interval (Y-axis) was plotted in a graph to the germline length (0-100% when relativized or absolute units when not, X-axis). The standard deviation was plotted in each interval, represented as the error bar.

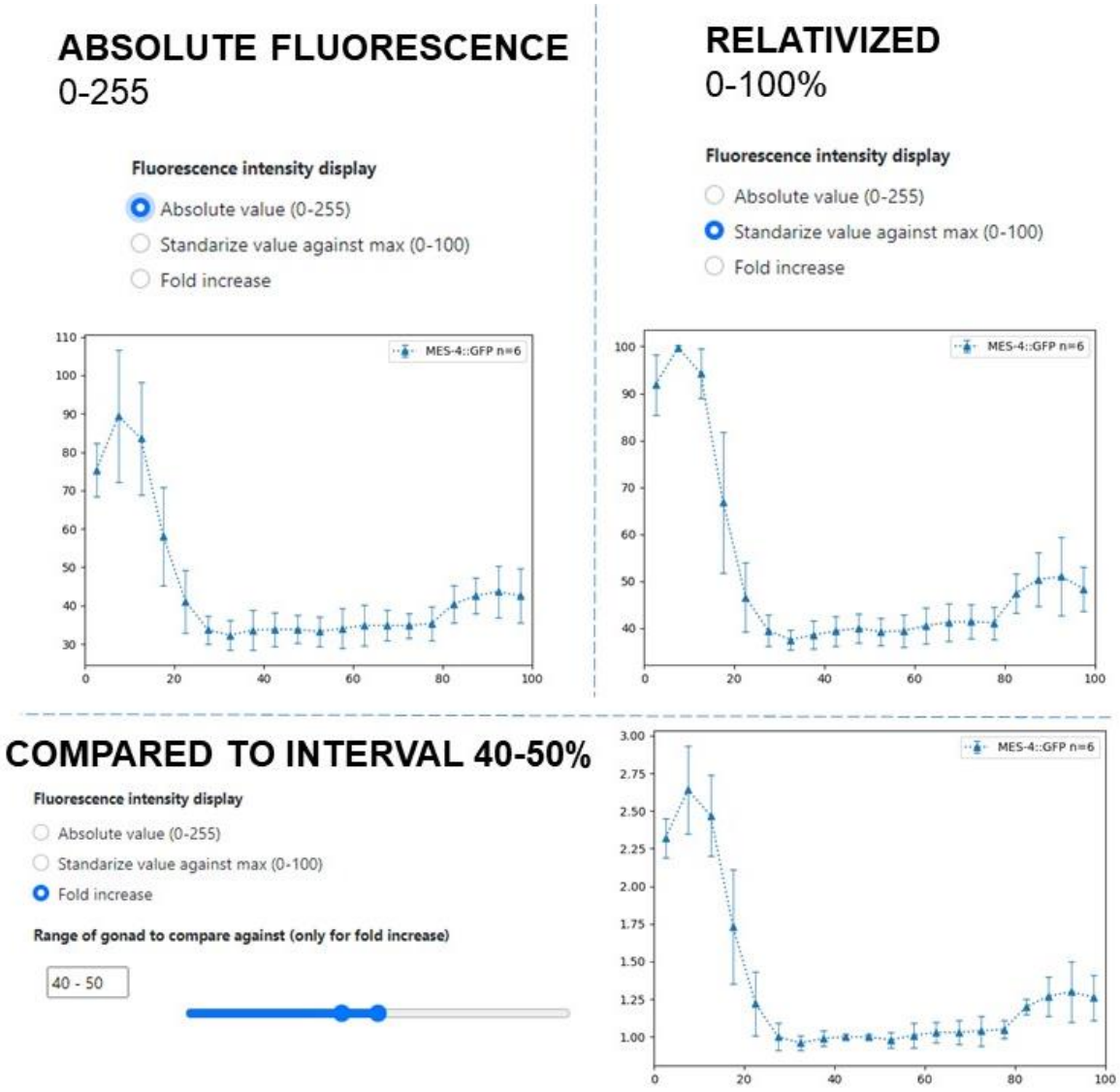

Figure 2.2: Different transformations to display fluorescence intensity.
All of the graphs represent relative germline length (0-100%) in the X axis. The Y axis shows the average fluorescence intensity for the sample. The first graph (top-left) shows **absolute fluorescence** (0-255) without any transformations. The second graph (top-right) shows **relativized fluorescence**, each interval was divided by the maximum interval before averaging, this explains why the second point (representing second interval) is near 100%, as that was the maximum interval in all germlines averaged. The third graph (bottom-side) shows the fluorescence intensity of each interval **compared** to the interval of 40-50% of the germline. This allows a comparison of each interval to the 40-50% interval.

To represent the extent of the mitotic zone, we followed a simple procedure: The length of the mitotic zone from the distal end to the start of the germline transition zone was measured. The germline transition zone was determined by the presence of at least two crescent-shaped cells in the same row. The total length of the germline was measured from the distal end to the first single-row diplotene cell. Dividing the length of the mitotic zone with the total length gave a relative value for each germline that was averaged between different germlines to obtain the sample average and sample standard deviation. For example, we could have a strain with a 23% average mitotic length and a 3% standard deviation (**Figure 2.3** shows an example).

$$mitotic\ length\ (\%) = \frac{\text{distal to transition zone length (absolute units)}}{\text{distal to first single row diplotene cell (absolute units)}}$$

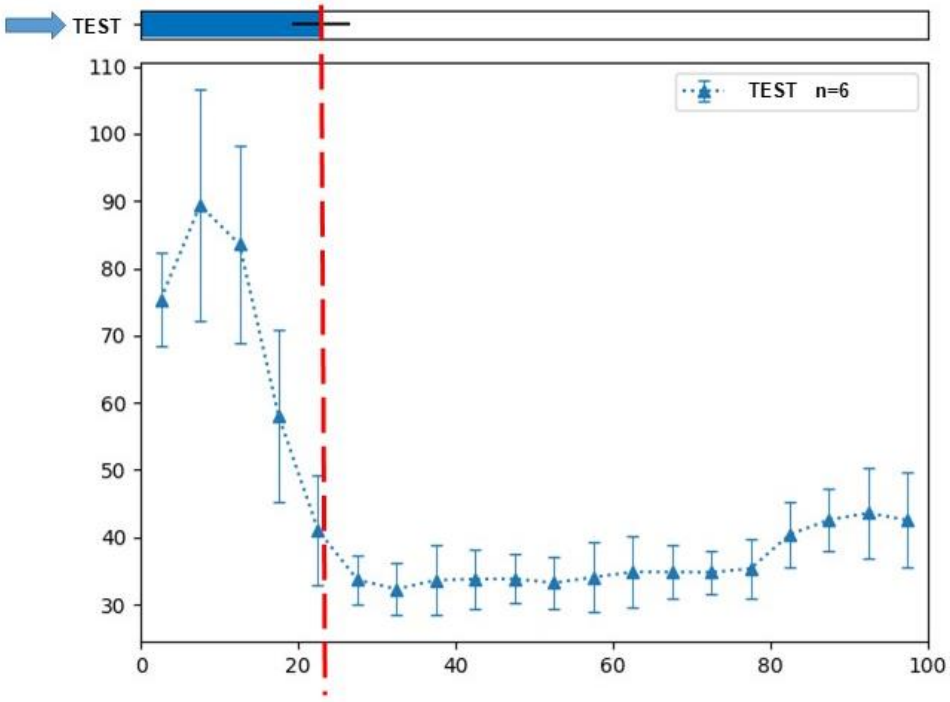

Figure 2.3: Mitotic length graph (blue arrowhead) was included on top of the fluorescence intensity graph.

This sample used to show the procedure presents an average mitotic length of around 23% with a standard deviation of 3% plotted as a line inside of the bar. The red dotted line shows the intersection with 23% germline length on the X-axis. The end of the mitotic zone is detected under DAPI staining by the presence of two crescent-shaped nuclei in the same row of cells.

To automate and simplify previous procedures an open source webapp was developed and used:
https://germline.deta.dev/

The webapp is hosted in DETA services to allow online to users. In case of future DETA hosting changes that impede access, the new hosting will be provided in the README file of the GitHub repository:
https://github.com/dpuertamartos/Germline-Analyzer

All the code of the webapp and therefore the code to run all the statistical analysis for fluorescence quantification and mitotic zone length quantification can be found and freely accessed and downloaded from the GitHub repository. The code is developed mostly in Python: Flask library for website interface and Numpy, Pandas and Matplotlib libraries to analyze and represent the data.

2.4.3 General statistics and data representation

For the statistical representation of other kinds of data non-related to fluorescence intensity quantification, we used Python code with open source libraries Numpy and Pandas for statistical calculations and Matplotlib and/or Seaborn library for data representation. These libraries include well-tested and studied functions to calculate descriptive statistics and represent the data with customizable graphs. For testing statistical significance calculation (for example, one-way ANOVA), we used STATGRAPHICS centurion.

2.4.4 Prediction of KEN-box and D-box motifs: GPS-ARM and ELM

To validate the presence of a KEN-box or D-box motif in a protein, we used GPS-ARM 1.0 (http://arm.biocuckoo.org/down.php). This software predicts the existence of both KEN-box and D-box and gives them a score based on previously experimentally identified ones (Liu et al., 2012).

The search for APC/C signatures was complemented using the Eukaryotic Linear Motif (ELM) resource (http://elm.eu.org/). This software, which can detect the presence of KEN-box and D-box motifs, allows us to predict the organization of a protein region. APC/C recognition motifs used to be located at accessible protein region. Motifs with high score in GPS-ARM, and located in a disorganized region (upon analysis with ELM) were selected as most likely APC/C motifs.

2.5 Alleles constructed, strains used and primers used

2.5.1 cye-1(sal42[cye-1::GFP^3xFlag::cye-1-3UTR])

The (Dickinson et al., 2015) method was used to label the C-terminus of CYE-1 with GFP. N2 were microinjected with CRISPR-Cas9 mix described in **2.1.3**, 2µg of plasmid pCye-1::GFP were used as a repair template. The used crRNA was designed and then tested *in vitro*, to check the correct and specific cutting of the CRISPR-Cas9 mix near *cye-1* C-terminus sequence.

The repair template plasmid construction started by amplifying 1kbp homology arms of *cye-1* with high fidelity Q5 polymerase, the fragments amplified were purified from a gel. 5' homology arm was amplified with oligos "5 fw cye-1" and "5 rev cye-1", 3' homology arm was amplified with oligos "3 fw cye-1" and "3 rev cye-1". Plasmid pDD285 was digested with *Avr*II and *Spe*I enzymes following (Dickinson et al., 2015) and assembled with previously mentioned 5' and 3' homology arms to generate pCye-1::GFP. NEBuilder HiFi DNA assembly mix (from NEB) was used for the assembly reaction. 5µl of the reaction product was transformed into *E. coli* DH5-alpha, colonies were selected by digesting plasmid with appropriate restriction enzymes.

Microinjected worms were grown for 5 days at 25ºC. Then, we added 300 µL hygromycin (250 µg/mL) per plate. After some days, hygromycin resistant and roller worms were selected, as described in (Dickinson et al., 2015). Both extremes of the insertion were checked: left side was checked with oligonucleotides "5 ext cye-1" and "GFP Crispr Rev", right side was checked with oligos "Hyg direct" and "3 ext cye-1".

Cre-Lox induction was carried by heat-shocking (32ºC) L1 larvae for 4h, allowing the excision of the hygro-rol cassette, and causing the coupling of the GFP with *cye-1* 3' UTR. Correct excision was checked in the following generation of the heat-shocked worms by PCR with oligos "GFP Utr dir" and "3 ext cye-1", plus "Hyg direct" with "3 ext cye-1". The fragment produced by the reaction carried out with the first pair of oligos is amplified and has size of 1.5kbp only when Lox recombination was produced, the second PCR, with the second pair of oligos, shows no amplification when Lox recombination was produced.

2.5.2 cye-1(sal57[K44A,E45A,N46A][R469A,L471A,L472A])

This allele was the result of two successive and independent CRISPR-Cas9 mutations over the *cye-1* coding sequence in the N2 strain: First, the highest scoring D-box by GPS-Arm algorithm was mutated (R469A, L471A, L472A) using "cye-1 dbox crRNA" and "cye-1 dbox ssDNA template". Secondly, the stable strain obtained by the previous CRISPR protocol, had the KEN-box motif mutated to triple alanine (K44A, E45A, N46A) using "cye-1 kenbox crRNA" and "cye-1 kenbox ssDNA template". Both mutations were performed at the same time as mutations in *dpy-10*, therefore guide RNA and ssDNA template for *dpy-10* were added in the mix used for both D-box and KEN-box mutations, as described in **2.1.3 table 5**. This allowed selecting mutated worms, since the mutation in dpy-10 causes "roller" phenotype. *Dpy-10* mutations were afterwards selected off the strain by selecting the absence of roller phenotype. The co-injection marker protocol is described by (Kim et al., 2014).

Insertion of the D-box and KEN-box mutations were checked by PCR amplification and digestion with a restriction enzyme. The mutated templates introduced included a *Pst*I restriction enzyme site in both, mutated D-box and KEN-box templates. To check the presence of the D-box mutation these oligonucleotides were used in the PCR: "5 ext cye-1" and 3 "ext cye-1". Then, the fragments were digested with *Pst*I, wild type allele shows a 2kbp band and the mutated allele shows two 1.2-0.8kbp bands. To check the presence of the KEN-box mutation these oligonucleotides were used: "cye-1 check 1" and "cye-1 check

2". After digestion with *Pst*I, wild type allele shows a 1.1kbp band and mutated allele shows two 550-450bp bands.

2.5.3 cye-1(sal58[cye-1 (K44A,E45A,N46A) (R469A,L471A,L472A)::GFP^3xFlag::cye-1-3UTR])

This allele was the result of the same two successive mutations carried for allele cye-1(sal57[K44A,E45A,N46A][R469A,L471A,L472A]) described in **2.5.2**, but we used cye-1(sal42[cye-1::GFP^3xFlag::cye-1-3UTR]) described in **2.5.1** as starting allele. This allowed us to have a cye-1 gfp tagged allele with mutated KEN-box and D-box. Intermediate *cye-1::gfp* strains with only KEN-box mutation or D-box mutation were also used in this thesis and are shown in the list of strains.

To check the presence of the KEN-box mutation in *cye-1::gfp* the procedure was the same as in the previous point **2.5.2**. To check the presence of the D-box mutation these oligonucleotides were used: "5 ext cye-1" and "GFP Crispr Rev". Then, the fragments were digested with *Pst*I, wild type allele shows a 1.1kbp band and the mutated allele shows two 0.8-0.3kbp bands.

2.5.4 cya-1(sal35[cya-1::GFP^3xFlag::cya-1 3'UTR])

This allele was built in a very similar way to the *cye-1::gfp* (**2.5.1**), (Dickinson et al., 2015) methodology was also used. We used crRNA "cya-1::gfp" to cut near the C-terminus of CYA-1 coding sequence and 2 µg of cya-1::gfp plasmid was added to the microinjection mix to act as a template.

To build cya-1::gfp plasmid, *cya-1* homology arms were amplified by using the following oligonucleotides: for 5' homology arm "CYA1GFP-2" and "CYA1GFP-3", for 3' homology arm "CYA1GFP-4" and "CYA1GFP-5". These fragments were assembled to pDD285 that was digested with *Avr*II and *Spe*I as described by (Dickinson et al., 2015).

After the microinjection procedure, worms were selected as described in **2.5.1** and for insertion confirmation by PCR we used the following oligonucleotides: before the excision of the hygromycin cassette, we used

“CYA1GFP-1” and “GFP Crispr rev” for one extreme and “Hyg direct” and “CYA1GFP-6” for the other. To check for correct excision of hygromycin after heat shock we used the following oligonucleotides “GFP Utr direct” and “CYA1GFP-6” that showed amplification plus “Hyg direct” and “CYA1GFP-6” that showed no amplification.

2.5.5 cya-1(sal39[R2A,L5A][K78A,E79A,N80A])

In a similar way to allele **2.5.2**, this allele was a product of two successive CRISPR mutations. First, we mutated the KEN-box motif (K78A, E79A, N80A), for that, in the CRISPR mix, we used “cya-1 kenbox” crRNA and “cya-1 kenbox” ssDNA template that included a new *Pst*I restriction site. Again, worms were first pre-selected by using CO-CRISPR with *dpy-10* mutation (Kim et al., 2014). Afterwards, they were confirmed as mutants by PCR with oligonucleotides: “Cya-1 kenbox check1” and “Cya-1 kenbox check2”, amplified fragments were digested with *Pst*I. Wild type allele shows 1 band of 1.1kbp and the mutated allele shows 2 bands of 0.6-0.5kbp.

Secondly, we mutated the D-box motif (R2A, L4A), to achieve that, we used “cya-1 dbox” crRNA and “cya-1 dbox” ssDNA template that included a new *PstI* restriction site. CO-CRISPR with the *dpy-10* mutation was used to pre-select and for the final check by PCR, we used oligonucleotides “CYA1 DBOX check 1” and “CYA1 DBOX check 2” and digestion with *Pst*I. Wild type allele shows 1 band of 800bp and the mutated allele shows 2 bands of 450-350bp.

2.5.6 cya-1(sal40[cya-1(R2A,L5A)(K78A,E79A,N80A)::GFP^3xFlag::cya-1 3'UTR])

To obtain a *cya-1::gfp* allele with KEN-box and D-box motifs mutated we followed the same procedure as **2.5.5** but as a starting strain, we used the one carrying *cya-1(sal35[cya-1::GFP^3xFlag::cya-1 3'UTR])* allele (strain JPM277) instead of wild type *cya-1*. CRISPR oligonucleotides and PCR oligonucleotides for checking were the same that the ones used in **2.5.5**. Intermediate strain with

only KEN-box mutation was also used in this thesis and it's shown in the strain list (strain JPM286).

2.5.7 fzr-1(sal14[GFP^3xFlag::fzr-1])

Strain constructed by (Fragoso *PhD thesis*, 2020). The (Dickinson et al., 2015) method was used to label N-terminus of FZR-1 with GFP. The attempts to label C-terminus were unsuccessful. The process was similar to the one described to label CYE-1 with GFP (**2.5.1**). Required CRISPR-Cas9 crRNA "gfp::fzr-1" was designed to cut near the N-terminus coding sequence of FZR-1.

Dickinson plasmid was constructed as follows: 5' Homology arm was amplified with oligos: "5 fzr1 nt fw" and "5 fzr1 nt rev". 3' homology arm was amplified with oligos: "3 fzr1 nt fw" and "3 fzr1 nt rev". Plasmid pDD282 was digested with *Cla*I and *Spe*I and assembled with homology arms following (Dickinson et al., 2015).

Selected worms for hygromycin resistance and roller phenotype were tested to check if the insertion was correctly integrated. Both extremes of the insertion were checked by PCR: using "hyg direct" and "3 ext FZR1 Nt" for one extreme, and "5 ext FZR1 Nt" and GFP "Crispr Rev" for the other. Positive bands could only happen if the insertion was located in the correct place of the genome. To check the expulsion of the hygro-roller cassette after heat shock, PCR with oligos "GFP utr dir" and "3 ext FZR1 Nt" was carried out. Amplification of 1.2kbp could only happen when the cassette is excised. To further verify that hygro cassette was expulsed PCR with oligos "hyg direct" and "3 ext FZR1 Nt" was performed, showing no amplification.

2.5.8 fzr-1(sal60[R23A,R24A,L26A)])

The highest scoring (by GPS-Algorithm) D-box sequence in *fzr-1* was mutated (R23A, R24A, L26A) by CRISPR-Cas9 in a wild-type worm, *Pst*I restriction site was introduced in the mutated sequence. Oligonucleotide

sequences of crRNA and template ssDNA can be found in the “Oligonucleotides used” section (**2.5.12**).

Co-CRISPR as described in (Kim et al., 2014) was used to filter candidate worms, positive worms were finally selected by PCR amplification using oligonucleotides: “Fzr-1 dbox check 1” and “Fzr-1 dbox check 2” and digesting with *PstI.* Wild type allele produces a 900 bp band and the mutated allele produces two 550-330 bp bands.

2.5.9 fzr-1(sal50[GFP^3xFlag::fzr-1(R23A,R24A,L26A)])

To produce a *gfp::fzr-1* allele carrying D-box mutation, we used the same procedure described in **2.5.8** but the mutated allele was *fzr-1(sal14[GFP^3xFlag::fzr-1])* described in **2.5.7**. In this case, the PCR checking was done using oligonucleotides “GFP Utr direct” and” Fzr-1 dbox check 2”, and then, the amplified fragment was digested with *Pst*I. Alleles without D-box mutation produced an 800 bp band and the allele with D-box mutation two 550-250 bp bands.

2.5.10 fzr-1(q1290[fzr-1::5xV5])

(Allele created by Kimble’s lab in the University of Madison-Wisconsin) A low conservation region near FZR-1 N-terminus was selected to insert a 5xV5 tag. The small size insertion was done by CRISPR-Cas9 using crRNA and template ssDNA that can be found in the “Oligonucleotides used” section (**2.5.12**). Positive worms were confirmed by amplifying by PCR with oligos “slc316” and “slc317” and sequencing.

2.5.11 salSi73 (Pfzr1::fzr-1::cye-1 3' UTR)

This allele was created because we needed to have a functional and working copy of *fzr-1* without its wild-type 3' UTR. To achieve this the *fzr-1* 5' UTR sequence (3.5kbp upstream of *fzr-1* start codon), *fzr-1* ORF sequence, and *cye-1* 3' UTR sequence were included in the pMosII vector.

For the plasmid construction, we used *pMosfzr-1p::fzr-1::3'UTR fzr-1* plasmid as the starting cloning vector, construction of this plasmid was described in (Fragoso *PhD thesis*, 2020), and we digested it with *Afe*I and *Sbf*I. We used oligos: "fzr1 ORF AfeI F" and "fzr1 ORF PacI SbfI" to amplify the last part of *fzr-1* ORF without including its 3' UTR but including two restriction sites *Pac*I *Sbf*I adjacent to the termination codon. The PCR product was digested with *Afe*I and *Sbf*I and then purified, finally, it was ligated into *Afe*I and *Sbf*I sites of *pMosfzr-1p::fzr-1::3'UTR fzr-1*. This way we obtained a version of *pMosfzr-1p::fzr-1::3'UTR fzr-1* without any 3' UTR but with *Pac*I and *Sbf*I sites to clone in any desired 3' UTR (*pMosfzr-1p::fzr-1::PacI-SbfI).* Finally, we ligated the *cye-1* 3' UTR, digested with *Pac*I and *Sbf*I, into the former plasmid, obtaining *pMosfzr-1p::fzr-1::3'UTR cye-1.* The *cye-1* 3' UTR was amplified using the following oligonucleotides: "Cye-1 utr PacI" and "Cye-1 utr SbfI" which flanked it with *Pac*I and *Sbf*I restriction sites.

The final constructed plasmid *pMosfzr-1p::fzr-1::3'UTR cye-1* was microinjected in EG8082 strain for insertion in chromosome V, following Universal MosSCI protocol (Frøkjær-Jensen et al., 2008, 2012). The microinjection mix was composed of: 100ng/ µL of pMos *pMosfzr-1p::fzr-1::3'UTR cye-1*, 50 ng/µL of pCFJ601 (coding for transposase) and a cocktail of plasmids coding for extrachromosomal markers (20 ng/µL of pGH8, 20 ng/µL of pMA122, 5 ng/µL of pCFJ90 and 10 ng/µL of pCFJ104). Insertion-carrying worms were selected by screening normal moving worms since insertion rescues the uncoordinated (unc) phenotype of the EG8082 strain. Insertion of the construction was then checked by PCR using the following oligonucleotides: "MosRIN" and "MosIIRout".

This insertion successfully complemented the full deletion of wild-type *fzr-1* locus, *fzr-1(sal19),* it restored fertility and did not present obvious phenotypes.

All the experiments carried out with the intention of using this allele were done using strains that had also the *fzr-1(sal19)* deletion. This way we ensured that the only functional copy of *fzr-1* did not have wild-type *fzr-1* 3' UTR but had *cye-1* 3' UTR.

2.5.12 Construction of *fzr-1*, *cye-1* and *tbb-2* 3' UTR reporter

We followed (Merritt et al., 2008) to create an *fzr-1* 3' UTR reporter allele expressed in the germline, *SalSi71[Ppie1::GFP::h2b::3' UTR fzr-1 (1kb) + unc-119(+)]*. This allele is under *pie-1* promoter control to allow germline expression and contains a GFP fused to histone h2b for nuclear localization, the pattern of expression varies depending on what 3' UTR you fuse to the construction, in our case we used *fzr-1* 3' UTR.

To create the plasmid, we used 1kbp of *fzr-1* 3' UTR. We amplified it using oligonucleotides: "fzr-1 utr-1 pacI" and "fzr-1 utr sbfI". The fragment was cloned into pJET and sequenced to ensure fidelity to the genomic sequence. Afterwards, the fragment was digested with *Pac*I and *Sbf*I and directly cloned into a pMos II vector carrying *pie-1* promoter fused to *gfp::h2b* ORF. The vector has convenient *Pac*I *Sbf*I sites after the stop codon of the ORF, allowing easy swap of different 3' UTRs. The resulting plasmid after the introduction of *fzr-1* 3' UTR was used for microinjection into EG8080 strain for insertion in chromosome III, following MosSCI universal protocol (Frøkjær-Jensen et al., 2008), (Frøkjær-Jensen et al., 2012).

The microinjection mix was composed of: 100ng/ µL of pMos *Ppie-1::GFP::h2b::fzr-1 3' UTR*, 50 ng/µL of pCFJ601 (coding for transposase) and a cocktail of plasmids coding for extrachromosomal markers (20 ng/µL of pGH8, 20 ng/µL of pMA122, 5 ng/µL of pCFJ90 and 10 ng/µL of pCFJ104). Insertion-carrying worms were selected by screening normal moving worms since insertion rescues the uncoordinated (unc) phenotype of the EG8080 strain. Insertion of the construction was then checked by PCR using the following oligonucleotides: "MosRIN" and "MosIIRout".

The same procedure was followed to create *cye-1* and *tbb-2 3' UTR reporters*. In these cases, the only change was the 3' UTR region amplified and

cloned into the pMos II vector with *Ppie-1::gfp-h2b* using *Pac*I *Sbf*I restriction sites. The following oligos were used. For *cye-1* 3' UTR: "Cye-1 utr PacI" and "Cye-1 utr SbfI". And for tbb-2 3' UTR: "Tbb-2 utr PacI" and "Tbb-2 utr SbfI".

2.5.13 mes-4 alleles

Some mes-4 alleles were very important for this work. They were built using similar methods to the ones described in this work and they were also previously described in (Rivera-Martin *PhD thesis*, 2018):

Mes-4(sal9[mes-4::mGFP::mes-4 utr]) was constructed by following (Dickinson et al., 2015).

Mes-4(sal3[mes-4::mCherry + FRT hpt FRT]) was constructed by CRISPR insertion using mes-4::mCherry plasmid with Hygromycin resistance as the selection marker.

Mes-4(sal11[mes-4(AAA)::mGFP]) was created using CRISPR with ssDNA template, methods described in this thesis for other alleles.

2.5.14 *C. elegans* strains used

Table 6. Strains used in this work.

Name	Genotype	Origin
EG8080	oxTi444 unc-1198(ed3) III	CGC
EG8082	unc-119(ed3) III; oxTi365 V	CGC
JPM45	mes-4(sal3[mes-4::mCherry + FRT hpt FRT]) V	CRISPR N2
JPM76	mes-4(sal9[mes-4::mGFP::mes-4 utr]) V	CRISPR N2
JPM78	mes-4(sal11[mes-4(K10A, E11A, N12A)::mGFP::mes-4 utr]) V	JPM76
JPM119	fzr-1(sal13[GFP^3xFlag::fzr-1]) II	CRISPR N2
JPM128	salIs40 [Ppie1::GFP::h2b::tbb'2 UTR + unc-119(+)] V	EG8082
JPM275	cye-1(sal42 [cye-1::GFP^3xFlag::cye-1-3UTR]) I	CRISPR N2
JPM277	cya-1(sal35 [cya-1::GFP^3xFlag::cya-1 3'UTR]) III	CRISPR N2
JPM278	cye-1(sal36 [cye-1(K44A,E45A,N46A)::GFP^3xFlag::cye-1-3UTR]) I	JPM275
JPM286	cya-1(sal38[cya-1(K78A,E79A,N80A)::GFP^3xFlag::cya-1 3'UTR]) III	JPM276

JPM289	cye-1(sal17[cye-1::mkate2^3xFlag::cye-1-3UTR]) I; cya-1(sal35 [cya-1::GFP^3xFlag::cya-1 3'UTR]) III	JPM127, JPM277
JPM291	cye-1(sal42 [cye-1::GFP^3xFlag::cye-1-3UTR]) I; mes-4(sal3[mes-4::mCherry + FRT hpt FRT]) V	JPM45, JPM275
JPM294	cya-1(sal40[cya-1(R2A,L5A)(K78A,E79A,N80A)::GFP^3xFlag::cya-1 3'UTR]) III	JPM286

JPM305	cye-1(sal42 [cye-1::GFP^3xFlag::cye-1-3UTR]) I;
	cya-1(sal39[cya-1(R2A,L5A)(K78A,E79A,N80A]) III;
	mes-4(sal3[mes-4::mCherry + FRT hpt FRT]) V
		JPM291
		JPM293

JPM318	prom-1(ok1140) I; mes-4(sal3[mes-4::mCherry + FRT hpt FRT]) V	RB1183, JPM45
JPM329	cye-1(sal56[cye-1(R469A,L471A,L472A):GFP^3xFlag::CYE-1-3UTR]) I	JPM275
JPM330	fzr-1(sal55[GFP::fzr-1(R23A,R24A,L26A)]) II	JPM119
JPM337	SalSi68 [Ppie1::GFP::h2b::3' UTR cya-1 + unc-119(+)] III	EG8080
JPM341	cye-1(sal57[cye-1(K44A,E45A,N46A)(R469A,L471A,L472A)::GFP^3xFlag::cye-1-3UTR]) I	JPM329
JPM342	cye-1(sal57[cye-1(K44A,E45A,N46A)(R469A,L471A,L472A)]) I; mes-4GFP V	JPM76, JPM336
JPM344	SalSi70 [Ppie1::GFP::h2b::3' UTR cye-1 + unc-119(+)] (III)	EG8080
JPM349	SalSi71 [Ppie1::GFP::h2b::3' UTR fzr-1 (1kb) + unc-119(+)] III	EG8080
JPM380	fzr-1 utr reporter(sal64[Ppie1::GFP::h2b::3' UTR fzr-1 with predicted FBE mutation + unc-119(+)]) III	JPM349

JPM393	fzr-1(sal13[GFP^3xFlag::fzr-1]) II;
	salSi43 [Pfzr1::fzr1::fzr1UTR + unc-119(+)] V;
	mes-4(sal3[mes-4::mCherry + FRT hpt FRT]) V
		JPM291, JPM353

JPM399	fzr-1(sal19) (II); SalSi73 (Pfzr1::fzr-1::cye-1 3' utr + unc-119(+)) III; mes-4(sal9[mes-4::mGFP::mes-4 utr]) V	JPM157, JPM394
JPM404	fzr-1(q1290[fzr-1::5xV5)]) II; mes-4(sal9[mes-4::mGFP::mes-4 utr]) V	fzr-1(q1290[fzr-1::5xV5)]) Judith Kimble, JPM76
JPM410	prom-1(ok1140) I; fzr-1 (sal19) II; SalSi73 (Pfzr1::fzr-1::cye-1 3' utr + unc-119(+)) III; mes-4(sal9[mes-4::GFP^3xFlag::mes-4UTR]) V	JPM318, JPM399

2.5.15 Oligonucleotides used

Table 7. Sequences for CRISPR guide RNAs and single strain DNAs used as template.

Name	Sequence (5'-3')
Cye-1::gfp crRNA	TTTCTAAAATAACCCGCAAT
Cye-1 dbox crRNA	GTCAAGAAGTTGTCGTTGTT
Cye-1 dbox template	TTTATGCAGGCTCAACTTGAAAAAGTTATTGAATATGTTGAACCGGTG TGCCGGGCGTTCGCTAAGCAAGCACAAGCTGCAGATGATGTTATTCCA AAACATGAATCAATAAAATCGGATGATTCACACAATATTCAAGTATAC GTTAAA
Cye-1 kenbox crRNA	GGAGACTGCAATTGATATGA
Cye-1 kenbox template	GAAAAATTTTAATTTTCAGATCTCCACATGACGAACTGCGTGAACGTC TTCTGGAGACTGCAATTGATATGGCTGCAGCAATATTCCACAACGAA ATACCCGAAATTCGAGCGTTGGAAGTCAGAAATCAGATTGTTCTGAG ACAAGAAAAC
Cya-1::gfp crRNA	GAGAATTCAAGAATATAACA
Cya-1 dbox crRNA	GCGGTCGGCACTTAGTTTGA
Cya-1 dbox template	TTTTTTACAGATTCCGACACAGCGCACGCGCCTAGGGACCAATTATCA AGCGCTTTTGAGAGCAGCAGATCGCGACGAGTATGGCATCTGCAGCCT CACTTAAGGTAAGTATTTTCTGAAATTGTAAAAAATATATTTACAATG CGACTGTCAAATTAGTTACATTTATTTATTCGCGATCT
Cya-1 kenbox crRNA	ATGAAAAATAGCCGGAGAGT
	AAGAAAATAGATGAATCACCAATTATCAAAATAGATGCAAAAGACAGT

Cya-1 kenbox template	TTTAAAGTATTTGAGGATCAGGAGCCAGAGGCTGCAGCCTCTTCTGAAAATGTTGATGCAACGGAGAAAGATTCTAACGTAATACCTGCTGAGGATAACAAT
Gfp::fzr-1 crRNA	TCATCCATTTTATGTGCAAA
Fzr-1 dbox crRNA	GATGCCGGTGAGACGAACCC
Fzr-1 dbox template	ATGGATGAGCAGCAACCGCCAGCCAACTCTCCGGCTATTTTTCATTCGCCACAAGCGATGCCTGTAGCTGCTACTGCAGGACCACACAACTCACCCGTTAAATCAATGTCCACAAACTCATCGGTAAGAAATTTTTTACATTTTGGAAAAAAT
Fzr-1 V5 crRNA	ATGAAAAATAGCCGGAGAGT
Fzr-1 V5 template	TAAAATGGATGAGCAGCAACCGCCAGCCAACGGATCTGGTAAGCCTATCCCTAACCCTCTCCTCGGTCTAGATAGTACTGGAAAGCCAATCCCAAACCCACTCCTCGGACTTGATAGCACCGGTAAGCCTATCCCTAACCCACTCCTCGGACTTGATAGCACCGGATCTTCTCCGGCTATTTTTCATTCGCCACAAGCGA

Table 8. Oligonucleotides used for PCR amplification

Name	Sequence (5'-3')
5 fw cye-1	ACGTTGTAAAACGACGGCCAGTCGCCGGCACACTTCAAAATCGATAGTTCTCAAACG
5 rev cye-1	CATCGATGCTCCTGAGGCTCCCGATGCTCCGAAAAGTCGTTGCGGATGAAGACGGCG
3 fw cye-1	CGTGATTACAAGGATGACGATGACAAGAGATAATAGGATTCTTTTATCATCGAAATTTC

3 rev cye-1	GGAAACAGCTATGACCATGTTATCGATTTCAAACATTAATTAGAAATTCACGCAAAC
5 ext cye-1	ATACGAGGTAACAATCAGGGGTTTCAC
3 ext cye-1	TTTAGCCAAGAAACTAAATAATGATTC
GFP Crispr Rev	TCCGTAGGTGGCGTCTCCCTCTCCCTCTCC
GFP Utr dir	GGAATCACCCACGGAATGGACGAGCTC
Hyg direct	CCCAAAATCTACACAATGTTCTGTGTACAC
Cye-1 check 1	GTTTATATTTTAAATTCACACCTAATTCA
Cye-1 check 2	ACCCAGACTACTCAATATTGAGCGTTTGAC
CYA1GFP-1	AAAGTCTCCGTCGCCTCTTCAACCTTCACC
CYA1GFP-2	ACGTTGTAAAACGACGGCCAGTCGCCGGCACAAGCGTCCGTGCAACCTTCTCATCATTCC
CYA1GFP-3	CATCGATGCTCCTGAGGCTCCCGATGCTCCCTGGGGACTACTACTATCGTTGGAAGATTT
CYA1GFP-4	CGTGATTACAAGGATGACGATGACAAGAGATATTCTTGAATTCTCCAAATTTCCCGACTT
CYA1GFP-5	GGAAACAGCTATGACCATGTTATCGATTTCGTTTTCTGATTCAAAAACTTAAATATAACA
CYA1GFP-6	AAGTTCATTTTTCATAGTTTTCCGATAACA

CYA1 kenbox check1	ATGCGGTCGGCACTTAGTTTGAAGGTA
CYA1 kenbox Check2	TCACGACATCGCTGAACCAATCGATGA
CYA1 DBOX Check 1	TCTTCACCGTCTGTCCTGCCTTGAATG
CYA1 DBOX Check 2	CTTGCTTGGTAGAGCTTGTTGAAGCAA
5 fzr1 nt fw	ACGTTGTAAAACGACGGCCAGTCGCCGGCATTAAGACGGCCGTCATTAGTTG AAAAG
5 fzr1 nt rev	TCCAGTGAACAATTCTTCTCCTTTACTCATTGTGCAAAAGGGTAAAGTTGAGG AGAA
3 fzr1 nt fw	CGTGATTACAAGGATGACGATGACAAGAGAATGGATGAGCAGCAACCGCCAG CCAAC
3 fzr1 nt rev	GGAAACAGCTATGACCATGTTATCGATTTCCTCGTAACATCAATAATTCCTTCG TTG
5 ext FZR1 Nt	TTATCATGAATCTCTTGGTTTGAAGAG
3 ext FZR1 Nt	AACTTTTAACGGAAAATATTGGAACAG
Fzr-1 dbox check 1	TCATAAGATGAGTTAGTTGACCTGACA
Fzr-1 dbox check 2	CACTACTTCTGGTGTCATCCATACAAG
Slc316	GCTTTTGCGTGTTCTCCTCA
Slc317	TGAATCCTGAGTCATCATCCGAGT
fzr1 ORF AfeI F	TGTGAAAGCGCTCGCGTGGTCGCCACA

fzr1 ORF PacI SbfI R	TATCCTGCAGGGCTTAATTAACTACCGGATGGTAGAATGCAAATTCAA
Fzr-1 utr PacI	ATTTAATTAATTTCATTTTCACATGTTTTTTGTTTTTTTTTTTCTG
Fzr-1 utr SbfI	ATCCTGCAGGTACGACACATTTGACTATTCCACTTAA
Cye-1 utr PacI	GCTTAATTAATAACCCGCAATAGGATTCTTTTATC
Cye-1 utr SbfI	TATCCTGCAGGACTCGTTAAAAATTGTATTTCGTATAA
Cya-1 utr PacI	GCTTAATTAATCCATGTTATATTCTTGAATTCTC
Cya-1 utr SbfI	CTTTGTCAAATAAATCTTTTAAATAAACCTGCAGGATA
Tbb-2 utr PacI	GCTTAATTAATGCAAGATCCTTTCAAGCATTCCCTT
Tbb-2 utr SbfI	TATCCTGCAGGATAGCATTCACTTCACTCAGATGCAA
MOSR in	CATGGTCATAGCTGTTTCCTGCCCGTG
MOSIIR out	GGGAGGCGAACCTAACTGTAAAAGTCC

Table 9. Oligonucleotides used for cloning inserts for RNAi producing plasmids

Gene sequence inserted	**Primer 1 sequence**	**Primer 2 sequence**	**Origin of the plasmid**
None (control)	-	-	Control pL4440
cya-1	ATACCATGGCCGAGCAACGGAAACGCGGCGAAAAGT	TATGCGGCCGCCTGCGATCATCATCGACGTCGTTCCAA	Lab cloned pL4440
cyb-1	AGTCGAAACTGCGCAAAAGT	AAGGAGCCGAAAAGAAAAGC	Ahringer library pl4440
cye-1	ATACTGCAGAAGGTCCAGCTGCAAAACGTCATTCG	TATCCATGGCTCGTATTTAGCAGCTATAAATAGAGC	Lab cloned pL4440
cyd-1	TCTTCATTCTCAAAAATCCCAAA	TGGACTAGGTGGAATGAAAGAAA	Ahringer library pl4440
cyb-3	TGGGAAAGTCGAGAACGAGT	GGTGAACAGTTGAGAGGGGA	Ahringer library pl4440
fbf (fbf-1 and fbf-2)	ATACCATGGCCCACATCTACAGAGGTTGGAAATCA	TATGCGGCCGCATCACGAGGTAGAGCTTGAACAAGTT	Lab cloned pL4440
cdk-1	ATGCGGCCGCATGGATCCTATTCGCGAAGGAGAAGTG	GCAGATCTTCAAGAAGAGAGAATGCAGTATCGTC	Lab cloned pL4440

cdk-2	ATACTGCAGAAAGAGACCTGCAAGGTCGCTTTTGCT	TATCCATGGCTTGCCAATCCGAAATCCGCAATTTTG	Lab cloned pL4440
prom-1	ATACCATGGATGGATAAATCAACACCCAGGCGGACT	TATGCGGCCGCCAGCTCTCGATCCGTTTCGGGGGTGA	Lab cloned pL4440
gld-1	ATGCGGCCGCATGCCGTCGTGCACCACTCCAACTTAC	GCAGATCTGAACACGATTCTCAGTGTCTTCGCAT	Lab cloned pL4440
gld-2	ATACTGCAGATCGATTCTCGAACAAAGTTGATGTTC	TATCCATGGAGATCGTGGTCCAGTAGATCCGTTTCC	Lab cloned pL4440
cki-2	GGCAACAACAAAGAGTTTGAATC	AATTGAACCCATATGTTTGAACG	Ahringer library pl4440
apc-6	TTGCTTCATTCAGCCTTCCT	GCTCAGAATGGTTCCAGCTC	Ahringer library pl4440
fzr-1	GCAAGCTTATGGATGAGCAGCAACCGCCAGCCAAC	ATCTGCAGTCGTAACATCAATAATTCCTTCGTTGG	Lab cloned pL4440
fzy-1	TGTCACAATTGGGTTGCAGT	TCGACGTTGAACAATTGGAA	Ahringer library pl4440

RESULTS

3. RESULTS

CHAPTER 1: APC/C^{FZR-1} down-regulation in the mitotic zone of the germline

3.1.1 FZR-1 and his target MES-4 are both present in mitotic germline

We wondered where FZR-1 was expressed in the *C. elegans* germline. For that, we took advantage of a fully-functional allele of FZR-1 tagged at its N-terminal region with the V5 epitope (a gift from Prof. J. Kimble). We have analyzed worms carrying the tagged FZR-1 allele and an MES-4::GFP allele. We have found that FZR-1 was expressed along the distal part of the germline, roughly overlapping with the MES-4 expression pattern (**Fig. 3.1A and B**). Quantification of the fluorescence signal indicated that FZR-1 levels were lower at the most distal part, increasing as cells reached the transition zone, where it gets to its peak and dropping in a parallel manner as the MES-4 signal.

The overlap in the signal coming from MES-4 and FZR-1 strongly suggested that some regulation has to be exerted over APC/C^{FZR-1} to preclude premature MES-4 degradation in the mitotic region of the germline. This negative regulation has to be alleviated as cells reach the transition zone enabling timely MES-4 degradation.

Along this work, we will use the MES-4 levels as the reporter of the APC/C^{FZR-1} activity. Previous research in our laboratory indicated that MES-4 levels were exclusively controlled by the APC/C^{FZR-1} activity, with no other elements affecting its distribution pattern along the germline (Fragoso-Luna *PhD thesis*, 2020; Rivera-Martín *PhD thesis*, 2018). In addition, when fused to different fluorescent proteins, its signal was very intense at microscopy. Its expression pattern was very reproducible: the levels of MES-4 dramatically decreased near the transition zone from mitosis to meiosis. Any decrease in the APC/C^{FZR-1} activity resulted in the extension of the presence of MES-4 protein in the pachytene region (see **Figure 1.7**).

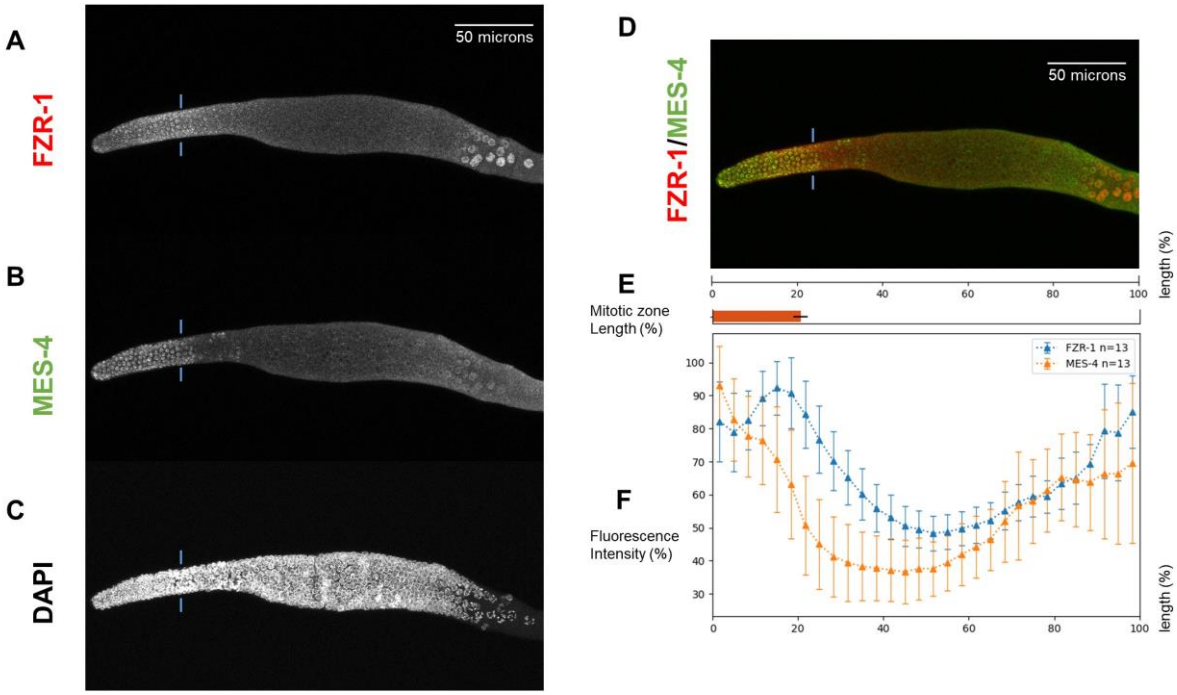

Figure 3.1: Expression of MES-4 and FZR-1 co-localize in the mitotic region of the germline.

To study FZR-1::V5 and MES-4::GFP expression, anti-V5 and anti-GFP immunostaining was carried out using strain JPM404 (A, B). Germlines were also stained with DAPI (C). The superposition of FZR-1 and MES-4 can be observed in the mitotic region (D). Fluorescence intensity levels were measured and relativized (%), germline length was also relativized (F). The end of the mitotic zone and the start of the transition zone were measured by detecting crescent-shaped cells in DAPI and it was marked in the image with blue lines, mitotic germline length was averaged and plotted (E).

3.1.2 CYE-1 maintains APC/C^{FZR-1} activity low in mitotic germline

The APC/C^{Cdh1} complex assembly is negatively regulated by the CDK-mediated phosphorylation of the Cdh1/Fzr1 coactivator. This control has been extensively shown in other models such as yeast, *Drosophila,* and mammal cells (Keck et al., 2007; Kramer et al., 2000; Reber et al., 2006b; L. Wan et al., 2017; Zachariae et al., 1998). In *C. elegans*, it has been shown that FZR-1 can be phosphorylated by CDK complexes, at least using *in vitro* assays. We wondered whether the high CDK activity in the mitotic zone could be responsible for the proposed down-regulation in the APC/C^{FZR-1} activity in the distal part of the gonad. The main CDK activity in the mitotic zone of the gonad is caused by the complexing of CDK-2 to S-phase cyclins (mostly CYE-1) and CDK-1 complexed with M-phase cyclins (mostly CYB-3 and secondly CYB-1). Therefore, we silenced *cdk-1* and *cdk-2*, individually. In both cases, we did not observe a dramatic effect in the distribution pattern of MES-4 on the gonad. We observed a slightly faint fluorescence signal of MES-4 and a decrease in the number of MES-4 positive cells (probably, a consequence of the impaired cell cycle). Because CDK-1 and CDK-2 can be redundant, we tried double silencing, although with a similar outcome (**Figure 3.2**). Whether the absence of a more dramatic effect on MES-4 distribution was a consequence of diminished silencing (the cell cycle was still active in the gonad) or redundancy with other catalytic subunits (like CDK-4) was not addressed. We decided to repeat the approach but using the silencing of cyclins, which we considered more specific.

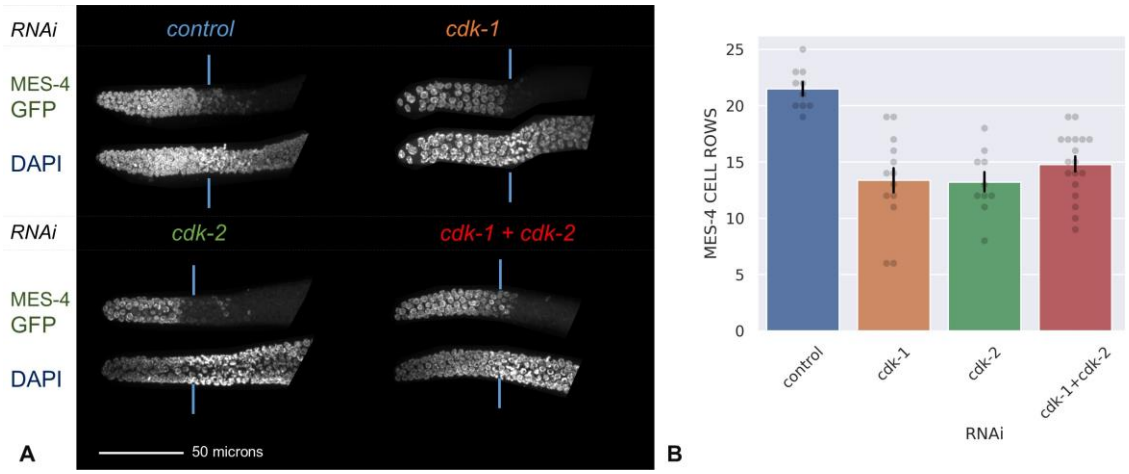

Figure 3.2: Silencing of *cdk-1, cdk-2 or* both does not replicate *cye-1* silencing.
(A) Confocal images (strain JPM76) of germlines of worms with different RNAi treatments. MES-4::GFP fluorescence and DAPI staining are displayed in the images. The RNAis that silence *cdk-1*, *cdk-2*, or *cdk-1* + *cdk-2* cannot replicate *cye-1* RNAi causing MES-4::GFP premature degradation in the mitotic zone of the germline.
(B) Bar and swarm plot of the number of cell rows (counted from the distal tip of germline) that are MES-4::GFP positive in different RNAi conditions.

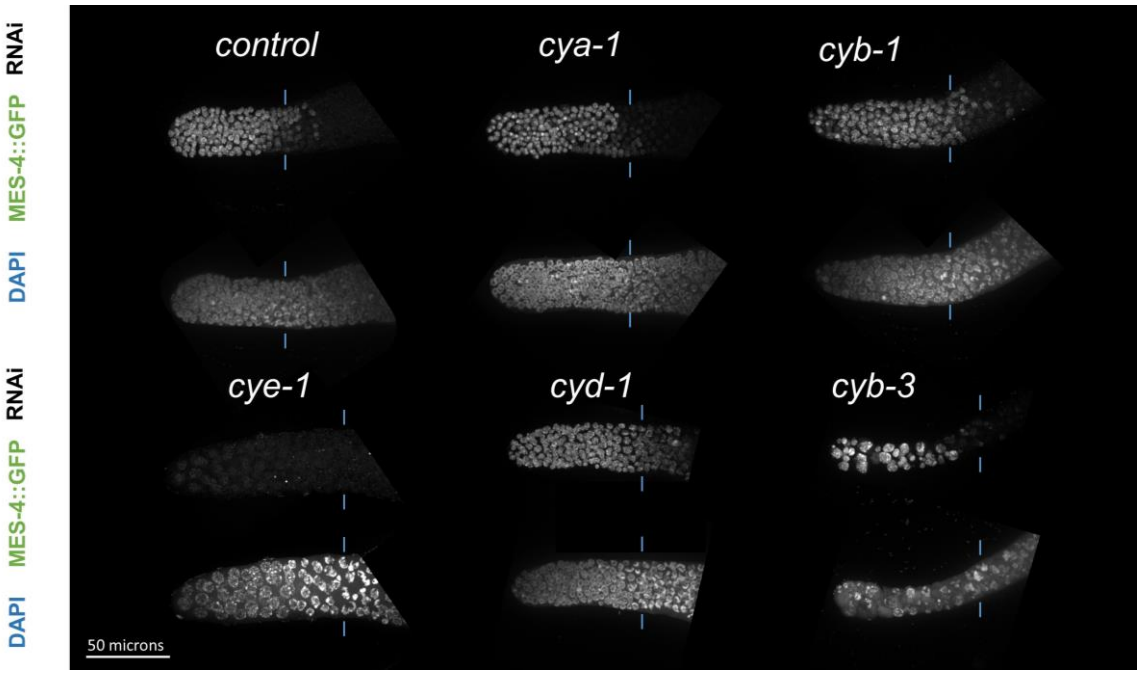

Figure 3.3: Silencing of cyclins over *mes-4::gfp* strain.
MES-4 was only prematurely degraded when *cye-1* was silenced, suggesting that CYE-1 could inhibit APC/C^{FZR-1} activity. The transition zone of each germline is marked with blue lines.

We have silenced the G1 cyclin, CYD-1, the S-phase cyclins CYE-1, and CYA-1, and the M-phase cyclins CYB-1 and CYB-3. From these, we observed a significant premature degradation of MES-4 when *cye-1* was silenced (**Figure 3.3**), suggesting that CYE-1, most likely complexed with CDK-2, was involved in the downregulation of FZR-1. To discard that the drop in MES-4 levels was some indirect effect on the gonad cells because of the silencing of *cye-1*, such as the decrease in the transcriptional expression of *mes-4*, we carried out *cye-1* silencing in strain JPM78, which carries a non-FZR-1 recognized version of MES-4 (KEN-box mutated [K10A, E11A, N12A]) tagged with GFP. In this case, MES-4 was not prematurely degraded. (**Figure 3.4B and D**) strongly suggesting that the observed effect, when *cye-1* is silenced, was a consequence of overactivated APC/C^{FZR-1} activity.

We have observed that the decrease in MES-4 levels upon *cye-1* RNAi was less evident at the most distal part of the gonad. One possible explanation was that the *cye-1* RNAi silencing at the most distal part was not as efficient as in the rest of the gonad. To address this possibility, we took advantage of a strain carrying an endogenous *cye-1::gfp* allele (strain JPM275) created by CRISPR knock-in. We observed that the protein was detected in control RNAi conditions but not when *cye-1* RNAi was used. This illustrates that *cye-1* silencing worked effectively along the entire gonad (**Figure 3.5**). Altogether, these results suggested that it could be possible that additional controls, apart from CYE-1, were exerted over FZR-1 to reduce his activity in the most distal part of the mitotic gonad.

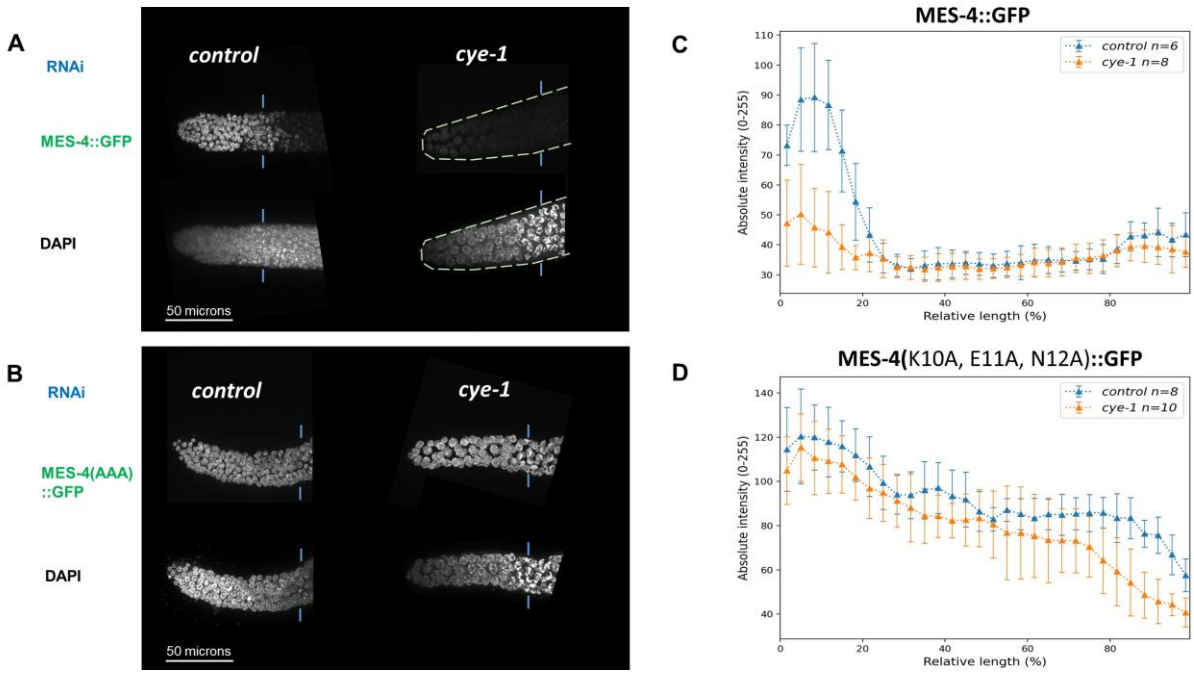

Figure 3.4: Silencing of *cye-1* shows decreased MES-4 levels in the mitotic zone because of APC/C^{FZR-1} premature activation.

MES-4 was prematurely degraded when *cye-1* was silenced (A, C). In the same conditions but using an MES-4::GFP allele with FZR-1 recognition motif KEN-box mutated, MES-4 was not prematurely degraded (B, D). MES-4::GFP with KEN-box mutated (K10A, E11A, N12A) is marked as MES-4(AAA)::GFP. Plots show absolute fluorescence intensity comparison of *control/cye-1* silencing for MES-4::GFP protein intensity (C) or MES-4(AAA)::GFP protein (D).

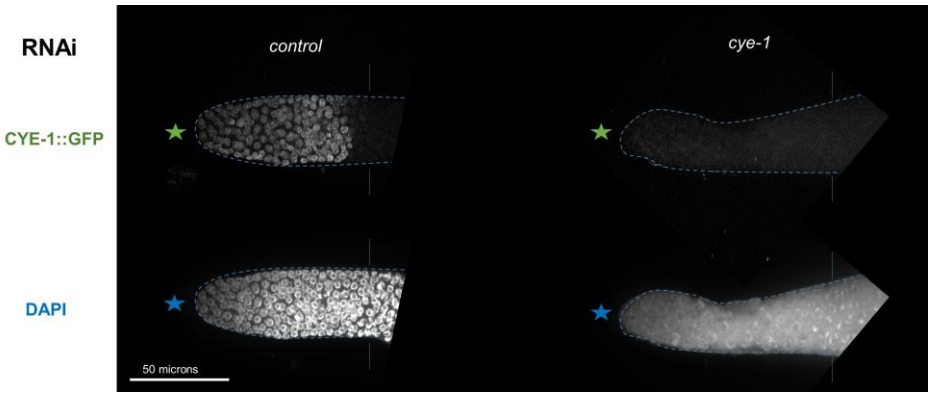

Figure 3.5: Silencing of *cye-1* shows non-detectable CYE-1::GFP levels.

Cye-1::gfp strain shows that CYE-1 is expressed through the distal region of the germline. When *cye-1* silencing was carried over the strain, the CYE-1::GFP signal disappeared, showing that *cye-1* RNAi was efficient. The distal tip of the germline is marked with green (GFP) or blue (DAPI) stars, the transition zone is marked with blue vertical lines.

3.1.3 FBF proteins control FZR-1 expression and activity in mitotic germline

A detailed observation of the FZR-1 fluorescence in the mitotic region of the gonad reveals lower levels in the most distal part of the region, reaching the peak of fluorescence just before the transition zone, in which it seems that APC/C^{FZR-1} upregulation causes the MES-4 degradation. We believe these levels faithfully reflect the actual protein levels because this pattern was observed in two different tagged alleles from FZR-1: *gfp::fzr-1* (strain JPM78) by direct GFP observation, and *V5::fzr-1* (strain JPM404), observed with immunostaining anti-V5. **Figure 3.6.**

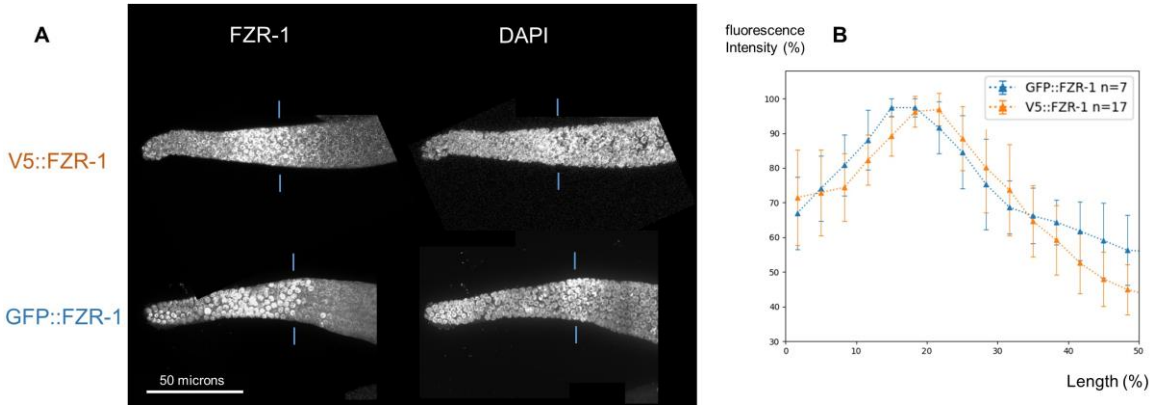

Figure 3.6: FZR-1 protein levels are lower in the most distal part of the mitotic region, reaching a peak of expression just before the transition zone.

(A) FZR-1 protein levels were observed using two different tagged strains and techniques. The upper side shows V5::FZR-1 (strain JPM404) observed by using immunostaining with anti-V5 antibodies. The lower side shows GFP::FZR-1 (strain JPM119) analyzed with direct observation of GFP. The transition zone start is marked with blue lines.

(B) Plot of relativized fluorescence intensity (%) for V5 strain (orange, averaged n=17) and GFP strain (blue, averaged for n=7). The first 50% of the total gonad length is shown.

On the basis of these observations, we believe that a post-transcriptional control over *fzr-1* could exist, reducing FZR-1 protein expression and, therefore, its activity at the most distal part of the gonad. In this region, the primary regulation was exerted by the FBF proteins (FBF-1 and FBF-2), which are RNA-binding proteins under the control of the NOTCH pathway. For that reason, we entertained the hypothesis that the FBF activity could control FZR-1 levels. We addressed this possibility with an *fbf* RNAi plasmid that can silence *fbf-1* and *fbf-2* due to their very similar sequence.

When *fbf* was silenced, we observed no differences in the MES-4 pattern of expression comparing to control RNAi. However, if we co-silenced both fbf and cye-1 we observed that MES-4::GFP presence in the mitotic zone was abolished **(Figure 3.7A, 3.7C).**

To confirm that the results in *cye-1 + fbf* silencing were due to increased FZR-1 activity and no other indirect causes, we performed the same experiments over a strain that carried *mes-4::gfp* with KEN-box mutated (strain JPM78). This showed that when MES-4 is not degraded through FZR-1, removing CYE-1 and FBF control does not cause premature MES-4 degradation **(Figure 3.7B, 3.7D).**

As shown in the previous results, *fbf*+*cye-1* silencing increases the premature upregulation of APC/C^{FZR-1} compared to *cye-1* silencing. Because of this, we hypothesized that *fbf* RNAi could also sensitize the upregulation of APC/C^{FZR-1} when *CDKs* were silenced. To address this possibility, we silenced *fbf*+*cdk-1*, *fbf*+*cdk-2* and *fbf*+*cdk-1*+*cdk-2* in JPM76 (*mes-4::gfp*) strain (**Figure 3.8**). We observed a significant upregulation of APC/C^{FZR-1} with *fbf*+*cdk-1*+*cdk-2* but it did not fully replicate *fbf*+*cye-1* silencing. Only minor premature upregulation of APC/C^{FZR-1} was obtained with *fbf*+*cdk-1* and *fbf*+*cdk-2*. Although CDK silencing by itself does not cause APC/C^{FZR-1} premature upregulation (**Figure 3.2**), it does in a sensitized background with *fbf* silenced. These results suggest that FZR-1 inactivation acted by CYE-1 could be mediated through CDK-1, CDK-2, and possibly, in a minor way, other CDKs.

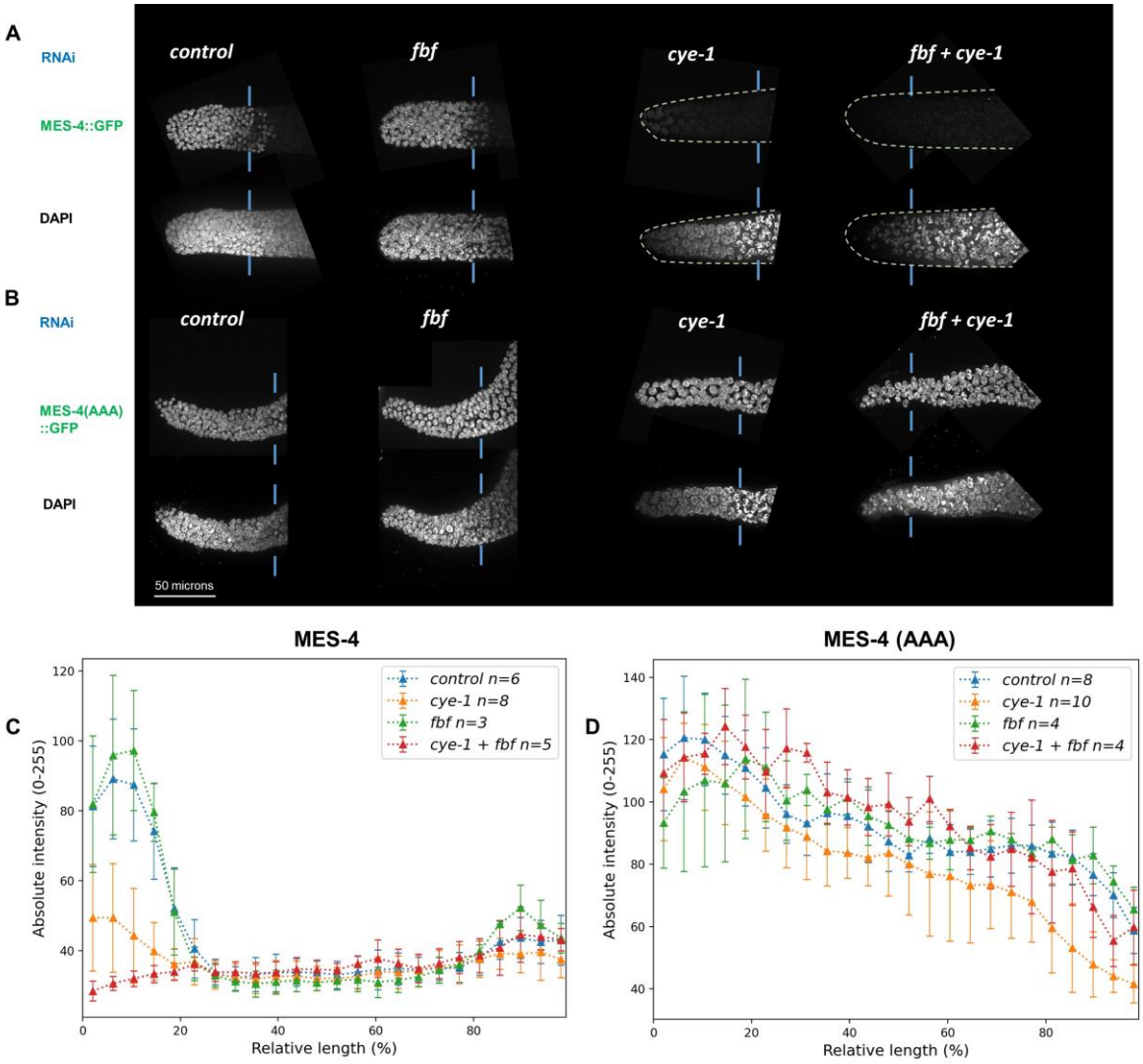

Figure 3.7: MES-4 is prematurely degraded when both *cye-1* and *fbf* are silenced.

(A) MES-4::GFP images are displayed on the top side and DAPI on the bottom side. When *cye-1* is silenced MES-4 is prematurely degraded, and when both *cye-1* and *fbf* are silenced MES-4 disappears completely at the mitotic zone. Absolute intensity is plotted and compared in **(C).**

(B) MES-4(AAA)::GFP and DAPI images are displayed. This strain (JPM78) cannot have MES-4 recognized by FZR-1. Absolute intensity is plotted and compared in **(D).** When *cye-1, fbf,* or both are silenced, we do not see the drastic changes observed in A and C.

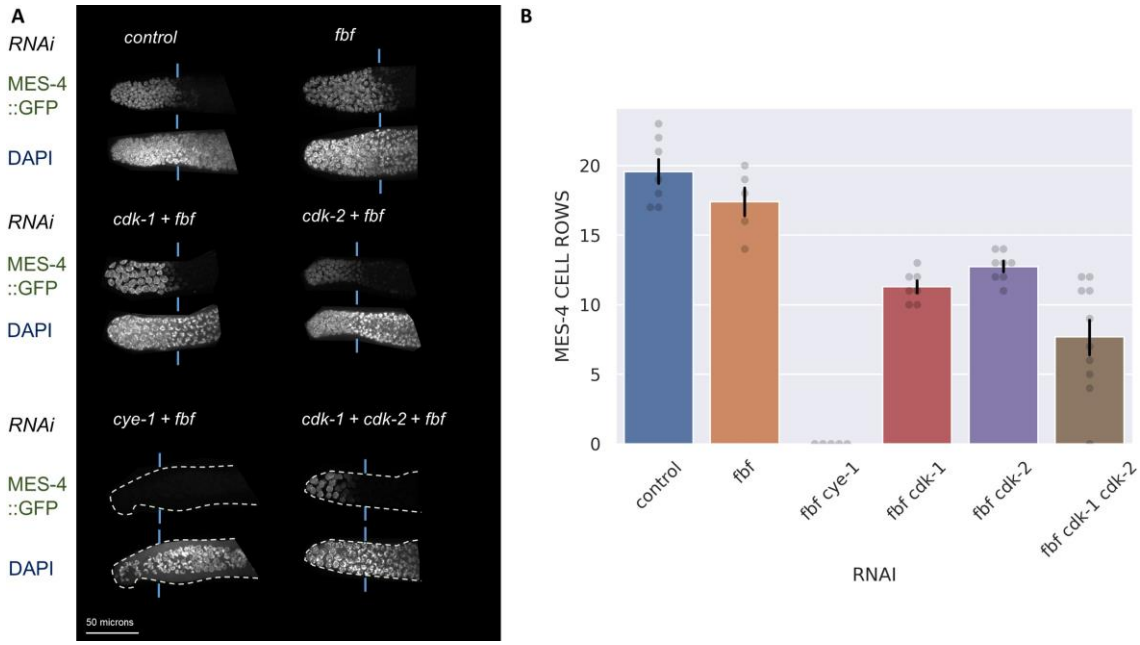

Figure 3.8: Silencing of *cdk-1/cdk-2/fbf* partially replicates *cye-1/fbf* silencing.
(A) MES-4::GFP confocal images with different RNAis applied. *Cye-1 + fbf* prematurely removes all MES-4::GFP. *Cdk-1 + cdk-2 + fbf* shows strong but variant premature degradation. *Cdk-1 + fbf* and *cdk-2 + fbf* only show partial premature degradation of MES-4::GFP.
(B) Bar and swarm plot of the number of cell rows (counted from the distal tip of germline) that are MES-4::GFP positive in different RNAi conditions.

Together, these results strongly suggested that FBF proteins could be acting as additional control over *fzr-1* activity. To support this conclusion we analyzed, using a strain carrying the *V5::fzr-1* allele, whether the levels of FZR-1 were affected by the down-regulation of FBF proteins. Encouragingly, we observed that FZR-1 expression was greatly increased in the mitotic region of the germline in response to the silencing of FBF proteins. (**Figure 3.9**)

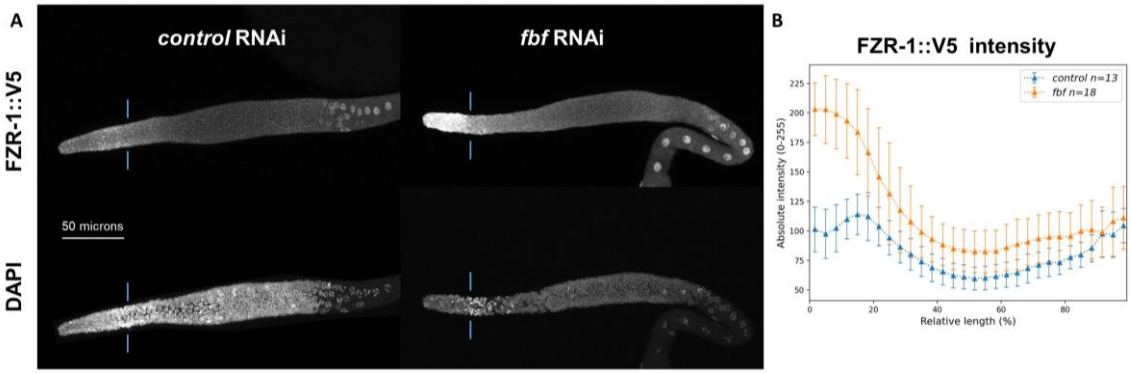

Figure 3.9: Silencing of *fbf* increases V5::FZR-1 protein levels.

(A) Control RNAi shows previously seen FZR-1 pattern of expression with the peak of expression around the transition zone. In opposition, *fbf* silencing greatly increases V5::FZR-1 expression levels throughout the mitotic region of the germline. The transition zone is marked with blue lines. Fluorescence signaling was obtained by immunostaining with anti-V5 in a strain carrying *V5::fzr-1(q1290)* allele.

(B) V5::FZR-1 absolute fluorescence intensity levels (Y axis) are averaged and plotted for control (blue, n=13) and *fbf* RNAi (orange, n=18) to relative germline length (X-axis).

3.1.4 FBF control over *fzr-1* is mediated through *fzr-1* 3' UTR sequence

FBF proteins interact with mRNA, typically in the 3' UTR region (Haupt et al., 2020). To study if this was the case for *fzr-1*, we created a 3' UTR reporter using *fzr-1* 3' UTR (Merritt et al., 2008). This reporter contains the *pie-1* promoter, a GFP fused to H2B, and the 3' UTR of *fzr-1* (1kb length). The reporter was inserted in strain JPM349 in a single copy by the Mos system. We analyzed the pattern of expression of this reporter in comparison to a control 3' UTR reporter, such as *tbb-2* (**Figure 3.10 B and C**), inserted in strain JPM128. We observed that 3' UTR of *fzr-1* causes low expression of the reporter in the mitotic zone, showing an expression peak near the transition zone. FBF proteins exert their effect in the mitotic region, gradually decreasing repression as cells enter meiosis. These results were in concordance with the possibility that post-transcriptional repression of *fzr-1* in the mitotic zone was caused by the binding of FBF to its 3' UTR. To confirm this, we silenced *fbf* in the strain carrying the *fzr-1* 3' UTR reporter, and we have observed that in this case, the downregulation observed at the most distal part was lost, supporting a direct correlation between FBF and *fzr-1* 3' UTR. (**Figure 3.10 C and F**)

FBF binding sites to mRNA (FBEs) are characterized by a consensus recognition sequence. We have found a single canonical FBF-recognition sequence in the 3' UTR region of *fzr-1*. We have constructed a *fzr-1* 3' UTR reporter strain carrying this putative FBF binding site removed by several substitutions. Disappointingly, this mutant reporter was indistinguishable from wild-type reporter (**Figure 3.10 D and G**). One possible explanation for this negative result was that additional non-canonical sites were responsible for the FBF activity on *fzr-1* UTR. This possibility is supported by *fzr-1* having multiple sequences in his 3' UTR that only differs from the canonical FBE "**TGT**xxx**AT**" by having one less or one more spacer nucleotides in the variable region: "**TGT**xx**AT**" or "**TGT**xxxx**AT**". These close-to-canonical sequences are also considered as usual FBF binding sites (Aman et al., 2016). Since a targeted mutation of all the proposed non-canonical FBF sites (7 in total) was not possible without heavily affect the sequence of the UTR region, we carried out an

alternative approach to address the importance of the 3'UTR in the control over FZR-1 levels on the most distal part of the gonad. We decided to swap the whole *fzr-1* 3' UTR for a 3' UTR sequence that was not repressed in the mitotic zone. The *cye-1* 3' UTR region showed no repression in the mitotic zone when incorporated into the *pie-1::GFP-H2B* reporter **(Figure 3.11 A)**, thus being a good candidate for swapping with the original *fzr-1* 3' UTR region. Therefore we constructed a strain carrying *fzr-1::cye-1 3' UTR* (described in **2.5.11**) as the only copy of *fzr-1* and *mes-4::gfp* as APC/C^{FZR-1} activity reporter (strain JPM399).

We hypothesized that in this strain, we will able to disable the FBF repression through *fzr-1* 3' UTR because we swapped the whole *fzr-1* 3' UTR region. Under this hypothesis, APC/C^{FZR-1} activity should be controlled only by the CDK activity on FZR-1. To test this, we carried *cye-1* RNAi in the *fzr-1* swapped UTR strain. In agreement with our hypothesis we observed that in this strain MES-4 was fully degraded in the mitotic region of the germline, (**Figure 3.11**).

Altogether, these results indicate that FZR-1 levels were controlled by FBF proteins, most likely through interaction with the *fzr-1* 3' UTR.

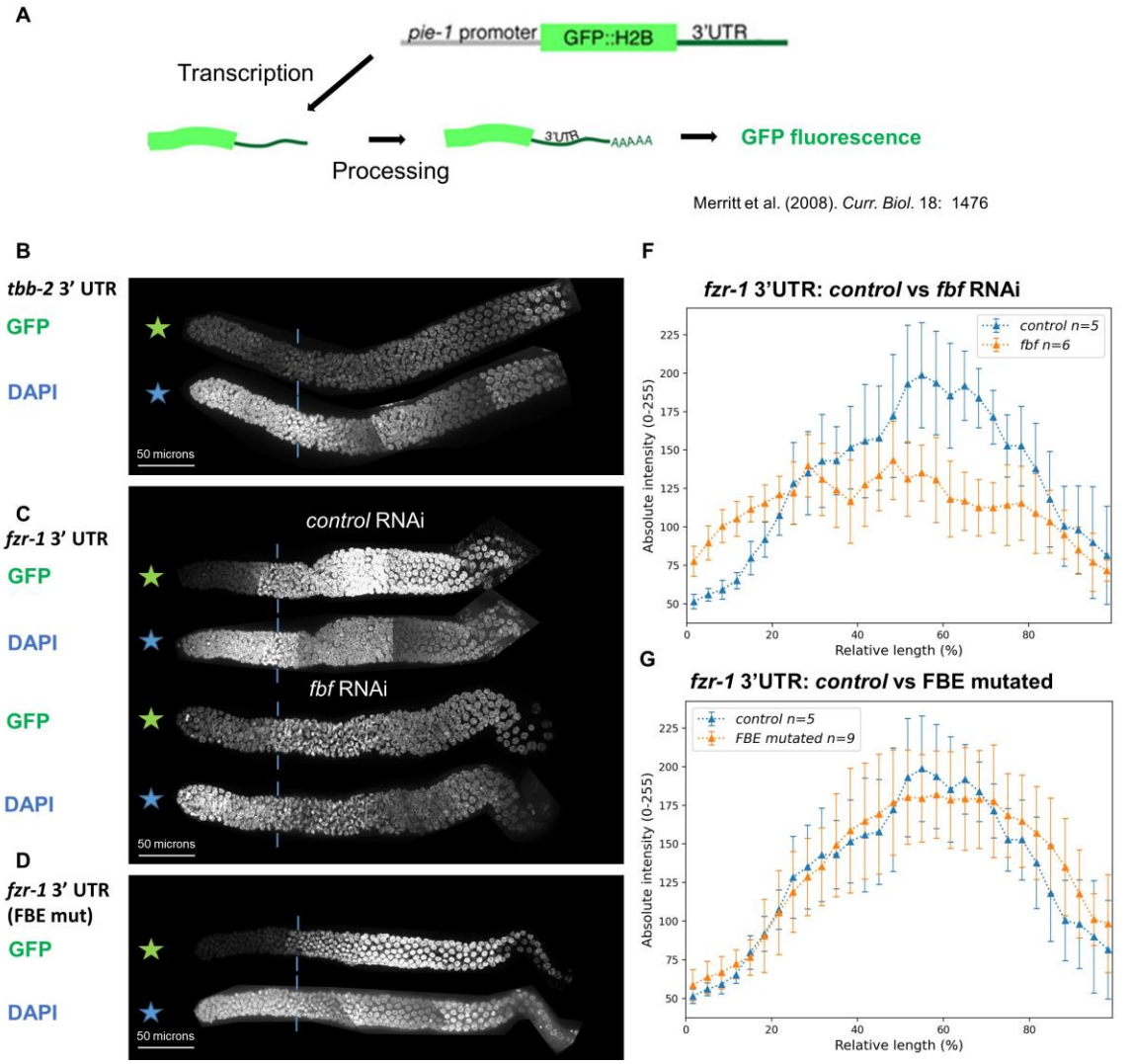

Figure 3.10: *fzr-1* 3' UTR reporter shows a low signal in the mitotic region with a peak in the meiosis region, this pattern is broken with *fbf* silencing.

(A) Construction of 3' UTR reporters following Merritt et al. 2008 guidelines

(B) *tbb-2* 3' UTR reporter shows uniform distribution along the germline. Strain JPM128.

(C) *fzr-1* 3' UTR reporter (strain JPM349) shows a low signal in the distal region and peak intensity more proximally. When *fbf* is silenced that pattern is broken. Control vs *fbf* silencing is plotted in (F).

(D) *fzr-1* 3' UTR reporter with canonical FBF binding site mutated (strain JPM378) shows no change in the distribution of the signal. The fluorescence of unchanged *fzr-1* 3'UTR vs mutated is plotted in (G).

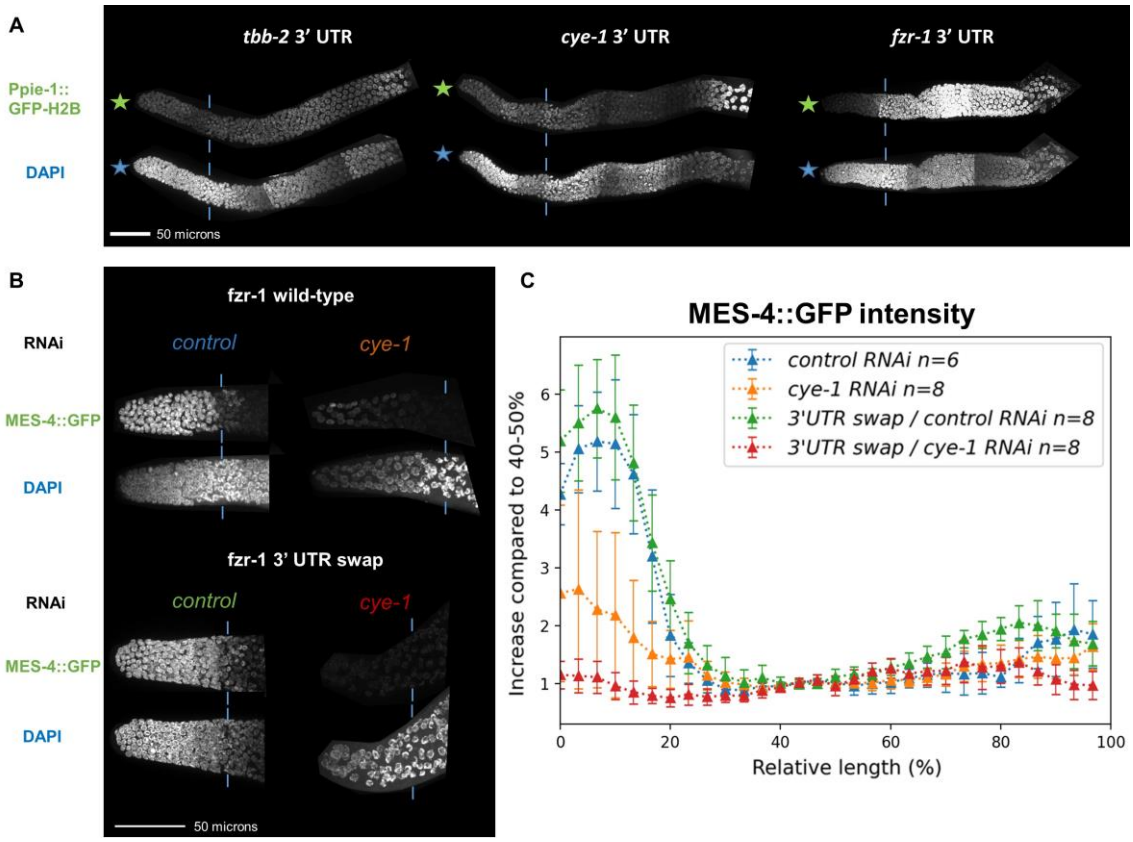

Figure 3.11: Strain carrying *fzr-1* allele with swapped 3' UTR sequence can fully degrade MES-4 when *cye-1* is silenced.

In an *fzr-1* wild-type strain (JPM76) when *cye-1* is silenced residual levels of MES-4 are maintained. In an *fzr-1* allele with 3' UTR sequence swapped (strain JPM399) *cye-1* silencing causes MES-4 protein to fully disappear (A), suggesting that FBF additional control is not exerted.

MES-4 levels are plotted in (B), blue for wild type *fzr-1* with control RNAi, orange for wild type fzr-1 treated with *cye-1* RNAi, green for *fzr-1* with swapped 3' UTR (JPM399 strain) treated with control RNAi and red for *fzr-1* with swapped 3'UTR (JPM399 strain) treated with *cye-1* RNAi. Y axis shows the relative ratio of MES-4::GFP fluorescence intensity compared to the pachytene region (the pachytene region was determined as the interval 40-50% of germline length) described as "FOLD-INCREASE", the X axis shows the relative length of germline (%).

CHAPTER 2: APC/C^{FZR-1} up-regulation in the transition to meiosis

3.2.5 CYE-1 degradation is promoted by SCF^{PROM-1} and APC/C^{FZR-1} but is not the sole cause of APC/C^{FZR-1} upregulation

The results shown above supported the idea that APC/C^{FZR-1} activity was negatively regulated at two levels along the mitotic region of the gonad. We were interested to address how this repression was alleviated to allow the timely activation of APC/C^{FZR-1} to degrade known targets such as MES-3 and MES-4. The easiest hypothesis was that the decrease in the CYE-1/CDK activity at the end of the mitotic zone, allowed the presence of non-phosphorylated active FZR-1. This hypothesis fits well with the observation that CYE-1 levels dropped before MES-4 degradation, suggesting a causal relationship between both processes (**Figure 3.12**)

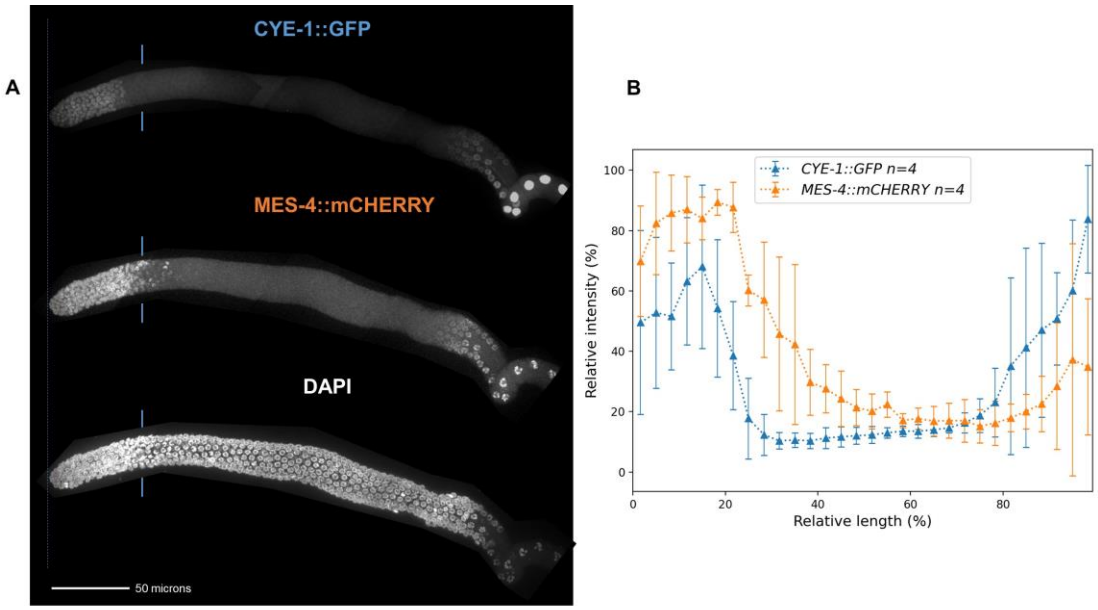

Figure 3.12: CYE-1 levels drop before MES-4 is degraded.

(A) Top-side we can observe CYE-1::GFP levels, mid-side MES-4::mCHERRY levels, and bottom-side DAPI staining in strain JPM291. The transition zone is marked with blue lines.

(B) Graphic representation of CYE-1::GFP and MES-4::mCHERRY relativized fluorescence intensity. CYE-1 levels drop before MES-4 levels drop.

To address this possibility, we decided to maintain high the levels of CYE-1 protein throughout the whole germline, and then analyze the levels of MES-4. For that, first, we needed to obtain a genetic background in which CYE-1 was stabilized throughout the germline. CYE-1 is described to be degraded by the E3 ubiquitin ligase complex SCF^{PROM-1} (Mohammad et al., 2018). However, in concordance with published observations (Mohammad et al., 2018), we have observed that when *prom-1* was silenced in a *cye-1::gfp* strain (JPM275), CYE-1 was still downregulated once cells reach the pachytene region (**Figure 3.13B**), suggesting additional controls. Following the previous published report suggesting that GLD-1 was also involved in this down-regulation (Mohammad et al., 2018), we carried out double silencing of *prom-1* + *gld-1*. Downregulation of GLD-1 activity resulted in a tumorous germline, in which germ cells progress to the pachytene stage of meiosis and then re-enter the mitotic cell cycle. Strikingly, the presence of CYE-1 on the tumorous gonad was interrupted by clear band in which CYE-1 disappeared, overlapping the region corresponding to the transition zone (**Figure 3.13C**). Since the transition zone correspond to the region of highest activity of APC/C^{FZR-1} in wild-type gonads, we entertained the hypothesis that this band was caused by the degradation of CYE-1 by the APC/C^{FZR-1} complex. We based this idea on the observation that CYE-1 has a KEN-box and multiple D-box motifs, suggesting the possibility that is recognized and degraded by APC/C^{FZR-1}. To test if CYE-1 was degraded by APC/C^{FZR-1} we analyzed the levels of CYE-1 in worms submitted to *fzr-1* RNAi, *prom-1* RNAi, and a combination of *fzr-1* + *prom-1* RNAi (**Figure 3.13A**). The results indicated that that CYE-1 levels dropped in pachytene when either *prom-1* **or** *fzr-1* were individually silenced. However, when both *prom-1* **and** *fzr-1* were silenced, CYE-1 was stabilized throughout the germline. This result strongly suggested that CYE-1 was targeted by SCF^{PROM-1} and APC/C^{FZR-1}.

To add further support to the idea that CYE-1 was targeted by APC/C^{FZR-1} we sequentially mutated the KEN-box, and the highest score (under GPS-ARM algorithm) D-box to alanine residues in a strain carrying the *cye-1::gfp* allele (strains JPM278, JPM329, JPM341). In these strains we carried out *control* and *prom-1* silencing. We observed that CYE-1 downregulation was only impaired when KEN-box and highest score D-box were mutated and *prom-1* was silenced

(*prom-1* silenced, *fzr-1* recognition mutated). In consonance, CYE-1 was degraded in *prom-1* RNAi used over a *cye-1::gfp* allele with no mutations (*prom-1* silenced, *fzr-1* recognition wild type) and in *control* RNAi used over a *cye-1::gfp* allele with KEN-box and D-box mutations (*prom-1* not silenced, *fzr-1* recognition mutated). This shows that both APC/C^{FZR-1} and SCF^{PROM-1} can degrade CYE-1 without the other (**Figure 3.13B**). Finally, to address whether the observed down-regulated CYE-1 band in *prom-1* + *gld-1* silencing was due to APC/C^{FZR-1} we carried out *prom-1* + *gld-1* double silencing in *cye-1(KEN-box)(D-box)::gfp* allele showing that in that case, the band disappears (**Figure 3.13C**).

All the results showed that both APC/C^{FZR-1} and SCF^{PROM-1} activity need to be impaired to allow CYE-1 stabilization throughout the germline because both complexes are independently sufficient to cause CYE-1 degradation. In addition, it supports the idea that CYE-1/CDK-2 and APC/C^{FZR-1} are acting as a toggle-switch, showing a mutual repression, with CYE-1/CDK-2 being able to repress APC/C^{FZR-1} activity through phosphorylation and APC/C^{FZR-1} being able to recognize and mark for degradation CYE-1.

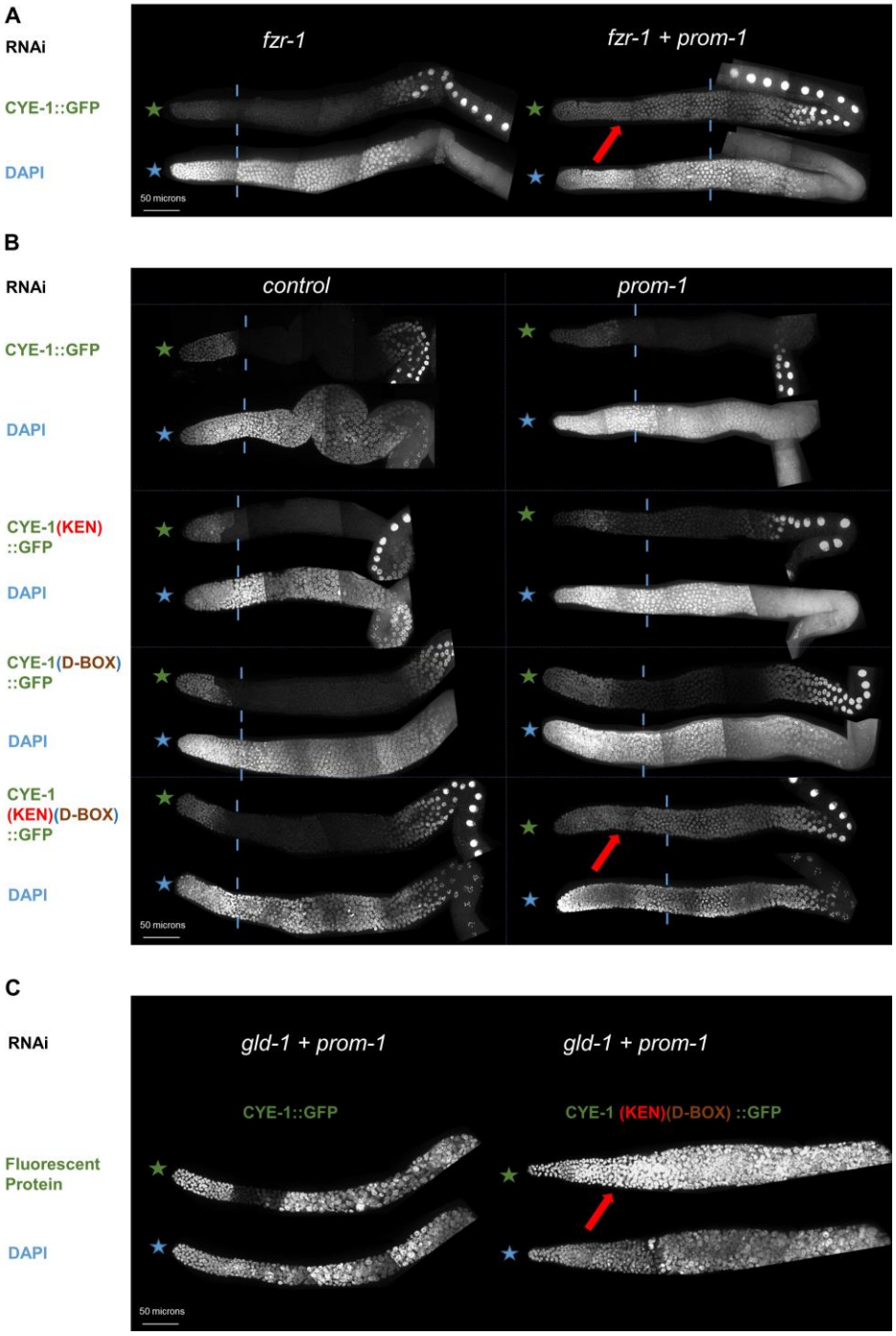

Figure 3.13: CYE-1 degradation is promoted by SCF^{PROM-1} and APC/C^{FZR-1}.
Red arrowheads point to backgrounds where CYE-1 is stabilized throughout the germline.

(A) In *fzr-1* silenced germlines, CYE-1 is degraded (left), but when *prom-1* is also silenced CYE-1 is present throughout the germline (right).

(B) When *prom-1* is silenced, CYE-1 is degraded. Nevertheless, if both *fzr-1* recognition motifs (KEN-box and D-box) are mutated and *prom-1* is silenced CYE-1 is not degraded (bottom right).

(C) In the Gld-1 Prom-1 background CYE-1 is still degraded due to APC/C^{FZR-1} activity (left). Under the same background, if *fzr-1* recognition motives are mutated, CYE-1 is not degraded (right).

The purpose of studying CYE-1 degradation was to analyze whether the downregulation of CYE-1 occurring at the transition zone was the sole cause of the upregulation of APC/C^{FZR-1} activity and therefore MES-4 degradation. To test this, we analyzed the MES-4::GFP pattern of expression in worms unable to degrade CYE-1. For that, we carried out *prom-1* silencing in a strain carrying *cye-1(KEN-box)(D-box)* allele (strain JPM342). In these conditions, the levels of CYE-1 were kept high throughout the gonad (**Figure 3.13B**). Strikingly, despite that CYE-1 was present throughout the germline, MES-4 is downregulated, indicating that the activity of APC/C^{FZR-1} remains at the transition zone. These results strongly suggested that the decrease in the levels of CYE-1 is not the sole cause responsible of the promotion of APC/C^{FZR1} activity (**Figure 3.14**), and therefore implying additional factors in the APC/C^{FZR-1} activation.

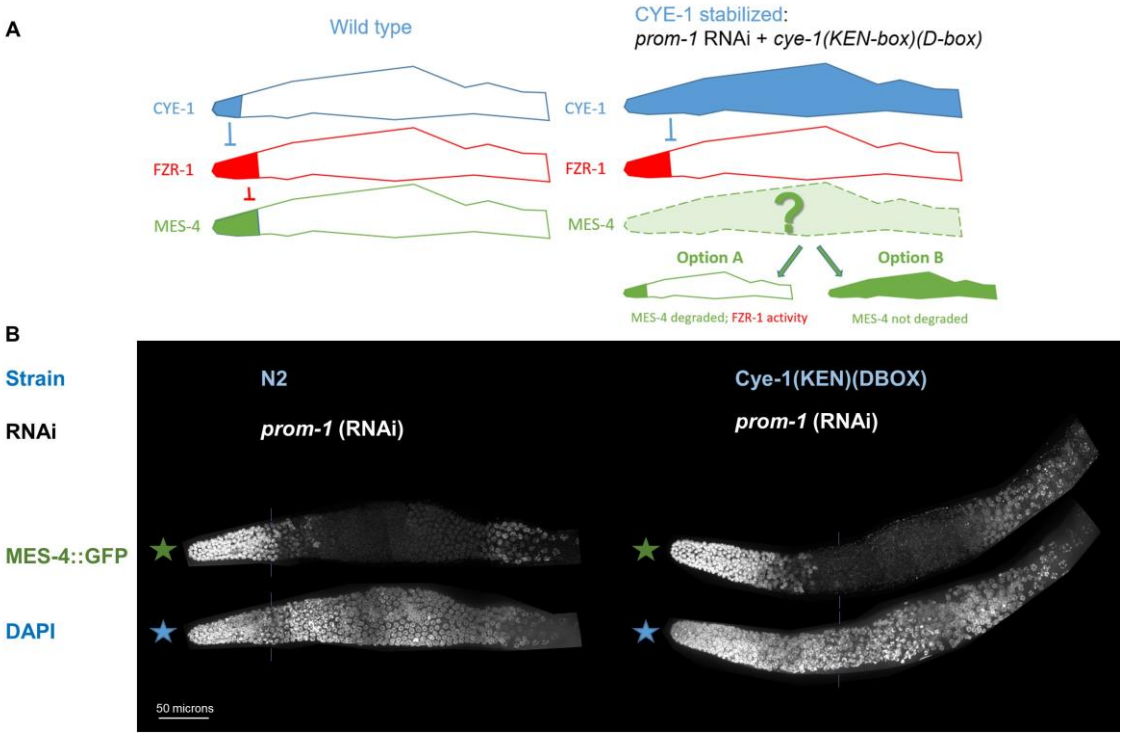

Figure 3.14: APC/C^{FZR-1} activity takes place when CYE-1 is present throughout the germline.

In (A), we lay the basis of the experiment: In the wild type, CYE-1 levels drop before APC/C^{FZR-1} degrades MES-4, we wanted to test what happens when CYE-1 was present throughout the germline. As shown in (B), when we used *prom-1* RNAi and an allele of *cye-1* with *fzr-1* recognition motifs mutated (strain JPM342), MES-4 was still degraded.

3.2.6 CYA-1 is a target of APC/C^{FZR-1} in C. elegans germline and its degradation marks the start of APC/C^{FZR-1} activity in the transition from mitosis to meiosis

We wondered whether other cyclins, which are predicted to be targeted by APC/C^{FZR-1}, would be supporting the CYE-1/CDK control of APC/C^{FZR-1} in a redundant manner. CYB-1 and CYB-3 had D-box motifs but their pattern of expression did not change after *fzr-1* silencing. Interestingly, CYA-1 had a high score D-box and KEN-box. Moreover, Cyclin A is a well-described target of APC/C^{FZR-1} and plays a role in its regulation in other organisms (Reber et al., 2006b).

We have constructed an endogenously GFP-tagged allele of CYA-1. We observed that CYA-1 GFP signal was present in the most proximal part of the mitotic region, just before the transition zone (**Figure 3.15, Figure 3.17**). This band of expression overlaps with the germline region in which germ cells enter the last mitotic division and start the meiosis S-phase. This defined localization agrees with the proposed role of Cyclin A in other organisms, working at the S/G2 phase (Desdouets et al., 1995). We have observed that the levels of CYA-1 dramatically decrease as cells progress into the transition zone (leptotene-zygotene) (there is no GFP signal in crescent-shaped nuclei cells). More important, when *fzr-1* was silenced, CYA-1 levels did not drop in the transition zone and the fluorescent signal was present throughout pachytene (**Figure 3.15**). Since this result strongly suggested that CYA-1 could be a target of APC/C^{FZR1}, we have mutated the KEN-box motif and the D-box motif of *cya-1* in a GFP-tagged allele. In agreement with the idea of CYA-1 as a new target of APC/C^{FZR-1} in the gonad of *C. elegans*, we have observed that CYA-1::GFP with mutations in the two APC/C^{FZR-1} recognition motifs was stabilized in the germline (strain JPM294). (**Figure 3.15**).

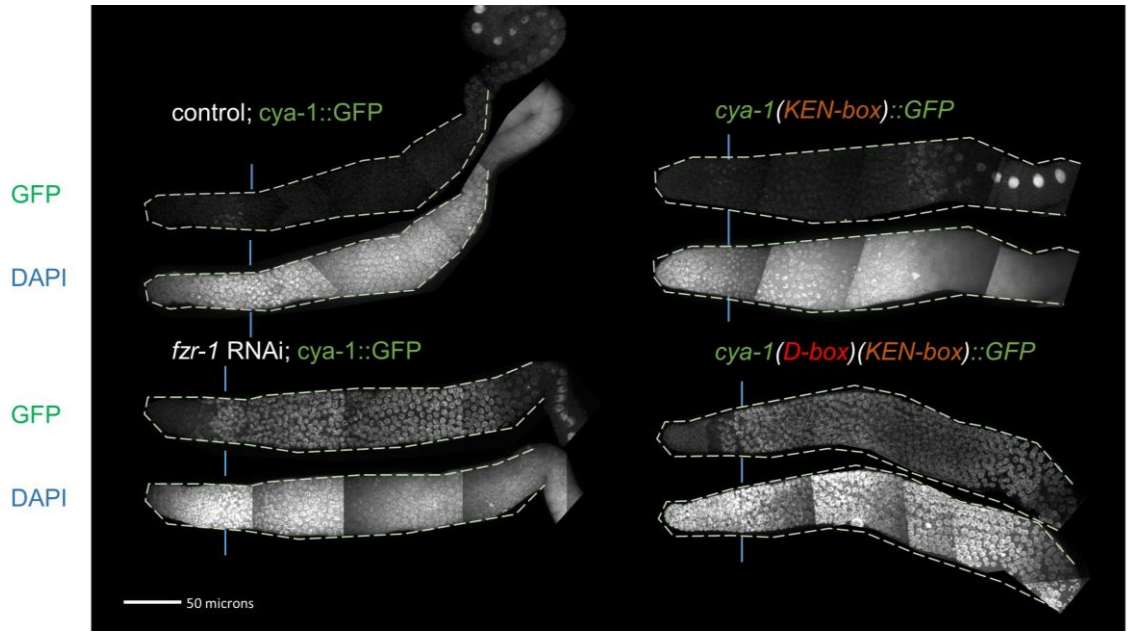

Figure 3.15: APC/C^{FZR-1} promotes degradation of CYA-1 in *C. elegans* germline. CYA-1 is a cyclin briefly present at the end of the mitotic zone, just before the transition zone. When *fzr-1* is silenced, CYA-1 is present throughout all pachytene. Mutations in the *cya-1* sequence of APC/C^{FZR-1} recognition motifs, the D-box and the KEN-box, impair CYA-1 degradation (strain JPM294). However, the single mutation of the KEN-box motif does not impair degradation (strain JPM286).

To study whether CYA—associated CDK activity was able to downregulate APC/C^{FZR-1} activity we tested if APC/C^{FZR-1} promoted MES-4 degradation when CYA-1 is stabilized and present throughout the germline. For this we used a non-degradable allele of *cya-1* with KEN-box and D-box motifs mutated and a *mes-4::mCherry* allele (strain JPM305). We observed that when CYA-1 is present throughout pachytene MES-4 is still degraded by APC/C^{FZR-1} at the transition zone, showing that CYA-1 presence is not sufficient to control APC/C^{FZR-1} activity (**Figure 3.16**)

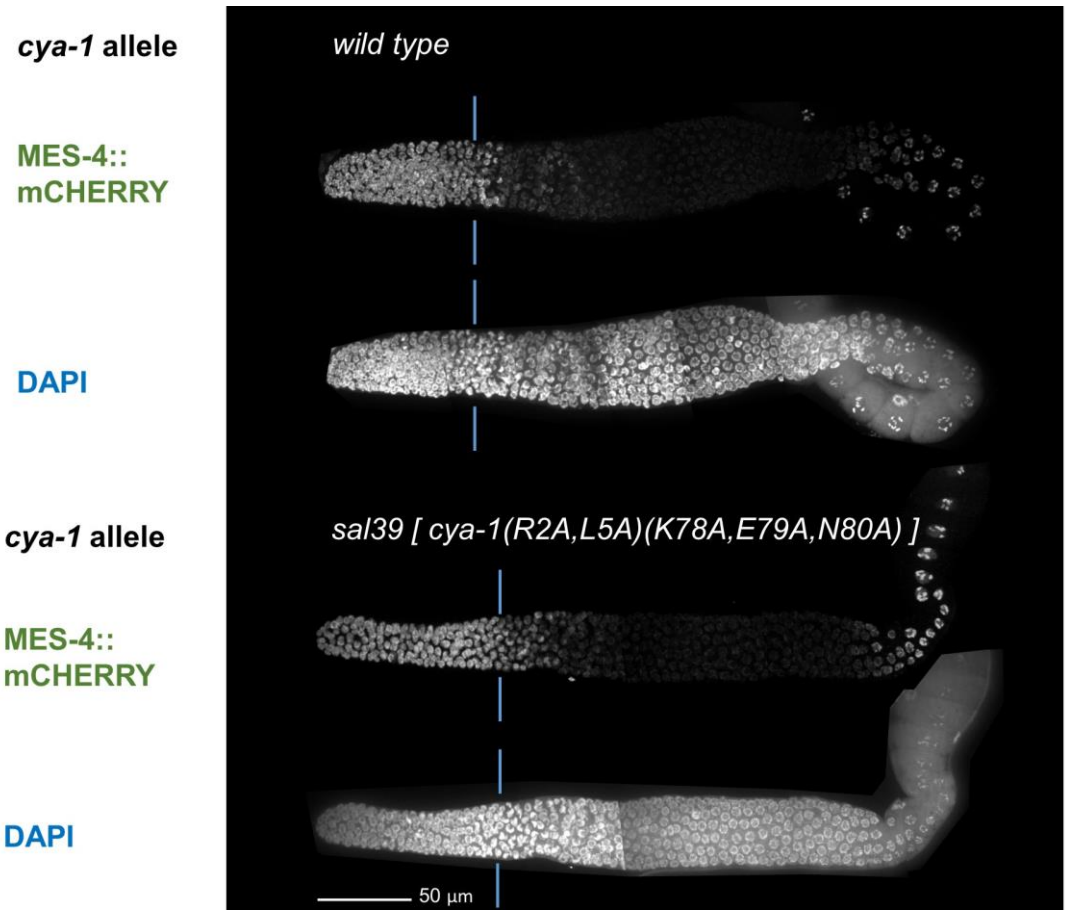

Figure 3.16: APC/C^{FZR-1} can degrade MES-4 when CYA-1 is present throughout pachytene.

The topside shows MES-4::mCHERRY fluorescence and DAPI staining in a strain carrying wild-type cya-1 (strain JPM291). The bottom side shows MES-4::mCHERRY fluorescence and DAPI staining in a strain carrying allele *sal39*, which has mutations in D-box and KEN-box motifs of *cya-1* (strain JPM305), these mutations impede CYA-1 degradation in the transition to meiosis, The transition zone is marked with blue lines.

3.2.7 SCF^{PROM-1} activity, promoting CYE-1 degradation, precedes APC/C^{FZR-1} upregulation

The study of the CYA-1 levels was an excellent tool to understand the regulation of APC/C^{FZR-1} activity in the transition zone of the germline. As showed above, CYE-1 degradation was promoted by both SCF^{PROM-1} and APC/C^{FZR-1} but CYA-1 degradation seems to be solely dependent on APC/C^{FZR-1}. To analyze the spatiotemporal differences between the activation of SCF^{PROM-1} and APC/C^{FZR-1} we compared the distribution pattern of CYE-1 and CYA-1 in the same gonads, and for that we have constructed a strain carrying both *cye-1::mkate* and *cya-1::gfp* tagged alleles (strain JPM289).

CYA-1 and CYE-1 overlaps at the end of the mitotic zone and were degraded as cells enter pachytene. However, CYE-1 degradation seems to occur a couple of cell rows before the transition zone (defined by the presence of crescent-shaped nuclei), just after meiosis S-phase (Mohammad et al., 2018) while CYA-1 seems to extend further and it was degraded just in the start of the transition zone. On the basis of these observation we hypothesized that most likely, CYE-1 is started to be degraded by the activity of SCF^{PROM-1} and later on APC/C^{FZR-1} is activated and both CYE-1 and CYA-1 are fully degraded. To prove this hypothesis, we analyzed the pattern of distribution of CYE-1 and CYA-1 when silencing *prom-1*. In concordance with our hypothesis, we have found that in these conditions, both CYA-1 and CYE-1 are degraded in the same cell rows. **(Figure 3.17**)

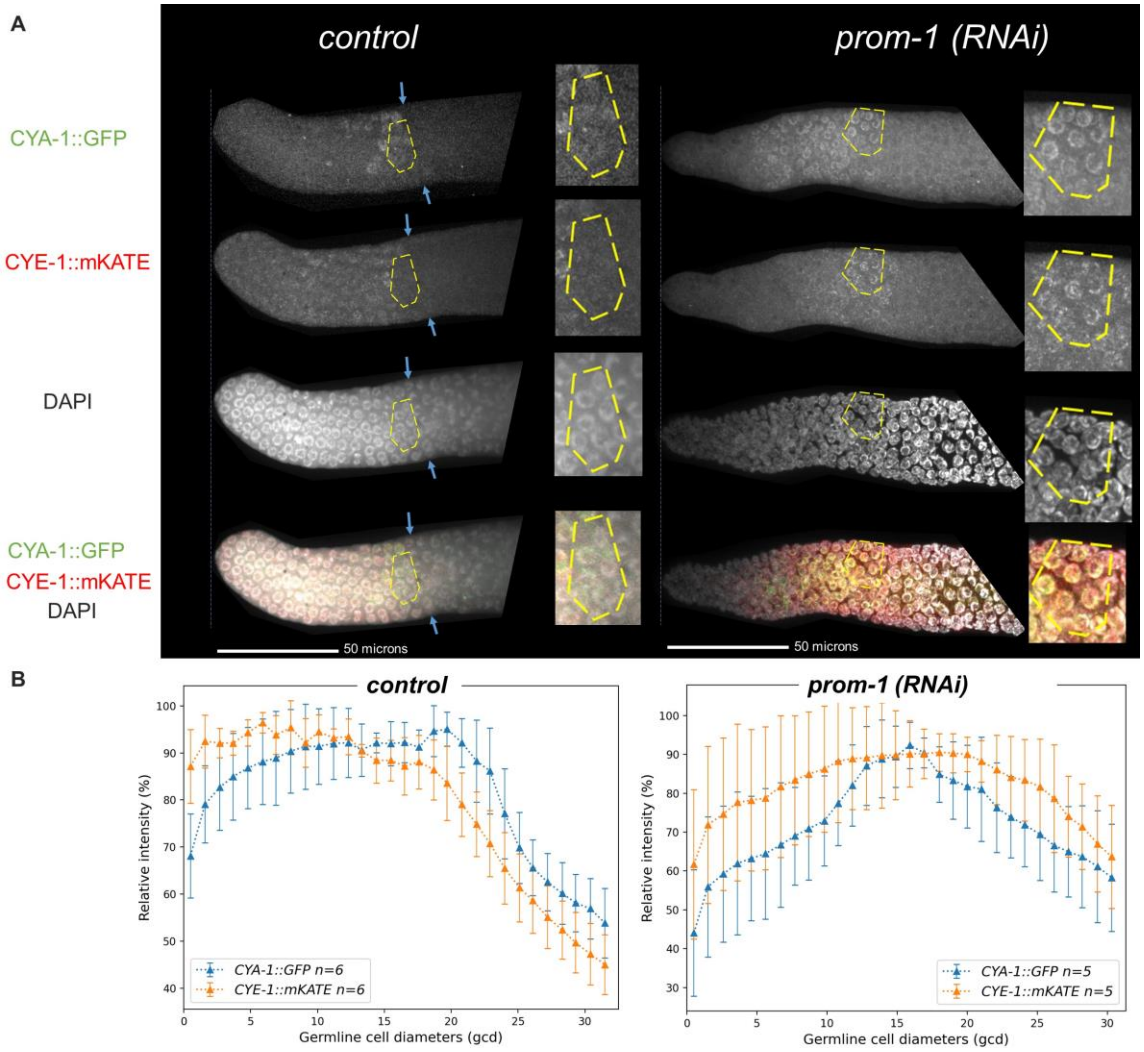

Figure 3.17: CYE-1::mKATE, CYA-1::GFP, and DAPI simultaneous observation in *control* and *prom-1* silencing (strain JPM289).

In (A) we can observe images of CYE-1::mKATE, CYA-1::GFP, DAPI, and the merge in both *control* and *prom-1* RNAi conditions. In **control RNAi,** the CYE::mKATE levels start to drop (yellow marked zone) while CYA-1::GFP is still present. Crescent-shaped nuclei under DAPI staining are characteristic of the transition zone (leptotene-zygotene) and were marked with blue arrows. Interestingly, CYA-1 abruptly drops in these crescent-shaped nuclei. The model proposed is that SCF^{PROM-1} starts to degrade CYE-1 while APC/C^{FZR-1} is still inactive, afterwards APC/C^{FZR-1} degrades CYA-1. In ***prom-1* RNAi,** CYE-1::mKATE is still present in the last rows of cells with CYA-1::GFP (yellow marked zone).

In (B) we can observe two graphs (one for *control* and the other for *prom-1* RNAi) of the relativized fluorescence intensity of CYA-1::GFP (blue) and CYE-1::mKATE (orange) plotted, representing the first 30-31 germline cell diameters (*control* n=6, *prom-1* n=5). Germline cell diameters were stablished as 3.5 microns.

To gather more information about the spatiotemporal coordination of SCF^{PROM-1} and APC/C^{FZR-1} activities, we decided to study the expression of MES-4 (exclusive APC/C^{FZR1} target) in comparison to CYE-1 (target of SCF^{PROM-1} and APC/C^{FZR-1}). We observed that in *control* conditions MES-4 degradation occurred some cell rows after CYE-1 degradation started but when *prom-1* is silenced MES-4 degradation coincides with CYE-1 degradation (**Figure 3.18**).

In summary, from these observations we conclude that APC/C^{FZR-1} activity seems to be triggered **after** SCF^{PROM-1} activity initiates CYE-1 degradation (which takes place, after meiosis S-phase (Mohammad et al., 2018)). APC/C^{FZR-1} activity (observed as the degradation of CYA-1 and MES-4) occurs in parallel with the appearance of the crescent-shaped nuclei characteristic of meiotic prophase I.

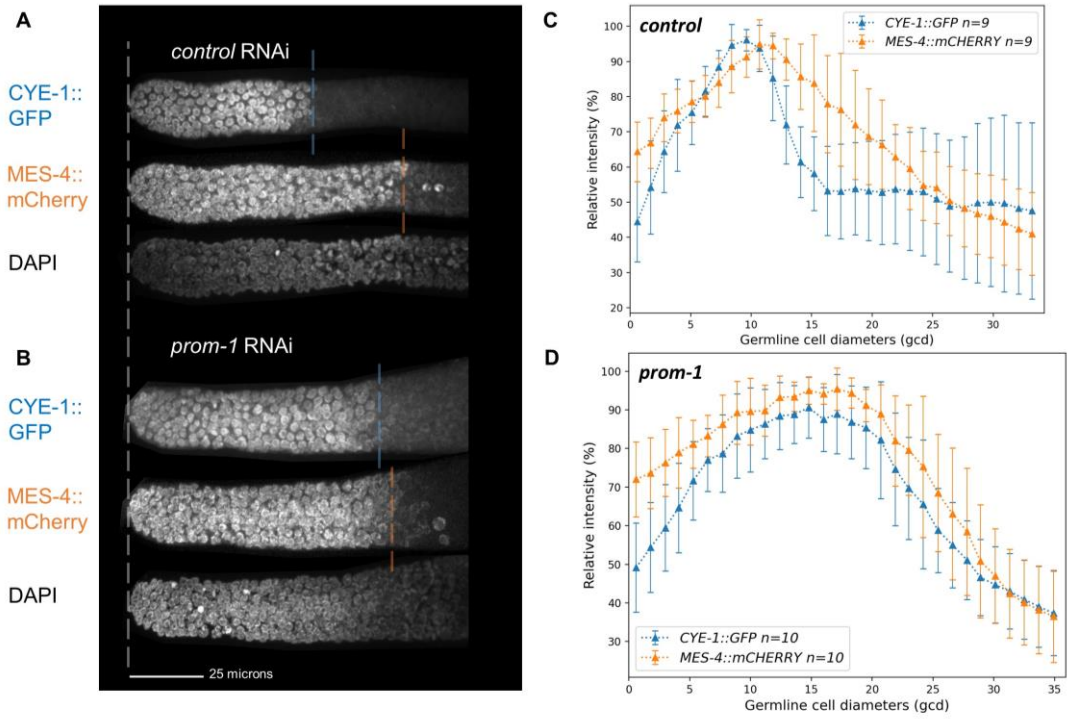

Figure 3.18: CYE-1::GFP, MES-4::mCHERRY, and DAPI simultaneous observation in *control* and *prom-1* silencing (strain JPM291).

In (A) we show images of strain JPM291 with *control* RNAi and we can observe CYE-1::GFP degradation (blue striped line) happening before MES-4::mCherry degradation (orange striped line). The graph displaying the average of the sample (n=9) is plotted in (C), relative fluorescence intensity is displayed on Y-axis and absolute length (from 0 to 34 germline cell diameters) is displayed on X-axis.

In (B) we show images of strain JPM291 with *prom-1* RNAi and we can observe CYE-1::GFP degradation (blue striped line) happening almost simultaneously with MES-4::mCherry degradation (orange striped line). The graph displaying the average of the sample (n=10) is plotted in (D), following (C) graph characteristics.

3.2.8 E3 ubiquitin ligase SCF^{PROM-1} and polyA-polymerase GLD-2 promote APC/C^{FZR-1} upregulation

From the above describe results, we entertained the hypothesis that SCF^{PROM-1} is acting as the trigger of APC/C^{FZR1} activation at the transition zone. This triggering activity could be a consequence of the decrease of CYE-1 levels promoted by the SCF^{PROM-1} activity. However, although this triggering activity most likely occurs, it seems that additional factors are required for the timely activation of APC/C^{FZR-1}, since stabilization of CYE-1 throughout the germline (silencing *prom-1* and mutating the D-box and KEN-box of *cye-1*) does not resulted in inability to activate APC/C^{FZR-1} (**Figure 3.14**).

To search for more factors promoting APC/C^{FZR-1} activity we carried out a RNAi screening in prom-*1(ok1140); mes-4::mCherry* strain (JPM318). We hypothesized that silencing other putative factors promoting APC/C^{FZR-1} activity in conditions that disable SCF^{PROM-1} would cause the pachytene invasion of MES-4. Among the silenced genes analyzed, we have included genes encoding protein phosphatase that in other systems were involved in the dephosphorylation of Cdh1/FZR-1 (and hence its activation) such as *cdc-14*, *lip-1,* and *let-92* (PP2A ortholog). Disappointingly, we did not observe any effect in these cases. However, we observed that silencing *gld-2* resulted in pachytene invasion of MES-4. This effect was dependent on the inactivation of SCF^{PROM-1}, supporting our hypothesis that several factors contributed to the timely activation of APC/C^{FZR-1} (**Figure 3.19**)

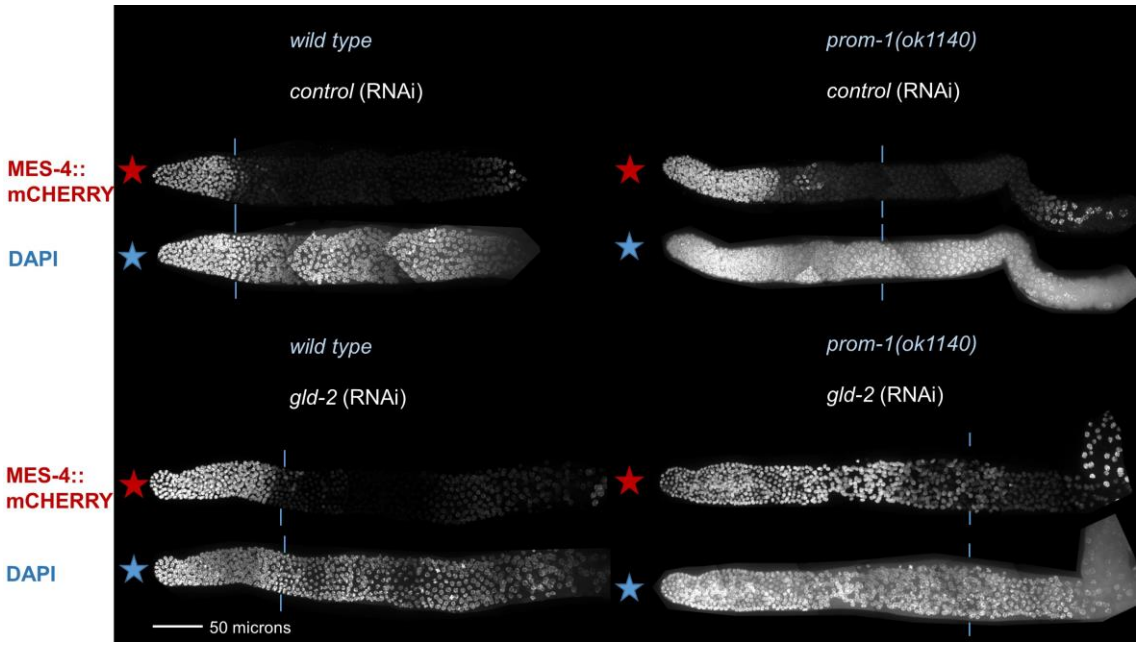

Figure 3.19: *Gld-2* silencing impairs APC/C^{FZR-1} activation in the *prom-1(ok1140)* mutant, strain JPM318.

Here we use the protein MES-4::mCHERRY to report FZR-1 activity. In the *prom-1(ok1140*) deletion mutant, FZR-1 can activate (top image). When *gld-2* RNAi is performed in the *prom-1* mutant, MES-4 degradation and therefore FZR-1 activation is hugely delayed (bottom image). This suggests that GLD-2 is involved in FZR-1 activation.

3.2.9 GLD-2 promotes APC/C^{FZR-1} upregulation by interacting with *fzr-1* 3' UTR and indirectly, by CKI-2 upregulation

Our screening proposed GLD-2 as a factor upregulating APC/C^{FZR-1}. GLD-2 is a polyA-polymerase involved in meiotic entry that promotes translation through interaction with 3' UTRs. Since we have observed an increase in the FZR-1 levels as cells reach the transition zone (the region where GLD-2 start to be operative), the easiest explanation is that GLD-2 could be promoting the translation of FZR-1. However, we made an observation that leads us to be cautious with this explanation. The interaction of GLD-2 with its mRNA targets is mediated by the GLD-3 protein. However, we observed that silencing *gld-3* does not reproduce the pachytene invasion observed when *gld-2* was silenced in the

prom-1 background. Although this discrepancy can be solved by arguing that a factor aside from GLD-3 directs GLD-2 to *fzr-1* mRNA, we need further support to this idea. For that we wondered whether GLD-2 could be promoting the translation of *fzr-1* via its 3' UTR. To test the interaction between GLD-2 and *fzr-1* 3' UTR we compared the expression of the *fzr-1 3' UTR reporter* (strain JPM349) in *control* and *gld-2* RNAi. We observed that when we silenced *gld-2* the peak of expression of the reporter decreased (although not dramatically) compared to the *control* (**Figure 3.20**), supporting the idea that GLD-2 was contributing to the increase levels of FZR-1 at the transition zone.

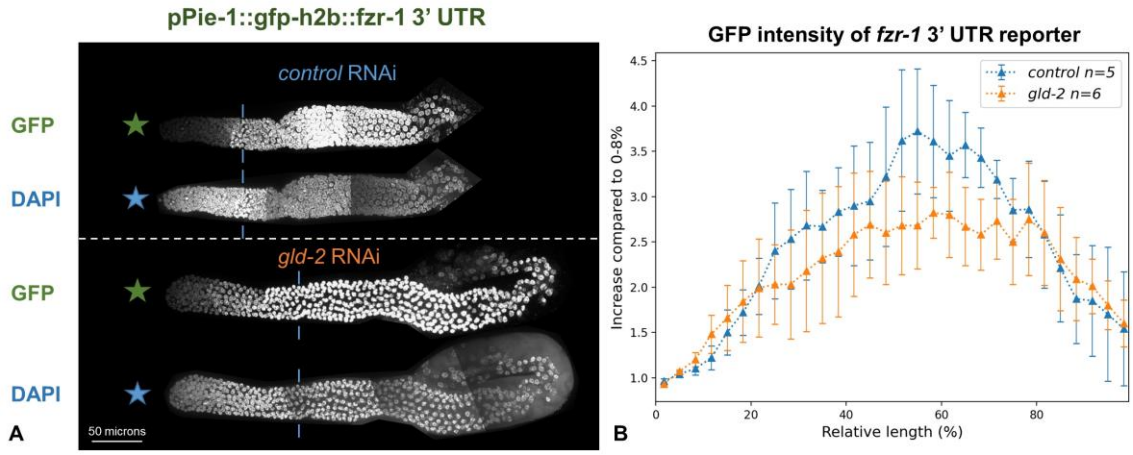

Figure 3.20: *gld-2* silencing partially reduces *fzr-1 3' UTR reporter* expression
In (A) images of *fzr-1 3' UTR reporter (pPie-1::gfp-h2b::fzr-1 3'utr), strain JPM349,* with *control* and *gld-2* RNAi. In (B) graphical representation of average fluorescence intensity for both samples, *gld-2* silencing partially decreases the peak of fluorescence intensity reached.

To address in a more direct manner the proposed role of GLD-2 upregulating FZR-1 activity, we took advantage of a strain with *prom-1* knock-out deletion *(ok1140)* and in which the only copy of *fzr-1* gene carried an alternative 3' UTR: *salSi73(Pfzr1::fzr-1::cye-1 3' UTR + unc-119(+)),* strain JPM410. In this strain, the putative GLD-2 interaction with *fzr-1* 3' UTR is proposed to be disabled, as the whole UTR was changed. As before, we analyzed the activity of APC/C^{FZR1} by observing the distribution pattern of MES-4::GFP. Strikingly, in this case we were not able to phenocopy the double knockdown of *prom-1* + *gld-2* (**Figure**

3.21 control). Although this result could indicate a partial involvement, if any, of the proposed role of GLD-2 upregulating the levels of FZR-1 it also can be explained by invoking an indirect role of GLD-2 upregulating APC/C^{FZR-1}, aside of activating FZR-1 translation via 3' UTR.

We have entertained the hypothesis that additional factors, also activated by GLD-2, could be contributing to the activation of APC/C^{FZR-1}. Among the proposed *in silico* target of GLD-2 it raised our attention the CDK inhibitor CKI-2. This CKI is highly expressed in the germline once the cells reach the transition zone and it has been proposed to help in the down-regulation of CYE-1/CDK-2 activity before meiosis entry. (Buck et al., 2009).

Therefore, we carried out *cki-2* RNAi in the previously described background with the *fzr-1* allele with swapped 3' UTR and with *prom-1* knock-out deletion (strain JPM410). Strikingly, when *cki-2* silencing was carried over this strain, more than 80% of germlines showed an ectopic presence of MES-4::GFP in mid-pachytene, replicating the effects of *gld-2* silencing (Figure **3.21**). *Cki-2* silencing over this strain also caused an exacerbated *prom-1 (ok1140)* phenotype regarding the crescent-shaped nuclei indicating meiosis entry, the transition to meiosis was very hard to identify and furthermore oogenesis was aberrant in some germlines. In concordance, *gld-2* silencing produced very similar results. These results suggest that CKI-2 could be the main target of GLD-2 promoting APC/C^{FZR-1} activity.

In summary, both ubiquitin-ligase SCF^{PROM-1} and polyA-polymerase GLD-2 are upstream of FZR-1 and contribute to his timely activation before the transition zone. SCF^{PROM-1} kick-starts CYE-1 degradation, and GLD-2 contributes to FZR-1 translation by interacting with *fzr-1* 3' UTR but it seems like it also upregulates APC/C^{FZR-1} indirectly. Genetic interaction analysis showed us that CKI-2 could be the main target of GLD-2 contributing to APC/C^{FZR-1} upregulation.

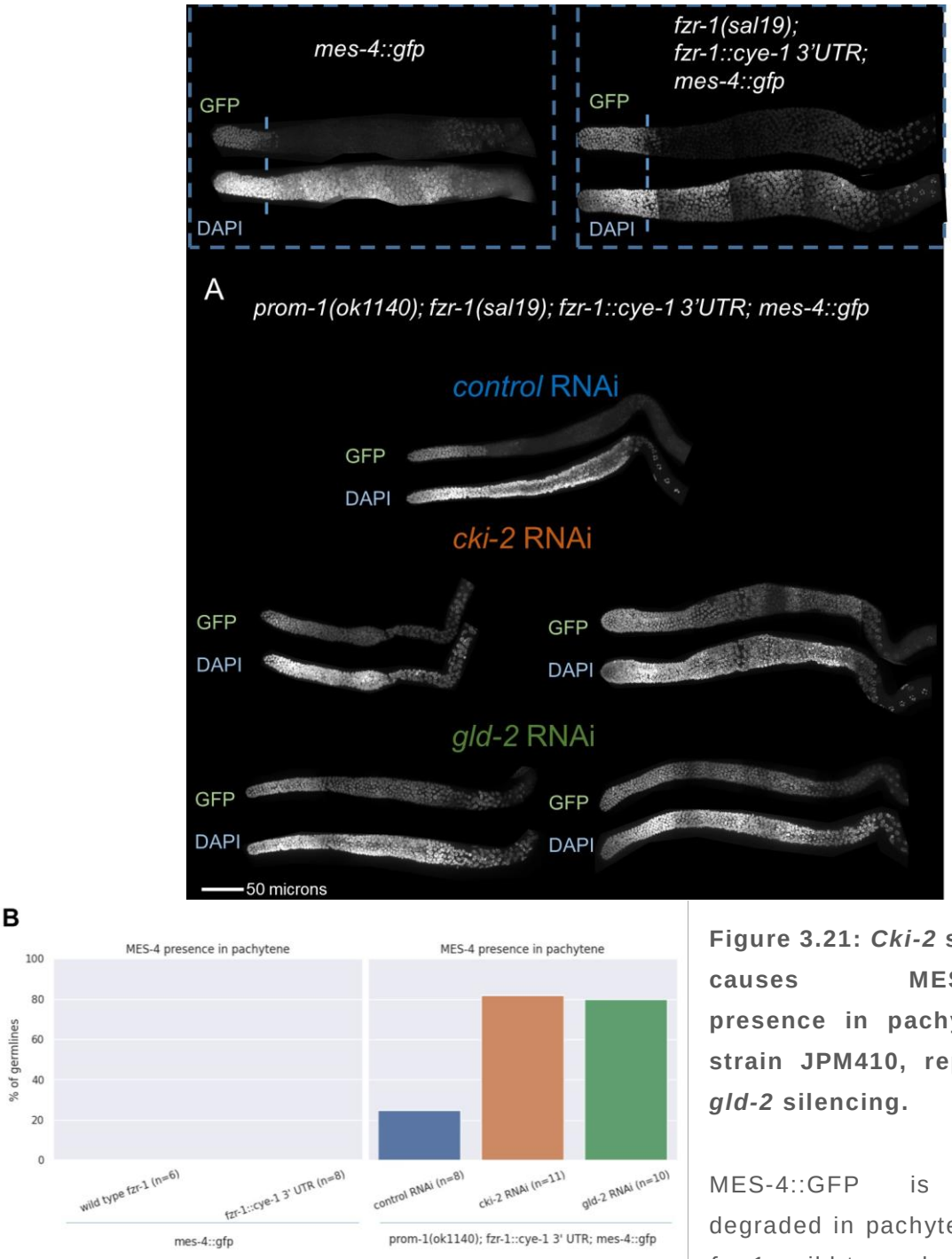

Figure 3.21: *Cki-2* silencing causes MES-4::GFP presence in pachytene in strain JPM410, replicating *gld-2* silencing.

MES-4::GFP is always degraded in pachytene in an *fzr-1* wild-type background (top-left, strain JPM76) and in a background with an *fzr-1* allele with *cye-1* 3' UTR (top-right, strain JPM399). However, when *prom-1(ok1140)* mutation is combined with an *fzr-1* allele with *cye-1* 3' UTR (strain JPM410), around 20% of the germlines show the presence of MES-4::GFP in pachytene (**A**, top-side image and blue bar in **B** graph). This phenotype is greatly exacerbated when *gld-2* is silenced (**A**, bottom-side images, and green bar in **B** graph). Interestingly, silencing the GLD-2 *in silico* target *cki-2*, fully replicates the silencing of gld-2 (**A**, mid-side images and orange bar in **B** graph)

3.2.10 GLD-1 pathway role in APC/C^{FZR-1} regulation

The current model is that three regulators control meiotic entry of *C. elegans* germ cells. These are the SCF^{PROM-1} ubiquitin ligase, the GLD-2 translation activator and the GLD-1 translation repressor (Mohammad et al., 2018). We have described that SCF^{PROM-1} and GLD-2 have roles in the APC/C^{FZR-1} upregulation. GLD-1 is a RNA-binding protein whose role is to inhibit the translation of mitotic genes and promote meiotic entry (Hansen et al., 2004). Interestingly, GLD-1 regulation is very similar to FZR-1 regulation: *gld-1* is phosphorylated by CYE-1/CDK-2 in the mitotic zone and GLD-1 negatively controls CYE-1 translation forming a toggle switch as we propose for APC/C^{FZR-1} (Jeong et al., 2011); *gld-1* mRNA translation is repressed in the mitotic zone by FBF proteins (Suh et al., 2009), and GLD-2 promotes *gld-1* mRNA translation in meiotic entry (Suh et al., 2006).

Previously we observed that silencing *gld-1* in a strain carrying *mes-4::gfp* (JPM76) resulted in a tumorous line in which MES-4 was present throughout the gonad with the exception of the transition zone. The down-regulation of MES-4 in this region was dependent of APC/C^{FZR-1} activity, double silencing of *gld-1* + *fzr-1* resulted in the presence of MES-4 throughout the germline (**Figure 3.22A**). This observation strongly suggested that APC/C^{FZR-1} upregulation seems to occur in a GLD-1 independent manner, since in GLD-1 defective mutants APC/C^{FZR-1} is able to promote the degradation of its targets near the transition zone, as it happens in wild type germlines.

The proposed independence between GLD-1 and APC/C^{FZR1} regulation prompted us to wonder whether the regulation control that we have previously described were operative in Gld-1 tumorous gonads. We combined *gld-1* silencing with conditions disabling the other observed controls of APC/C^{FZR-1} activity. While disabling SCF^{PROM-1} and the proposed GLD-2 control in *fzr-1* translation (via 3' UTR) we were able to still observe the MES-4 degradation band in Gld-1 tumorous gonads. However, when we silenced *gld-1* + *gld-2*, this degradation band disappears (**Figure 3.22B**). These results reinforce our working model that GLD-2 activates APC/C^{FZR-1} by at least two ways, via *fzr-1*

3'UTR and indirectly (we propose via CKI-2). Although it seems that APC/C^{FZR1} activation operates independently of GLD-1, we believe that there are some connections, in the sense that GLD-1 activity promotes the decrease of CYE-1/CDK-2 and FBF activity once cells reach the transition zone, and thereby is supporting the activation of APC/C^{FZR-1}. In the same way, it could be possible that the CYE-1 degradation promoted by SCF^{PROM-1} and APC/C^{FZR-1} also increases the activity of GLD-1 (which as FZR-1 is negatively controlled by CDK phosphorylation).

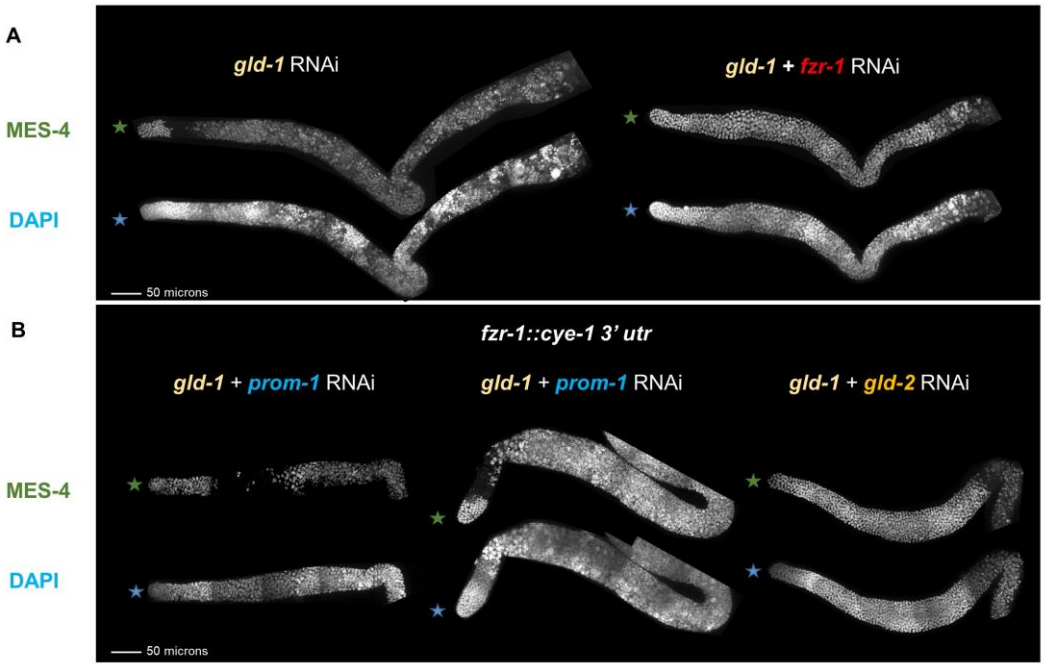

C

APC/C^{FZR-1} activity in different meiotic entry pathway deffective backgrounds

GLD-1	GLD-2	SCF^{PROM-1}	APC/C^{FZR-1} activity	Figure
✗	✓	✓	YES	3.22A
✓	✗	✓	YES	3.19
✓	✓	✗	YES	3.19
✗	✗	-	NO	3.22B
✓	✗	✗	NO	3.19
✗	✓	✗	YES	3.22B

Figure 3.22: APC/C^{FZR-1} regulation in Gld-1 tumorous germline.

(A) MES-4::GFP and DAPI signal of RNAi silencing carried out over JPM76 strain. In *gld-1* silencing, MES-4 is degraded at the transition zone and its levels are upregulated again when cells reenter mitosis. In *gld-1* + *fzr-1* silencing, MES-4 is not degraded, supporting the idea that in GLD-1-pathway-defective APC/C^{FZR-1} activity degrades MES-4.

(B) MES-4::GFP and DAPI signal of RNAi silencing carried out over JPM76 strain or JPM399 strain. In *gld-1* + *prom-1* silencing, MES-4 is degraded (strain JPM76). In *gld-1* + *prom-1* silencing + *fzr-1* copy with 3'UTR swapped (strain JPM399), MES-4 is also degraded. However, in *gld-1* + *gld-2* silencing (strain JPM76), MES-4 is not degraded.

(C) Table summarizing if we could observe APC/C^{FZR-1} activity when we impaired all the combinations of the three main meiotic entry pathways: GLD-1, GLD-2 and, SCF^{PROM-1}.

3.2.11 APC/C^{FZR-1} promotes the degradation of FZR-1

The levels of FZR-1 protein dramatically decrease in cells reaching the pachytene region, paralleling the behavior of MES-4. In other organisms, it has been reported that Cdh1 or Fzr1 are targeted by the APC/C^{Cdh1} complex. FZR-1 has an evolutionary conserved D-box in the *Caenorhabditis* genre*,* located near the N-terminus. This led to the hypothesis that APC/C could be mediating the destruction of FZR-1.

To support this hypothesis, we silenced *apc-6*, one of the subunits from APC/C and analyzed the GFP::FZR-1 pattern of expression (strain JPM119). Our results showed that FZR-1 down-regulation in the pachytene region was impaired (**Figure 3.23B**) replicating the pachytene invasion of MES-4 when *apc-6* was silenced (**Figure 3.23A**). These results indicated that FZR-1 down-regulation was mediated by APC/C. We wondered whether this APC/C-mediated downregulation was dependent of the *fzy-1* (*cdc20* in mammals) coactivator. For that, we silenced *fzy-1* and analyzed the levels of GFP::FZR-1. We observed that *fzy-1* RNAi was not able to reproduce the pachytene invasion by GFP::FZR-1 observed when *apc-6* was silenced. This observation gives us to propose that *fzr-1* could catalyze his own destruction.

To gain further support on this idea, we mutated key residues of the D-box to alanine (strain JPM330) and we observed that it caused the stabilization and presence of FZR-1 throughout the germline (**Figure 3.23C**). Together, these results led us to propose that APC/C^{FZR-1} recognizes FZR-1 and promotes self-degradation via the D-box motif, causing the absence of FZR-1 in pachytene.

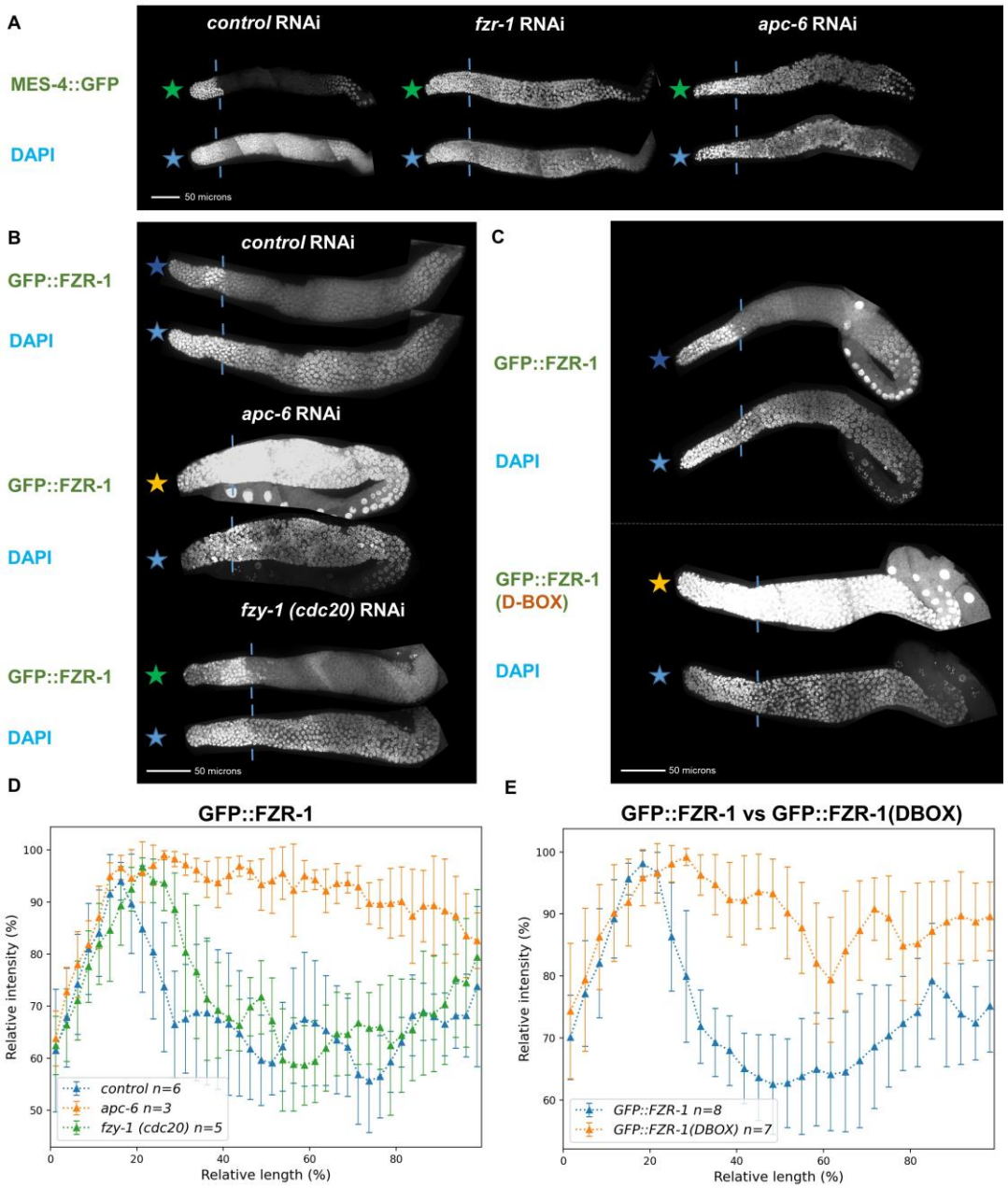

Figure 3.23: APC/C^{FZR-1} promotes degradation of FZR-1.

(A) We found an APC/C subunit *apc-6* that seems critical for APC/C^{FZR-1} activity in the germline. Silencing of *apc-6* replicated *fzr-1* silencing, impairing MES-4 degradation.

(B) GFP::FZR-1 (strain JPM119) is not present at pachytene in *control* RNAi conditions. However, when APC/C is impaired through silencing essential subunit *apc-6*, FZR-1 is not degraded. The silencing of *fzy-1* did not replicate the silencing of *apc-6*. These results suggest that *fzr-1* is the APC/C coactivator involved in FZR-1 degradation.

(C) When the *fzr-1* D-box motif is mutated, FZR-1 degradation is greatly reduced (strain JPM330).

(D) Graphic representation of (A) GFP::FZR-1 *control* (blue), GFP::FZR-1 when *apc-6* is silenced (orange), and GFP::FZR-1 when *fzy-1* is silenced (green).

(E) Graphic representation of (B) GFP::FZR-1 (blue) and GFP::FZR-1 with D-box motif mutated (orange).

DISCUSSION

4 DISCUSSION

During this Thesis, we have used the germline of *Caenorhabditis elegans* as a model to study how APC/C^{FZR-1} is regulated in the germline stem cells that are differentiating into meiosis. The starting point of this study was the observation that FZR-1, the co-activator of APC/C, overlaps with MES-4 and MES-3, two of the targets of APC/C^{FZR-1} along the mitotic region of the gonad, suggesting that somehow the activity of APC/C^{FZR1} was negatively controlled. We have found that this negative control takes place at least through two mechanisms, which in the last instance were dependent on the activity of the FBF proteins, which were downstream effectors of the Notch pathway. On one side, FBF proteins downregulate FZR-1 protein levels, most likely by interacting with *fzr-1* 3' UTR. This negative control was complemented by keeping high levels of CYE-1 (indirectly promoted by FBF by inhibiting GLD-1), which results in high CDK activity that we believe inhibits the interaction of FZR-1 with the APC/C core. As cells move away from the influence of the cell niche (the DTC) the signaling promoted by the Notch pathway fades, and thereby the action of FBF as translational repressors. As a consequence, a series of processes resulted in a rise of the APC/C^{FZR-1} activity, which overlaps with the entry into the meiotic cell cycle: The levels of FZR-1 protein rise, because the translational repression exerted by FBF is disabled and the polyA polymerase GLD-2 (which is also negatively regulated by FBF proteins) enhances the translation of FZR-1, most likely via its 3' UTR. The increase of FZR-1 levels was coincident with a decrease in the CDK activity, which was a consequence of at least two factors: a down-regulation in the levels of CYE-1 by the decrease in its translation, mediated by the RNA binding protein GLD-1 (another target of FBF proteins) and the triggering of its degradation promoted by the activity of the SCF^{PROM-1} complex. The decrease in the protein levels was accompanied by the decrease in the CDK activity because of the rise of CKI-2, repressed by FBF and most likely promoted by GLD-2. Altogether, these actions enabled the activity of APC/C^{FZR1}, which resulted in the destruction of CYE-1 and the other targets, including FZR-1.

Below we will discuss the experimental observations that support the above explanation.

4.1 APC/C^{FZR-1} down-regulation in the mitotic zone of the *C. elegans* germline

Along the mitotic cycle, APC/C^{FZR-1} is active only at the late M phase prolonging through the G1 phase. The reason for this pattern is the inhibition of the interaction between FZR-1 and the APC/C core upon CDK-promoted phosphorylation at several sites in FZR-1. Since CDK activity is absent at the end of mitosis and very low through G1 (until it reaches a peak, once the S phase started), previous reports correlated the length of G1 and the activation of APC/C^{FZR-1}: the longer the G1 phase, the higher the activity of APC/C^{FZR-1} and vice versa (Keck et al., 2007; Kramer et al., 2000; Reber et al., 2006a; L. Wan et al., 2017; Zachariae et al., 1998).

Interestingly, in the mitotic zone of the *C. elegans* germline, the cells are rapidly dividing and are found mainly in the S and G2 phases of the cycle, with a tiny amount of cells in G1 (<1%) (Kocsisova et al., 2018). This observation strongly suggested that APC/C^{FZR-1} is downregulated in the mitotic zone, correlating with the low percentage of cells in the G1 phase.

CYE-1, interacting mainly with CDK-2, is highly expressed in the mitotic zone of the *C. elegans* germline (Fox et al., 2011, **Figures 3.5, 3.12**). Gonads from worms with *cye-1* RNAi silenced showed significant premature downregulation of MES-4 in the mitotic zone, which was attributed to APC/C^{FZR-1} promoted degradation of MES-4 because when MES-4 was mutated in the APC/C^{FZR-1} recognition motif, the KEN-box, that premature downregulation was not observed (**Figure 3.4**). Strikingly, *cye-1* RNAi does not result in full down-regulation of MES-4 in the gonad: some fluorescent signal remains in the more distal region. These remains were not caused by defective silencing of cye-1 in this region, suggesting additional controls over APC/C^{FZR-1} activity.

The search for additional controls led us to observe that the FZR-1 protein levels were lower at the distal part of the mitotic region (**Figure 3.6**) and to conclude that the activity of FBF proteins caused this. FBF-1 and FBF-2 are part of the PUF (Pumilio and FBF) hub: a regulatory network of RNA binding proteins

under the control of the Notch signal emanating from the DTC (Haupt et al., 2020). FBF proteins regulate mRNA translation by binding to UTRs through conserved FBF binding elements (FBEs). We observed that *fbf* silencing increased FZR-1 protein levels throughout the mitotic germline (**Figure 3.9**). This observation was supported by studies using an *fzr-1* 3' UTR reporter that strengthened the idea that FBF regulated *fzr-1* mRNA via his 3' UTR. These results were concordant with previous research indicating that FZR-1 was an FBF interactor *in silico* (Supplementary data in (Kershner & Kimble, 2010) (Botta et al., 2022). The 3' UTR from *fzr-1* has a canonical FBF binding site in the 3' UTR (**TGT**xxx**AT**). However, the mutation of this putative binding site seems not to affect the expression pattern of the *fzr-1* 3' UTR reporter. We believe that additional non-canonical FBF binding sites in the 3' UTR could be acting redundantly. These non-canonical binding sites differ in the length of the variable spacer region (from canonical "**TGT**xxx**AT"** to non-canonical "**TGT**xx**AT**" or "**TGT**xxxx**AT**"), and they have been suggested as bona fide FBF binding sites (Aman et al., 2016). Interestingly, we have found a concentration of several of these putative binding sites in the *fzr-1* 3' UTR region believed to be interacting with FBF, extracted from iCLIP binding profiles data (Porter et al., 2019).

One interesting finding was that *fbf* silencing (impairing both *fbf-1* and *fbf-2*) not only eliminates the repression of *fzr-1* 3' UTR reporter in the mitotic zone but also eliminates the peak of expression later in meiosis. Recent studies are suggesting a dual regulatory effect of the FBF proteins: On one hand, the more classical mRNA translation repression (mediated by CCR4 de-adenylation) and, on the other hand, an activating mRNA role (Suh et al., 2009). The former study suggested a dual role (repression and activation) for both FBF-1 and FBF-2. However, some authors suggest a division of roles between FBF-1 (repression) and FBF-2 (activation) (Wang et al., 2020), although more evidence needs to be catered. We cannot exclude the possibility that FBF proteins are repressing the translation of *fzr-1* in the mitotic region but later on, in the transition to meiosis, they help to promote *fzr-1* translation. This dual role of FBF is currently being heavily studied and could throw light on *fzr-1* mRNA regulation in the germline.

The Notch signal emanating from the niche controls FZR-1 protein levels and indirectly controls APC/C^{FZR-1} activity through *cye-1* regulation. FBF proteins

downregulate the expression of RNA-binding protein GLD-1, one of the main proteins involved in meiotic entry (Suh et al., 2009). This is relevant as GLD-1 negatively regulates *cye-1* translation (Biedermann et al., 2009). The logic is that the niche inhibits GLD-1 expression, indirectly promoting high CYE-1 protein levels, which we propose enabled the downregulation of the APC/C^{FZR-1} activity.

CYE-1 partners with CDK-2 (Fox et al., 2011), and the inhibition of APC/C^{FZR-1} activity in the mitotic germline could be mediated by the CDK phosphorylation of FZR-1. We tried in different ways to introduce an ectopic copy of a phospho-null version of *fzr-1* with mutations of the CDK phosphorylation sites described previously (The et al., 2015), but we failed, most likely because it affects the fertility of the manipulated worms. As a control, inserting an ectopic wild-type version of *fzr-1* renders a viable and fertile strain. Although producing a negative result, this approach enhances our belief that CYE-1/CDK-2 repression is fundamental to maintaining APC/C^{FZR-1} activity low in the mitotic region and preserving essential germline proteins such as MES-3 and MES-4. In the same way, the observed control of FZR-1 protein levels by the proposed direct action of FBF proteins on *fzr-1* 3' UTR seems not so essential. Most likely, the role of FBF protein on FZR-1 levels is acting as a backup, as is suggested by the combination of *cye-1* and *fbf* RNAi's showing complete upregulation of APC/C^{FZR-1} activity in the mitotic zone.

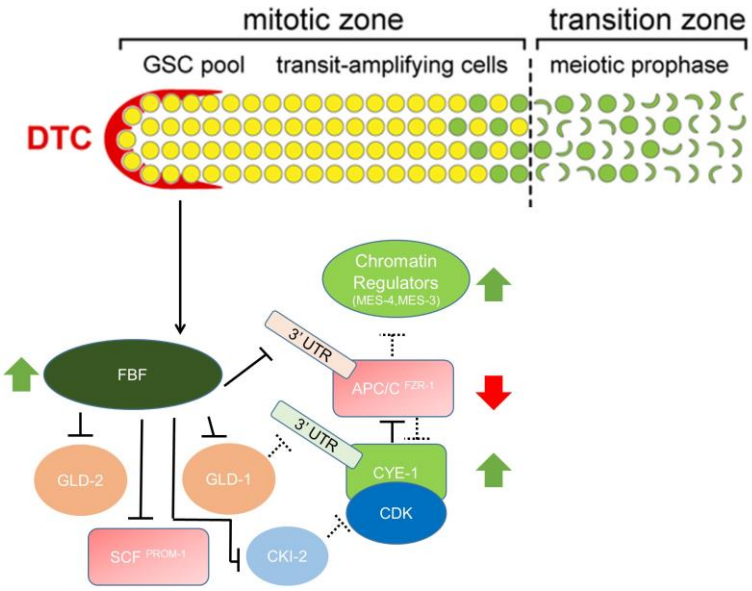

Figure 4.1: Proposed regulatory signaling in the mitotic zone.

4.2 APC/C^{FZR-1} up-regulation in the transition to meiosis

APC/C^{FZR-1} plays a role in meiosis in multiple other organisms, especially in those with no a specific APC/C coactivator for meiosis. In the *C. elegans* germline, APC/C^{FZR-1} activity is low in the mitotic zone, but we have observed that APC/C^{FZR-1} was active around the transition zone to meiosis, promoting the degradation of MES-3 and MES-4, as described in (Fragoso, *PhD thesis*, 2020; Rivera-Martin, *PhD thesis*, 2017).

We have shown that APC/C^{FZR-1} is kept inactive mainly because of the activity of CYE-1/CDK-2, which most likely phosphorylates FZR-1. The decrease of CYE-1/CDK-2 activity once cells enter meiosis and the increase in the FZR-1 levels resulted in the peak of APC/C^{FZR-1}-mediated degradation observed for MES-4 and MES-3. The decrease in CYE-1/CDK-2 activity was previously attributed to the activity of the ubiquitin ligase SCF^{PROM-1}(Mohammad et al., 2018). However, additional factors were claimed for the degradation of CYE-1 because the analysis of germlines from *prom-1* mutants or *prom-1* RNAi showed that CYE-1 was still sharply degraded once cells reached the transition zone. It was proposed that this additional factor was GLD-1, inhibiting *cye-1* translation (Biedermann et al., 2009). In this work, we proposed a modified model in which CYE-1 is promoted for degradation by the joint activity of SCF^{PROM-1} and APC/C^{FZR-1}. CYE-1 has multiple APC/C^{FZR-1} recognition motifs (one KEN-box and one high-scoring D-box, under GPS-Algorithm), and we showed that the mutation of these recognition motifs fully impairs CYE-1 degradation when *prom-1* is silenced (**Figure 3.13**). Furthermore, in double *gld-1* + *prom-1* silenced gonads, we observed a band of CYE-1 down-regulation, coinciding with the transition to meiosis. Strikingly, when we repeated the same *gld-1* + *prom-1* silencing using a *cye-1* allele with KEN-box and D-box mutated, this band disappeared, indicating that it was the result of the activity of the APC/C^{FZR-1} complex (**Figure 3.13C**). Our current model, supported by the data, is that both SCF^{PROM-1} and APC/C^{FZR-1} promote CYE-1 for degradation and that the GLD-1 activity, once cells enter meiosis, ensures that CYE-1 levels stay low by repressing *cye-1* mRNA translation.

Interestingly, we have found that another cyclin, CYA-1 was present in several cell rows just before cells acquired the crescent-shaped nuclei appearance, and afterward, its levels abruptly decreased (**Figure 3.17**). This CYA-1 downregulation was eliminated by *fzr-1* RNAi or by mutation of its KEN-box and D-box motifs (**Figure 3.15**), indicating that CYA-1 was an exclusive substrate of APC/C^{FZR-1} in the transition from mitosis to meiosis. We also observed that CYA-1 levels were maintained a couple of rows after CYE-1 levels started to decrease. Because CYA-1 is promoted for degradation by APC/C^{FZR-1} and CYE-1 is submitted to degradation by both SCF^{PROM-1} and APC/C^{FZR-1}, this observation suggested that SCF^{PROM-1} activity occurs before APC/C^{FZR-1}. This observation was reproduced when MES-4 levels were compared in the same gonad with the CYE-1 levels (**Figure 3.18**). Strikingly, in conditions of impaired SCF^{PROM-1} activity (by silencing *prom-1*), the cells expressing CYA-1 and CYE-1 overlap, suggesting that SCF^{PROM-1} acts before (spatiotemporally) and upstream of APC/C^{FZR-1} by initiating the degradation of FZR-1 inhibitor CYE-1.

While CYE-1 is a classic S-phase cyclin in other organisms, CYA-1 is an S/G2 phase cyclin (Desdouets et al., 1995). This correlates with the spatio-temporal succession of CYE-1 and CYA-1 occurring in the transition from mitosis to meiosis in the *C. elegans* germline. The role of CYA-1 in the germline is unknown. In contrast to its essential activity in embryos (where its loss of function seems to be lethal), *cya-1* silencing seems not to cause an evident defect in the germline (**Figure 3.3**). In other systems, like *Xenopus* oocytes, CYA-1 was involved in meiosis prophase I arrest (Lenka et al., 2020). The study of the role of CYA-1 in the *C. elegans* germline must be continued in the future. However, one possibility is that CYA-1 was acting as a buffer, maintaining CDK activity high temporally while CYE-1 is degraded by SCF^{PROM-1} and therefore avoiding a premature activation of APC/C^{FZR-1} during the transition into meiosis prophase I. The construction of conditional knock-out alleles of *cya-1* could be helpful to understand his function in the germline fully.

The observed APC/C^{FZR-1} upregulation in early meiosis was not exclusively attributable to the decrease in the levels of CYE-1. We have observed that in gonads where CYE-1 was stabilized throughout the germline (*prom-1* is silenced

+ *cye-1[KEN-box mut][D-box mut]* allele), the rise in APC/C^{FZR-1} activity was still detected (**Figure 3.14**) , indicating additional factors upregulating APC/C^{FZR-1}.

To search for these proposed additional factors, we carried out an educated RNAi screening in a *prom-1(ok1140)* mutant. We tested potential candidates such as phosphatases which in other organisms counteract the CDK phosphorylation of Cdh1/Fzr1 and other factors involved in the transition to meiosis. We found that silencing *gld-2* (encoding a polyA polymerase) in *prom-1(ok1140)* impaired APC/C^{FZR-1} activity and caused the MES-4 presence throughout pachytene (**Figure 3.19**). Interestingly, GLD-2, GLD-1, and SCF^{PROM-1} were proposed to be the three main pathways causing entry into meiosis (Mohammad et al., 2018).

The proposed role of GLD-2 in promoting APC/C^{FZR-1} activity is supported by pieces of evidence. FZR-1 protein levels were maintained low in the mitotic zone due to FBF activity but had a peak of expression in the transition zone to meiosis, which we believe was caused by GLD-2. Interestingly mRNAs repressed by FBFs are described to be later activated by polyA polymerase GLD-2. This is the case, for instance, of GLD-1 mRNA (Suh et al., 2006). One appealing hypothesis proposed in the study of GLD-1 was the involvement of GLD-2 in the activating mRNA role of FBF proteins: FBF represses mRNAs in the mitotic zone but later in the transition to meiosis, FBF proteins partner with factors such as GLD-2 and GLD-3 activating the translation of the same mRNAs (Suh et al., 2009). We believe that fzr-1 mRNA translation is submitted by a similar regulation: *fzr-1* mRNA 3' UTR is repressed mitotically by FBF, but silencing *fbf* also lowers the activation of the translation of the *fzr-1* 3' UTR reporter in meiosis. In addition, we observed that silencing *gld-2* also partially lowered the peak of expression in meiosis of the *fzr-1* 3' UTR reporter, suggesting positive interaction between GLD-2 and *fzr-1* 3' UTR (**Figure 3.20**).

To reinforce our hypothesis about GLD-2 interacting with *fzr-1* 3' UTR to promote the translation of FZR-1 at the transition zone, we created an allele of *fzr-1* which has swapped the whole 3' UTR with *cye-1* 3' UTR. We chose *cye-1* 3' UTR for two reasons: (1) We have observed that described "neutral" 3' UTR such as *tbb-2* 3' UTR resulted in a very low expression when fused to ORF encoding germline proteins (like the case of MES-3 (Fragoso, *PhD thesis*, 2020)

and therefore we worried that this could also be the case with *fzr-1;* (2) we observed that a *cye-1* 3' UTR reporter showed a high GFP expression in the distal mitotic region, while resulted in a deficient expression in meiosis (consequently to its targeting by GLD-1 (Biedermann et al., 2009)), this was the opposite pattern of expression observed for *fzr-1* 3' UTR reporter. Strikingly, the use of this *fzr-1* allele together with a *prom-1* mutant did not replicate the *gld-2* silencing + *prom-1* knockdown concerning the activity of APC/C^{FZR1}, indicating that GLD-2 was promoting APC/C^{FZR-1} activity by additional indirect ways. Supporting this suggestion, we have found that silencing *cki-2* over *prom-1(ok1140)*; *Pfzr-1::fzr-1::cye-1 3' UTR* replicated MES-4 pachytene invasion (APC/C^{FZR-1} downregulation) also observed with *gld-2* silencing (**Figure 3.21**). These results led us to propose that *cki-2* could be an additional target of GLD-2 promoting APC/C^{FZR-1} activity. CKI-2 is a CDK inhibitor of the family CIP/KIP and is the one mainly expressed in the *C. elegans* germline (Buck et al., 2009). CIP/KIP family work by directly inhibiting Cyclin E-CDK2 complex activity in other organisms (Polyak et al., 1994; Reynaud et al., 1999; Harper et al., 1993). Interestingly, CKI-2 is negatively regulated by FBF in the mitotic region (Kalchhauser et al., 2011), coinciding with high CYE-1/CDK-2 activity and low APC/C^{FZR-1} activity in the mitotic region. As stated before, mRNAs negatively regulated by FBF proteins are prone to be later activated by GLD-2: this happens with *gld-1* (Suh et al., 2009) and as we propose here in *fzr-1* (**Figure 3.10 and 3.20**). Our results also situate *cki-2* downstream of GLD-2, and interestingly, *prom-1* seems to be downregulated by FBF in the mitotic zone (Fox et al., 2011; Mohammad et al., 2018) and could be upregulated by GLD-2 in meiosis. This way, FBF/GLD-2 mRNA regulation network could work around maintaining high CYE-1/CDK activity in mitosis and low CYE-1/CDK activity after meiosis entry. In mitosis: (1) FBF proteins repress *gld-1* (Suh et al., 2009), promoting *cye-1* translation; (2) FBF repress CDK inhibitor *cki-2* (Kalchhauser et al., 2011); (3) FBF repress *prom-1* which inhibits CYE-1 degradation by SCF^{PROM-1} (Fox et al., 2011; Mohammad et al., 2018); (4) FBF repress *fzr-1* (**Figure 3.7, Figure 3.9**) which inhibits CYE-1 degradation by APC/C^{FZR-1}. In early meiosis, FBF mRNA repression activity fades away, and GLD-2 activation acts on *fzr-1* (**Figure 3.20 and 3.21**) and *gld-1* (Suh et al., 2009). We speculate that this could also be the

case for *prom-1* and *cki-2*. Therefore, we would like to propose that GLD-2 activation ensures a switch in the cell cycle, from high CDK activity to low CDK activity that could be necessary to maintain meiosis prophase I arrest.

Remarkably, GLD-2-pathway defective mutants have proximal tumors due to defective oogenesis, and we observed the same phenotype in some germlines under the background *prom-1 (ok1140*); *fzr-1::cye-1 3' UTR* + *cki-2* silencing (in which APC/C^{FZR-1} is downregulated), suggesting that *prom-1, fzr-1,* and *cki-2* could be some of the main targets of GLD-2 driving the Gld-2 tumorous phenotype.

Nonetheless, we must acknowledge the possibility that GLD-2 could enhance the translation of other factors that directly or indirectly promote APC/C^{FZR-1}. In the meiotic cycle, BubR1 stabilizes Cdh1/FZR-1 to ensure prophase I arrest and correct oogenesis (Homer et al., 2009). Remarkably, in C. elegans, the BubR1 homolog MAD-3 is an *in silico* target of GLD-2.

APC/C^{FZR-1} is tightly and redundantly regulated in the germline, but why? In this work, we described two new targets of APC/C^{FZR-1} in the *C. elegans* germline: CYE-1 and CYA-1, and in previous theses (Fragoso, 2020; Rivera-Martín, 2018) chromatin regulators MES-3 and MES-4 were described as targets. CYE-1, MES-3, and MES-4 are proteins highly expressed in the mitotic region of the germline, and knocking them down cause cell cycle arrest and sterility (for *cye-1*), and maternal sterility (for *mes-3* and *mes-4*), the tight downregulation of APC/C^{FZR-1} in the mitotic zone protects the cells from losing this germline stem cells drivers. Afterwards, in early meiosis, APC/C^{FZR-1} contributes to degrading these factors. For CYE-1 and CYA-1 degradation, the reasons seem straightforward. Meiosis prophase I is a specialized cell cycle arrest that needs low or at least not high CDK activity (Homer, 2013). However, it is not fully clear yet why APC/C^{FZR-1} must degrade chromatin regulators MES-3 and MES-4 before pachytene, as non-APC/C^{FZR-1} recognizable *mes-3(KEN-box)* and *mes-4(KEN-box)* mutants do not have evident phenotype. One hypothesis is that MES-3, MES-4, and possibly other factors must be degraded to permit the transcriptional program changes in early meiosis that cause oocyte differentiation.

Surprisingly *fzr-1* silencing or hypomorphic alleles such as *fzr-1(ku298)* (Fay et al., 2002) do not show an evident phenotype in the germline. Different

non-exclusive reasons could explain this: (1) the high level of redundancy in the germline (for example, both SCF^{PROM-1} and APC/C^{FZR-1} are E3 ubiquitin ligases that can target CYE-1 for degradation), or (2) it could be that even low levels of the protein or even a hypomorphic allele can alleviate more severe phenotypes. The complete deletion allele, *fzr-1(sal19)* shows strong phenotypes in the germline, with germlines being smaller, or not having a clear transition zone under DAPI staining and, in some cases, showing defective oocytes. Nevertheless, because *fzr-1* total loss of function has a strong role in somatic gonad, we cannot conclude that this is due to exclusive defects in the germline. Further studies on the *fzr-1* role are being carried out to clarify its importance in germline differentiation and the transcriptional program switch in gametogenesis.

Finally, although APC/C^{FZR-1} is upregulated and active in early meiosis, in mid and late pachytene FZR-1 protein levels drop. We showed that FZR-1 degradation is dependent on APC/C activity but is not dependent on coactivator FZY-1/CDC20, suggesting that APC/C^{FZR-1} could be promoting the degradation of the own FZR-1 subunit via his D-box **(Figure 3.23)**. This agrees with what was shown in mammals: $APC/C^{CDH1/FZR-1}$ can catalyze CDH1/FZR-1 destruction (Listovsky et al., 2004). One hypothesis of why this has to happen is related to $APC/C^{FZY-1/CDC20}$. APC/C^{CDH1} can degrade CDC20 in mammals (Thornton & Toczyski, 2003) and APC/C^{CDC20} seems to play an essential role in metaphase I of meiosis (Reviewed in (Homer, 2013). Although we do not know yet if FZY-1/CDC20 is a target of $APC/C^{FZR-1/CDH1}$ in *C. elegans*, if that is the case, it could be necessary that FZR-1 is degraded to allow the presence and activity of APC/C^{FZY-1} in metaphase I. There is another similar possibility to contemplate: In mitosis, APC/C^{FZR-1} complex works in G1 (after $APC/C^{FZY-1/CDC20}$) but in meiosis, the complex seems to work in prophase I ("G2-like" phase – before $APC/C^{FZY-1/CDC20}$ role in metaphase I), this could require FZR-1 degradation after his activity to prevent the interference with other putative APC/C^{FZR-1} targets that are required for G2/M transition, for example, promoters of CDK activity, which is necessary to activate $APC/C^{FZY-1/CDC20}$ (Kraft et al., 2003).

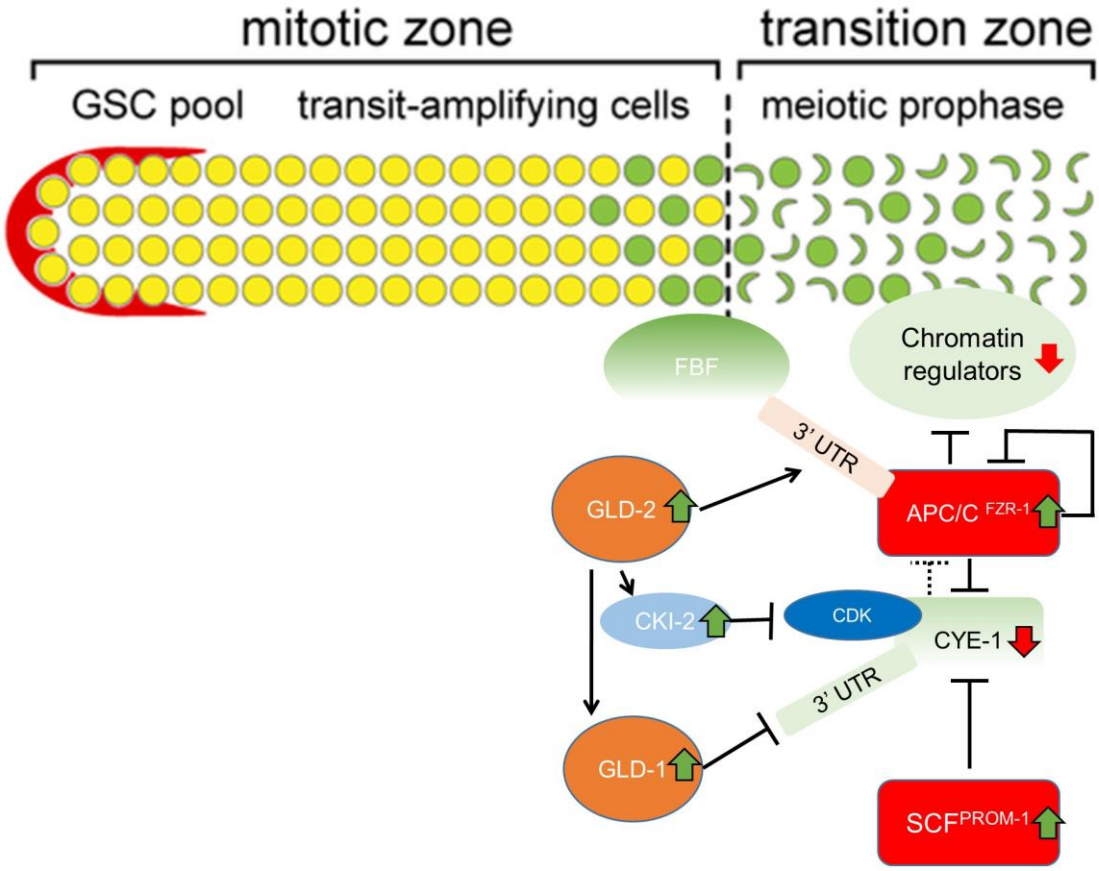

Figure 4.2: APC/C^{FZR-1} upregulation in early meiosis

CONCLUSIONS

5 CONCLUSIONS

1. In *C. elegans* germline, FZR-1 is present in the mitotic region with gradually increasing protein levels from distal to proximal and reaches a peak of expression in the mitosis-meiosis transition zone. However, the APC/C^{FZR-1} activity is impaired in the mitotic region to allow the presence of chromatin regulators MES-3 and MES-4 and possibly other targets.
2. Cyclin E inhibits APC/C^{FZR-1} activity throughout the mitotic region.
3. The niche signaling, the Notch Pathway, inhibits *fzr-1* expression in the mitotic region. This is caused by the interaction of RNA-binding-proteins FBF with *fzr-1* 3' UTR.
4. CYE-1 is degraded by SCF^{PROM-1} and APC/C^{FZR-1} in the germline. SCF^{PROM-1} promotes APC/C^{FZR-1} activity by initiating the degradation of CYE-1. But impairing CYE-1 degradation is not enough to impede APC/C^{FZR-1} activity.
5. PolyA polymerase GLD-2 promotes APC/C^{FZR-1} activity directly interacting with *fzr-1* 3' UTR and indirectly by enhancing translation of other factors. Our results suggest that the main downstream GLD-2 factor upregulating APC/C^{FZR-1} is CKI-2.
6. APC/C^{FZR-1} is upregulated in meiosis I prophase, downstream of meiotic pathways SCF^{PROM-1} and GLD-2. The spatiotemporal point of activation is observed thanks to Cyclin A-1. CYA-1 is present in the last rows of the mitotic zone co-localizing with CYE-1 until this one is degraded by SCF^{PROM-1}. After CYE-1 is degraded, CYA-1 is still present until APC/C^{FZR-1} starts its activity.
7. APC/C^{FZR-1} promotes the degradation of MES-3, MES-4 and CYA-1 in meiosis I prophase and can recognize and degrade CYE-1 if SCF^{PROM-1} is impaired. MES-3 and MES-4 are recognized through KEN-box motifs, however, CYE-1 and CYA-1 are recognized through both KEN-box and D-box motifs.
8. APC/C^{FZR-1} mediates FZR-1 degradation through the D-box motif to restrict his presence in pachytene.

REFERENCES

6 REFERENCES

Albert Hubbard, E. J., & Schedl, T. (2019). Biology of the caenorhabditis elegans germline stem cell system. *Genetics*, *213*(4), 1145–1188. https://doi.org/10.1534/genetics.119.300238

Aman, P., Douglas, F. P., Peggy, L. K. C., Ipsita, M., Anne, R. R., Sarah, L. C., Marvin, W., & Judith, K. (2016). The PUF binding landscape in metazoan germ cells. *Rna*, *22*(7), 1026–1043. https://doi.org/10.1261/rna.055871.116

Austin, J., & Kimble, J. (1987). glp-1 Is required in the germ line for regulation of the decision between mitosis and meiosis in C. elegans. *Cell*, *51*(4), 589–599. https://doi.org/10.1016/0092-8674(87)90128-0

Barstead, R. J., Kleiman, L., & Waterston, R. H. (1991). Cloning, sequencing, and mapping of an α-actinin gene from the nematode Caenorhabditis elegans. *Cell Motility and the Cytoskeleton*, *20*(1), 69–78. https://doi.org/10.1002/cm.970200108

Bashir, T., Dorello, H. V., Amador, V., Guardavaccaro, D., & Pagano, M. (2004). Control of the SCFSkp2-Cks1 ubiquitin ligase by the APC/C Cdh1 ubiquitin ligase. *Nature*, *428*(6979), 190–193. https://doi.org/10.1038/nature02330

Baudrimont, A., Paouneskou, D., Mohammad, A., Lichtenberger, R., Blundon, J., Kim, Y., Hartl, M., Falk, S., Schedl, T., & Jantsch, V. (2022). Release of CHK-2 from PPM-1.D anchorage schedules meiotic entry. *Science Advances*, *8*(7), 1–18. https://doi.org/10.1126/sciadv.abl8861

Baugh, L. R. (2013). To grow or not to grow: Nutritional control of development during Caenorhabditis elegans L1 Arrest. *Genetics*, *194*(3), 539–555. https://doi.org/10.1534/genetics.113.150847

Bender, L. B., Suh, J., Caroll, C. R., Fong, Y., Fingerman, I. M., Briggs, S. D., Cao, R., Zhang, Y., Reinke, V., & Strome, S. (2006). MES-4: An autosome-associated histone methyltransferase that participates in silencing the X chromosomes in the C. elegans germ line. *Development*, *133*(19), 3907–3917. https://doi.org/10.1242/dev.02584

Benmaamar, R., & Pagano, M. (2005). Involvement of the SCF complex in the

control of Cdh1 degradation in S-phase. *Cell Cycle*, *4*(9), 1230–1232. https://doi.org/10.4161/cc.4.9.2048

Biedermann, B., Wright, J., Senften, M., Kalchhauser, I., Sarathy, G., Lee, M. H., & Ciosk, R. (2009). Translational Repression of Cyclin E Prevents Precocious Mitosis and Embryonic Gene Activation during C. elegans Meiosis. *Developmental Cell*, *17*(3), 355–364. https://doi.org/10.1016/j.devcel.2009.08.003

Blanco, M. A., Pelloquin, L., & Moreno, S. (2001). Fission yeast mfr1 activates APC and coordinates meiotic nuclear division with sporulation. *Journal of Cell Science*, *114*(11), 2135–2143. https://doi.org/10.1242/jcs.114.11.2135

Botta, S., Prisco, N. De, Chemiakine, A., Cabaj, M., Patel, P., & Doron-, E. (2022). *Dosage sensitivity in Pumilio1-related phenotypes reflects distinct disease mechanisms*.

Brenner, J. L., & Schedl, T. (2016). Germline stem cell differentiation entails regional control of cell fate regulator GLD-1 in Caenorhabditis elegans. *Genetics*, *202*(3), 1085–1103. https://doi.org/10.1534/genetics.115.185678

Buck, S. H., Chiu, D., & Saito, R. M. (2009). The cyclin-dependent kinase inhibitors, cki-1 and cki-2, act in overlapping but distinct pathways to control cell cycle quiescence during C. elegans development. *Cell Cycle*, *8*(16), 2613–2620. https://doi.org/10.4161/cc.8.16.9354

Byrd, D. T., & Kimble, J. (2009). Scratching the niche that controls Caenorhabditis elegans germline stem cells. *Seminars in Cell and Developmental Biology*, *20*(9), 1107–1113. https://doi.org/10.1016/j.semcdb.2009.09.005

Byrd, D. T., Knobel, K., Affeldt, K., Crittenden, S. L., & Kimble, J. (2014). A DTC niche plexus surrounds the germline stem cell pool in Caenorhabditis elegans. *PLoS ONE*, *9*(2). https://doi.org/10.1371/journal.pone.0088372

Cappell, S. D., Mark, K. G., Garbett, D., Pack, L. R., Rape, M., & Meyer, T. (2018). EMI1 switches from being a substrate to an inhibitor of APC/CCDH1 to start the cell cycle. *Nature*, *558*(7709), 313–317. https://doi.org/10.1038/s41586-018-0199-7

Ceol, C. J., & Horvitz, H. R. (2001). dpl-1 DP and efl-1 E2F act with lin-35 Rb to

antagonize Ras signaling in C. elegans vulval development. *Molecular Cell*, *7*(3), 461–473. https://doi.org/10.1016/S1097-2765(01)00194-0

Chao, W. C. H., Kulkarni, K., Zhang, Z., Kong, E. H., & Barford, D. (2012). Structure of the mitotic checkpoint complex. *Nature*, *484*(7393), 208–213. https://doi.org/10.1038/nature10896

Chen, J., Mohammad, A., Pazdernik, N., Huang, H., Bowman, B., Tycksen, E., & Schedl, T. (2020). GLP-1 Notch-LAG-1 CSL control of the germline stem cell fate is mediated by transcriptional targets lst-1 and sygl-1. In *PLoS Genetics* (Vol. 16, Issue 3). https://doi.org/10.1371/journal.pgen.1008650

Christopher Merritt, Rasoloson, D., Ko, D., & Seydoux1, G. (2008). 3' UTRs are the primary regulators of gene expression in the C. elegans germline. *Current Biology*, *18*(19). https://doi.org/10.1038/jid.2014.371

Chu, T., Henrion, G., Haegeli, V., & Strickland, S. (2001). Cortex, a drosophila gene required to complete oocyte meiosis, is a member of the Cdc20/fizzy protein family. *Genesis*, *29*(3), 141–152. https://doi.org/10.1002/gene.1017

Cinquin, O., Crittenden, S. L., Morgan, D. E., & Kimble, J. (2010). Progression from a stem cell-like state to early differentiation in the C. elegans germ line. *Proceedings of the National Academy of Sciences of the United States of America*, *107*(5), 2048–2053. https://doi.org/10.1073/pnas.0912704107

Cockrum, C. S., & Strome, S. (2022). Maternal H3K36 and H3K27 HMTs protect germline development via regulation of the transcription factor LIN-15B. *ELife*, *11*, 1–31. https://doi.org/10.7554/eLife.77951

Cooper, K. F., Mallory, M. J., Egeland, D. B., Jarnik, M., & Strich, R. (2000). Ama1p is a meiosis-specific regulator of the anaphase promoting complex/cyclosome in yeast. *Proceedings of the National Academy of Sciences of the United States of America*, *97*(26), 14548–14553. https://doi.org/10.1073/pnas.250351297

Corsi, A. K., Wightman, B., & Chalfie, M. (2015). A Transparent window into biology: A primer on Caenorhabditis elegans. *WormBook : The Online Review of C. Elegans Biology*, 1–31. https://doi.org/10.1895/wormbook.1.177.1

Crane, R., Kloepfer, A., & Ruderman, J. V. (2004). Requirements for the destruction of human Aurora-A. *Journal of Cell Science*, *117*(25), 5975–5983. https://doi.org/10.1242/jcs.01418

Crittenden, S. L., Seidel, H. S., & Kimble, J. (2017). Analysis of the C. elegans germline stem cell pool. In *Methods in Molecular Biology* (Vol. 1463, Issue January). https://doi.org/10.1007/978-1-4939-4017-2_1

Da Fonseca, P. C. A., Kong, E. H., Zhang, Z., Schreiber, A., Williams, M. A., Morris, E. P., & Barford, D. (2011). Structures of APC/CCdh1 with substrates identify Cdh1 and Apc10 as the D-box co-receptor. *Nature*, *470*(7333), 274–280. https://doi.org/10.1038/nature09625

Delgado-Esteban, M., García-Higuera, I., Maestre, C., Moreno, S., & Almeida, A. (2013). APC/C-Cdh1 coordinates neurogenesis and cortical size during development. *Nature Communications*, *4*. https://doi.org/10.1038/ncomms3879

Desdouets, C., Sobczak-Thépot, J., Murphy, M., & Bréchot, C. (1995). Cyclin A: function and expression during cell proliferation. *Progress in Cell Cycle Research*, *1*, 115–123. https://doi.org/10.1007/978-1-4615-1809-9_9

Dickinson, D. J., Pani, A. M., Heppert, J. K., Higgins, C. D., & Goldstein, B. (2015). Streamlined genome engineering with a self-excising drug selection cassette. *Genetics*, *200*(4), 1035–1049. https://doi.org/10.1534/genetics.115.178335

Djabrayan, N. J. V., & Casanova, J. (2016). Snoo and Dpp Act as Spatial and Temporal Regulators Respectively of Adult Progenitor Cells in the Drosophila Trachea. *PLoS Genetics*, *12*(3), 1–15. https://doi.org/10.1371/journal.pgen.1005909

Eckmann, C. R., Crittenden, S. L., Suh, N., & Kimble, J. (2004). GLD-3 and control of the mitosis/meiosis decision in the germline of Caenorhabditis elegans. *Genetics*, *168*(1), 147–160. https://doi.org/10.1534/genetics.104.029264

Eguren, M., Porlan, E., Manchado, E., García-Higuera, I., Cañamero, M., Fariñas, I., & Malumbres, M. (2013). The APC/C cofactor Cdh1 prevents

replicative stress and p53-dependent cell death in neural progenitors. *Nature Communications*, *4*. https://doi.org/10.1038/ncomms3880

Fay, D. S., Keenan, S., & Han, M. (2002). fzr-1 and lin-35/Rb function redundantly to control cell proliferation in C. elegans as revealed by a nonbiased synthetic screen. *Genes and Development*, *16*(4), 503–517. https://doi.org/10.1101/gad.952302

Fielenbach, N., & Antebi, A. (2008). C. elegans dauer formation and the molecular basis of plasticity. *Genes and Development*, *22*(16), 2149–2165. https://doi.org/10.1101/gad.1701508

Fox, P. M., Vought, V. E., Hanazawa, M., Lee, M. H., Maine, E. M., & Sched, T. (2011). Cyclin e and CDK-2 regulate proliferative cell fate and cell cycle progression in the C. elegans germline. *Development*, *138*(11), 2223–2234. https://doi.org/10.1242/dev.059535

Fragoso-Luna, A. (2020). The role of APC/C^{FZR-1} in the functionality of the gonad of Caenorhabditis elegans. *PhD thesis*.

Franks, J. L., Martinez-Chacin, R. C., Wang, X., Tiedemann, R. L., Bonacci, T., Choudhury, R., Bolhuis, D. L., Enrico, T. P., Mouery, R. D., Damrauer, J. S., Yan, F., Harrison, J. S., Major, M. Ben, Hoadley, K. A., Suzuki, A., Rothbart, S. B., Brown, N. G., & Emanuele, M. J. (2020). In silico APC/C substrate discovery reveals cell cycle-dependent degradation of UHRF1 and other chromatin regulators. In *PLoS Biology* (Vol. 18, Issue 12). https://doi.org/10.1371/journal.pbio.3000975

Frøkjær-Jensen, C., Davis, M. W., Ailion, M., & Jorgensen, E. M. (2012). Improved Mos1-mediated transgenesis in C. elegans. *Nature Methods*, *9*(2), 117–118. https://doi.org/10.1038/nmeth.1865

Frøkjær-Jensen, C., Wayne Davis, M., Hopkins, C. E., Newman, B. J., Thummel, J. M., Olesen, S. P., Grunnet, M., & Jorgensen, E. M. (2008). Single-copy insertion of transgenes in Caenorhabditis elegans. *Nature Genetics*, *40*(11), 1375–1383. https://doi.org/10.1038/ng.248

Fujita, M., Takeshita, H., & Sawa, H. (2007). Cyclin E and CDK2 repress the terminal differentiation of quiescent cells after asymmetric division in C.

elegans. *PLoS ONE*, *2*(5), 1–8. https://doi.org/10.1371/journal.pone.0000407

Fukushima, H., Ogura, K., Wan, L., Lu, Y., Li, V., Gao, D., Liu, P., Lau, A. W., Wu, T., Kirschner, M. W., Inuzuka, H., & Wei, W. (2013). SCF-mediated Cdh1 degradation defines a negative feedback system that coordinates cell-cycle progression. *Cell Reports*, *4*(4), 803–816. https://doi.org/10.1016/j.celrep.2013.07.031

Gao, S. wei, & Liu, F. (2019). Novel insights into cell cycle regulation of cell fate determination. *Journal of Zhejiang University: Science B*, *20*(6), 467–475. https://doi.org/10.1631/jzus.B1900197

Garvin, C., Holdeman, R., & Strome, S. (1998). The phenotype of mes-2, mes-3, mes-4 and mes-6, maternal-effect genes required for survival of the germline in Caenorhabditis elegans, is sensitive to chromosome dosage. *Genetics*, *148*(1), 167–185. https://doi.org/10.1093/genetics/148.1.167

Gaydos, L. J., Rechtsteiner, A., Egelhofer, T. A., Carroll, C. R., & Strome, S. (2012). Antagonism between MES-4 and Polycomb Repressive Complex 2 Promotes Appropriate Gene Expression in C. elegans Germ Cells. *Cell Reports*, *2*(5), 1169–1177. https://doi.org/10.1016/j.celrep.2012.09.019

Goetsch, P. D., Garrigues, J. M., & Strome, S. (2017). Loss of the Caenorhabditis elegans pocket protein LIN-35 reveals MuvB's innate function as the repressor of DREAM target genes. *PLoS Genetics*, *13*(11), 1–25. https://doi.org/10.1371/journal.pgen.1007088

Gouda, K., Matsunaga, Y., Iwasaki, T., & Kawano, T. (2010). An altered method of feeding RNAi that knocks down multiple genes simultaneously in the nematode Caenorhabditis elegans. *Bioscience, Biotechnology and Biochemistry*, *74*(11), 2361–2365. https://doi.org/10.1271/bbb.100579

Hanahan, D. (1983). Studies on transformation of Escherichia coli with plasmids. *Journal of Molecular Biology*, *166*(4), 557–580. https://doi.org/10.1016/S0022-2836(83)80284-8

Hansen, D., Wilson-Berry, L., Dang, T., & Schedl, T. (2004). Control of the proliferation versus meiotic development decision in the C. elegans germline

through regulation of GLD-1 protein accumulation. *Development*, *131*(1), 93–104. https://doi.org/10.1242/dev.00916

Hao, B., Zheng, N., Schulman, B. A., Wu, G., Miller, J. J., Pagano, M., & Pavletich, N. P. (2005). Structural basis of the Cks1-dependent recognition of p27 Kip1 by the SCF Skp2 ubiquitin ligase. *Molecular Cell*, *20*(1), 9–19. https://doi.org/10.1016/j.molcel.2005.09.003

Haupt, K. A., Law, K. T., Enright, A. L., Kanzler, C. R., Shin, H., Wickens, M., & Kimble, J. (2020). A PUF hub drives self-renewal in caenorhabditis elegans Germline stem cells. *Genetics*, *214*(1), 147–161. https://doi.org/10.1534/genetics.119.302772

He, J., Chao, W. C. H., Zhang, Z., Yang, J., Cronin, N., & Barford, D. (2013). Article Insights into Degron Recognition by APC / C Coactivators from the Structure of an Acm1-Cdh1 Complex. *Molecular Cell*, *50*(5), 649–660. https://doi.org/10.1016/j.molcel.2013.04.024

Henderson, S. T., Gao, D., Lambie, E. J., & Kimble, J. (1994). lag-2 may encode a signaling ligand for the GLP-1 and LIN-12 receptors of C. elegans. *Development*, *120*(10), 2913–2924. https://doi.org/10.1242/dev.120.10.2913

Hodgkin, J., Horvitz, H. R., & Brenner, S. (1979). Nondisjunction Mutants of the Nematode Caenorhabditis Elegans . *Genetics*, *91*(1), 67–94. https://doi.org/10.1093/genetics/91.1.67

Holdeman, R., Nehrt, S., & Strome, S. (1998). MES-2, a maternal protein essential for viability of the germline in Caenorhabditis elegans, is homologous to a Drosophila Polycomb group protein. *Development*, *125*(13), 2457–2467. https://doi.org/10.1242/dev.125.13.2457

Holt, L. J., Krutchinsky, A. N., & Morgan, D. O. (2008). Positive feedback sharpens the anaphase switch. *Nature*, *454*(7202), 353–357. https://doi.org/10.1038/nature07050

Homer, H. (2013). The APC/C in female mammalian meiosis i. *Reproduction*, *146*(2). https://doi.org/10.1530/REP-13-0163

Homer, H., Gui, L., & Carroll, J. (2009). *A Spindle Assembly Checkpoint Protein*

Functions in Prophase I Arrest and Prometaphase Progression. *326*(November), 991–994.

Jacobs, H. W., Richter, D. O., Venkatesh, T. R., & Lehner, C. F. (2002). Completion of Mitosis Requires Neither fzr/rap nor fzr2, a Male Germline-Specific Drosophila Cdh1 Homolog. *Trends in Biochemical Sciences*, *12*, 1435–1441. https://doi.org/10.1016/s0968-0004(05)00043-5

Jaquenoud, M., Van Drogen, F., & Peter, M. (2002). Cell cycle-dependent nuclear export of Cdh1p may contribute to the inactivation of APC/CCdh1. *EMBO Journal*, *21*(23), 6515–6526. https://doi.org/10.1093/emboj/cdf634

Jeong, J., Verheyden, J. M., & Kimble, J. (2011). Cyclin E and Cdk2 control GLD-1, the mitosis/meiosis decision, and germline stem cells in Caenorhabditis elegans. *PLoS Genetics*, *7*(3). https://doi.org/10.1371/journal.pgen.1001348

Jillian A. Pesin and Terry L. Orr-Weaver. (2010). *Regulation of APC/C Activators in Mitosis and Meiosis Jillian*. *48*(Suppl 2), 1–6. https://doi.org/10.1097/MPG.0b013e3181a15ae8.Screening

Kadyk, L. C., & Kimble, J. (1998). Genetic regulation of entry into meiosis in Caenorhabditis elegans. *Development*, *125*(10), 1803–1813. https://doi.org/10.1242/dev.125.10.1803

Kalchhauser, I., Farley, B. M., Pauli, S., Ryder, S. P., & Ciosk, R. (2011). FBF represses the Cip/Kip cell-cycle inhibitor CKI-2 to promote self-renewal of germline stem cells in C. elegans. *EMBO Journal*, *30*(18), 3823–3829. https://doi.org/10.1038/emboj.2011.263

Kamath, R. S., Martinez-Campos, M., Zipperlen, P., Fraser, A. G., & Ahringer, J. (2001). Effectiveness of specific RNA-mediated interference through ingested double-stranded RNA in Caenorhabditis elegans. *Genome Biology*, *2*(1), 1–10.

Kamath, Ravi S., & Ahringer, J. (2003). Genome-wide RNAi screening in Caenorhabditis elegans. *Methods*, *30*(4), 313–321. https://doi.org/10.1016/S1046-2023(03)00050-1

Keck, J. M., Summers, M. K., Tedesco, D., Ekholm-Reed, S., Chuang, L. C., Jackson, P. K., & Reed, S. I. (2007). Cyclin E overexpression impairs

progression through mitosis by inhibiting APCCdh1. *Journal of Cell Biology*, *178*(3), 371–385. https://doi.org/10.1083/jcb.200703202

Kernan, J., Bonacci, T., & Emanuele, M. J. (2018). Who guards the guardian? Mechanisms that restrain APC/C during the cell cycle. *Biochimica et Biophysica Acta - Molecular Cell Research*, *1865*(12), 1924–1933. https://doi.org/10.1016/j.bbamcr.2018.09.011

Kershner, A. M., & Kimble, J. (2010). Genome-wide analysis of mRNA targets for Caenorhabditis elegans FBF, a conserved stem cell regulator. *Proceedings of the National Academy of Sciences of the United States of America*, *107*(8), 3936–3941. https://doi.org/10.1073/pnas.1000495107

Ketel, C. S., Andersen, E. F., Vargas, M. L., Suh, J., Strome, S., & Simon, J. A. (2005). Subunit Contributions to Histone Methyltransferase Activities of Fly and Worm Polycomb Group Complexes. *Molecular and Cellular Biology*, *25*(16), 6857–6868. https://doi.org/10.1128/mcb.25.16.6857-6868.2005

Kim, H., Ishidate, T., Ghanta, K. S., Seth, M., Conte, D., Shirayama, M., & Mello, C. C. (2014). A Co-CRISPR strategy for efficient genome editing in Caenorhabditis elegans. *Genetics*, *197*(4), 1069–1080. https://doi.org/10.1534/genetics.114.166389

Kimata, Y. (2019). APC/C Ubiquitin Ligase: Coupling Cellular Differentiation to G1/G0 Phase in Multicellular Systems. *Trends in Cell Biology*, *29*(7), 591–603. https://doi.org/10.1016/j.tcb.2019.03.001

Kimble, J. E., & White, J. G. (1981). On the control of germ cell development in Caenorhabditis elegans. *Developmental Biology*, *81*(2), 208–219. https://doi.org/10.1016/0012-1606(81)90284-0

Kimble, J, & Petcherski, A. G. (2000). LAG-3 is a putative transcriptional activator in the C. elegans Notch pathway. *Nature*, *405*(6784), 364–368.

Kimble, Judith, & Hirsh, D. (1979). The postembryonic cell lineages of the hermaphrodite and male gonads in Caenorhabditis elegans. *Developmental Biology*, *70*(2), 396–417. https://doi.org/10.1016/0012-1606(79)90035-6

Kimble, Judith, & Seidel, H. (2008). C. elegans germline stem cells and their niche. *StemBook*, 1–12. https://doi.org/10.3824/stembook.1.95.1.1

Kimble, Judith, & Simpson, P. (1997). The LIN-12/notch signaling pathway and its regulation. *Annual Review of Cell and Developmental Biology*, *13*, 333–361. https://doi.org/10.1146/annurev.cellbio.13.1.333

Kitamura, K., Maekawa, H., & Shimoda, C. (1998). *Fission Yeast Ste9 , a Homolog of Hct1 / Cdh1 and Fizzy- related , Is a Novel Negative Regulator of Cell Cycle Progression during G 1 -Phase*. *9*(May), 1065–1080.

Kocsisova, Z., Mohammad, A., Kornfeld, K., & Schedl, T. (2018). Cell cycle analysis in the c. Elegans germline with the thymidine analog edu. *Journal of Visualized Experiments*, *2018*(140), 1–15. https://doi.org/10.3791/58339

Koepp, D. M., Schaefer, L. K., Ye, X., & Elledge, S. J. (2001). *Koepp-et-al-2001*. *294*(October), 173–177.

Kraft, C., Herzog, F., Gieffers, C., Mechtler, K., Hagting, A., Pines, J., & Peters, J. M. (2003). Mitotic regulation of the human anaphase-promoting complex by phosphorylation. *EMBO Journal*, *22*(24), 6598–6609. https://doi.org/10.1093/emboj/cdg627

Kramer, E. R., Scheuringer, N., Podtelejnikov, A. V., Mann, M., & Peters, J. M. (2000). Mitotic regulation of the APC activator proteins CDC20 and CDH1. *Molecular Biology of the Cell*, *11*(5), 1555–1569. https://doi.org/10.1091/mbc.11.5.1555

Lavia, P., & Jansen-Dürr, P. (1999). E2F target genes and cell-cycle checkpoint control. *BioEssays*, *21*(3), 221–230. https://doi.org/10.1002/(SICI)1521-1878(199903)21:3<221::AID-BIES6>3.0.CO;2-J

Lenka, R., Tereza, P., Denisa, J., Da, J., & Michal, S. (2020). *Cyclin A1 in Oocytes Prevents Chromosome Segregation And Anaphase Entry*. 1–12. https://doi.org/10.1038/s41598-020-64418-1

Listovsky, T., Oren, Y. S., Yudkovsky, Y., Mahbubani, H. M., Weiss, A. M., Lebendiker, M., & Brandeis, M. (2004). Mammalian Cdh1/Fzr mediates its own degradation. *EMBO Journal*, *23*(7), 1619–1626. https://doi.org/10.1038/sj.emboj.7600149

Liu, L., Michowski, W., Inuzuka, H., Shimizu, K., Nihira, N. T., Chick, J. M., Li, N., Geng, Y., Meng, A. Y., Ordureau, A., Kołodziejczyk, A., Ligon, K. L.,

Bronson, R. T., Polyak, K., Harper, J. W., Gygi, S. P., Wei, W., & Sicinski, P. (2017). G1 cyclins link proliferation, pluripotency and differentiation of embryonic stem cells. *Nature Cell Biology*, *19*(3), 177–188. https://doi.org/10.1038/ncb3474

Liu, L., Michowski, W., Kolodziejczyk, A., & Sicinski, P. (2019). The cell cycle in stem cell proliferation, pluripotency and differentiation. *Nature Cell Biology*, *21*(9), 1060–1067. https://doi.org/10.1038/s41556-019-0384-4

Liu, X., Zong, W., Li, T., Wang, Y., Xu, X., Zhou, Z., & Wang, Z. (2017). The E3 ubiquitin ligase APC / C C dh1 degrades MCPH 1 after MCPH1-βTr CP 2-Cdc25A-mediated mitotic entry to ensure neurogenesis . *The EMBO Journal*, *36*(24), 3666–3681. https://doi.org/10.15252/embj.201694443

Liu, Z., Yuan, F., Ren, J., Cao, J., Zhou, Y., Yang, Q., & Xue, Y. (2012). GPS-ARM: Computational analysis of the APC/C recognition motif by predicting D-boxes and KEN-boxes. *PLoS ONE*, *7*(3), 1–9. https://doi.org/10.1371/journal.pone.0034370

Lukas, J., Herzinger, T., Hansen, K., Moroni, M. C., Resnitzky, D., Helin, K., Reed, S. I., & Bartek, J. (1997). Cyclin E-induced S phase without activation of the pRb/E2F pathway. *Genes and Development*, *11*(11), 1479–1492. https://doi.org/10.1101/gad.11.11.1479

Lukas, J., Parry, D., Aagaard, L., Mann, D. J., Bartkova, J., Strauss, M., Peters, G., & Bartek, J. (1995). Retinoblastoma-protein-dependent cell-cycle inhibition by the tumour suppressor p16. In *Nature* (Vol. 375, Issue 6531, pp. 503–506). https://doi.org/10.1038/375503a0

Maestre, C., Delgado-Esteban, M., Gomez-Sanchez, J. C., Bolaños, J. P., & Almeida, A. (2008). Cdk5 phosphorylates Cdh1 and modulates cyclin B1 stability in excitotoxicity. *EMBO Journal*, *27*(20), 2736–2745. https://doi.org/10.1038/emboj.2008.195

Marangos, P., Verschuren, E. W., Chen, R., Jackson, P. K., & Carroll, J. (2007). Prophase I arrest and progression to metaphase I in mouse oocytes are controlled by Emi1-dependent regulation of APCCdh1. *Journal of Cell Biology*, *176*(1), 65–75. https://doi.org/10.1083/jcb.200607070

Martins, T., Meghini, F., Florio, F., & Kimata, Y. (2017). The APC/C Coordinates Retinal Differentiation with G1 Arrest through the Nek2-Dependent Modulation of Wingless Signaling. *Developmental Cell*, *40*(1), 67–80. https://doi.org/10.1016/j.devcel.2016.12.005

Mohammad, A., Kara Vanden, Broek Christopher, W., Daryabeigi, A., Jantsch, V., Hansen, D., & Schedl, T. (2018). Initiation of Meiotic Development Is Controlled by. *Genetics*, *209*(August), 1197–1224.

Möröy, T., & Geisen, C. (2004). Cyclin E. *International Journal of Biochemistry and Cell Biology*, *36*(8), 1424–1439. https://doi.org/10.1016/j.biocel.2003.12.005

Nurse, P., Thuriaux, P., & Nasmyth, K. (1976). *Genetic Control of the Cell Division Cycle in the Fission Yeast Schizosaccharomyces pombe*. *178*, 167–178.

Pajalunga, D., & Crescenzi, M. (2004). Regulation of cyclin E protein levels through E2F-mediated inhibition of degradation. *Cell Cycle*, *3*(12), 1572–1578. https://doi.org/10.4161/cc.3.12.1279

Pal, D., Torres, A. E., Stromberg, B. R., Messina, A. L., Dickson, A. S., De, K., Willard, B., Venere, M., & Summers, M. K. (2020). Chk1-mediated phosphorylation of Cdh1 promotes the SCFβTRCP-dependent degradation of Cdh1 during S-phase and efficient cell-cycle progression. *Cell Death and Disease*, *11*(4), 1–15. https://doi.org/10.1038/s41419-020-2493-1

Papin, C., Rouget, C., Lorca, T., Castro, A., & Mandart, E. (2004). XCdh1 is involved in progesterone-induced oocyte maturation. *Developmental Biology*, *272*(1), 66–75. https://doi.org/10.1016/j.ydbio.2004.04.018

Patel, T., Tursun, B., Rahe, D. P., & Hobert, O. (2012). Removal of Polycomb Repressive Complex 2 Makes C. elegans Germ Cells Susceptible to Direct Conversion into Specific Somatic Cell Types. *Cell Reports*, *2*(5), 1178–1186. https://doi.org/10.1016/j.celrep.2012.09.020

Penas, C., Govek, E. E., Fang, Y., Ramachandran, V., Daniel, M., Wang, W., Maloof, M. E., Rahaim, R. J., Bibian, M., Kawauchi, D., Finkelstein, D., Han, J. L., Long, J., Li, B., Robbins, D. J., Malumbres, M., Roussel, M. F., Roush, W. R., Hatten, M. E., & Ayad, N. G. (2015). Casein kinase 1δ is an

APC/CCdh1 substrate that regulates cerebellar granule cell neurogenesis. *Cell Reports*, *11*(2), 249–260. https://doi.org/10.1016/j.celrep.2015.03.016

Penkner, A. M., Prinz, S., Ferscha, S., & Klein, F. (2005). Mnd2, an essential antagonist of the anaphase-promoting complex during meiotic prophase. *Cell*, *120*(6), 789–801. https://doi.org/10.1016/j.cell.2005.01.017

Pesin, J. A., & Orr-Weaver, T. L. (2008). Regulation of APC/C activators in mitosis and meiosis. *Annual Review of Cell and Developmental Biology*, *24*, 475–499. https://doi.org/10.1146/annurev.cellbio.041408.115949

Polyak, K., Kato, J. Y., Solomon, M. J., Sherr, C. J., Massague, J., Roberts, J. M., & Koff, A. (1994). p27(Kip1), a cyclin-Cdk inhibitor, links transforming growth factor-β and contact inhibition to cell cycle arrest. *Genes and Development*, *8*(1), 9–22. https://doi.org/10.1101/gad.8.1.9

Porta-de-la-Riva, M., Fontrodona, L., Villanueva, A., & Cerón, J. (2012). Basic Caenorhabditis elegans methods: Synchronization and observation. *Journal of Visualized Experiments*, *64*, 1–9. https://doi.org/10.3791/4019

Porter, D. F., Prasad, A., Carrick, B. H., Kroll-Connor, P., Wickens, M., & Kimble, J. (2019). Toward identifying subnetworks from FBF binding landscapes in caenorhabditis spermatogenic or oogenic germlines. *G3: Genes, Genomes, Genetics*, *9*(1), 153–165. https://doi.org/10.1534/g3.118.200300

Qin, L., Guimarães, D. S. P. S. F., Melesse, M., & Hall, M. C. (2017). Erratum: Substrate recognition by the Cdh1 destruction box receptor is a general requirement for APC/CCdh1-mediated proteolysis (Journal of Biological Chemistry (2016) 291 (15564-15574) DOI: 10.1074/jbc.A116.731190). *Journal of Biological Chemistry*, *292*(12), 5125–5127. https://doi.org/10.1074/jbc.M116.731190

Raizen, D. M., Zimmerman, J. E., Maycock, M. H., Ta, U. D., You, Y. J., Sundaram, M. V., & Pack, A. I. (2008). Lethargus is a Caenorhabditis elegans sleep-like state. *Nature*, *451*(7178), 569–572. https://doi.org/10.1038/nature06535

Rape, M., & Kirschner, M. W. (2004). Autonomous regulation of the anaphase-promoting complex couples mitosis to S-phase entry. *Nature*, *432*(7017),

588–595. https://doi.org/10.1038/nature03023

Rape, M., Reddy, S. K., & Kirschner, M. W. (2006). The processivity of multiubiquitination by the APC determines the order of substrate degradation. *Cell*, *124*(1), 89–103. https://doi.org/10.1016/j.cell.2005.10.032

Reber, A., Lehner, C. F., & Jacobs, H. W. (2006a). Terminal mitoses require negative regulation of Fzr/Cdh1 by Cyclin A, preventing premature degradation of mitotic cyclins and String/Cdc25. *Development*, *133*(16), 3201–3211. https://doi.org/10.1242/dev.02488

Reber, A., Lehner, C. F., & Jacobs, H. W. (2006b). *Terminal mitoses require negative regulation of Fzr / Cdh1 by Cyclin A , preventing premature degradation of mitotic cyclins and String / Cdc25*. *3211*, 3201–3211. https://doi.org/10.1242/dev.02488

Rechtsteiner, A., Ercan, S., Takasaki, T., Phippen, T. M., Egelhofer, T. A., Wang, W., Kimura, H., Lieb, J. D., & Strome, S. (2010). The Histone H3K36 Methyltransferase MES-4 acts epigenetically to transmit the memory of germline gene expression to progeny. *PLoS Genetics*, *6*(9). https://doi.org/10.1371/journal.pgen.1001091

Reddy, K. L., Zullo, J. M., Bertolino, E., & Singh, H. (2008). Transcriptional repression mediated by repositioning of genes to the nuclear lamina. *Nature*, *452*(7184), 243–247. https://doi.org/10.1038/nature06727

Reis, A., Madgwick, S., Chang, H. Y., Nabti, I., Levasseur, M., & Jones, K. T. (2007). Prometaphase APCcdh1 activity prevents non-disjunction in mammalian oocytes. *Nature Cell Biology*, *9*(10), 1192–1198. https://doi.org/10.1038/ncb1640

Reynaud, E. G., Pelpel, K., Guillier, M., Leibovitch, M. P., & Leibovitch, S. A. (1999). p57 Kip2 Stabilizes the MyoD Protein by Inhibiting Cyclin E-Cdk2 Kinase Activity in Growing Myoblasts . *Molecular and Cellular Biology*, *19*(11), 7621–7629. https://doi.org/10.1128/mcb.19.11.7621

Rivera-Martin, S. (2018). MES-4 regulation through cell cycle during development in *Caenorhabditis elegans*. *PhD thesis*.

Roy, D., Michaelson, D., Hochman, T., Santella, A., Bao, Z., Goldberg, J. D., &

Hubbard, E. J. A. (2016). Cell cycle features of C. elegans germline stem/progenitor cells vary temporally and spatially. *Developmental Biology*, *409*(1), 261–271. https://doi.org/10.1016/j.ydbio.2015.10.031

Salomoni, P., & Calegari, F. (2010). Cell cycle control of mammalian neural stem cells: Putting a speed limit on G1. *Trends in Cell Biology*, *20*(5), 233–243. https://doi.org/10.1016/j.tcb.2010.01.006

Schade, A. E., Oser, M. G., Nicholson, H. E., & DeCaprio, J. A. (2019). Cyclin D–CDK4 relieves cooperative repression of proliferation and cell cycle gene expression by DREAM and RB. *Oncogene*, *38*(25), 4962–4976. https://doi.org/10.1038/s41388-019-0767-9

Schafer, K. A. (1998). The Cell Cycle: A Review. *Veterinary Pathology*, *35*(6), 461–478. https://doi.org/10.1177/030098589803500601

Schwarz, C., Johnson, A., Kõivomägi, M., Zatulovskiy, E., Kravitz, C. J., Doncic, A., & Skotheim, J. M. (2018). A Precise Cdk Activity Threshold Determines Passage through the Restriction Point. *Molecular Cell*, *69*(2), 253-264.e5. https://doi.org/10.1016/j.molcel.2017.12.017

Seidel, H. S., & Kimble, J. (2011). The oogenic germline starvation response in c. elegans. *PLoS ONE*, *6*(12). https://doi.org/10.1371/journal.pone.0028074

Seidel, H. S., & Kimble, J. (2015). Cell-cycle quiescence maintains Caenorhabditis elegans germline stem cells independent of GLP-1/Notch. *ELife*, *4*(NOVEMBER2015), 1–28. https://doi.org/10.7554/eLife.10832.001

Shin, H., Haupt, K. A., Kershner, A. M., Kroll-Conner, P., Wickens, M., & Kimble, J. (2017). SYGL-1 and LST-1 link niche signaling to PUF RNA repression for stem cell maintenance in Caenorhabditis elegans. In *PLoS Genetics* (Vol. 13, Issue 12). https://doi.org/10.1371/journal.pgen.1007121

Sigi, R., Wandkee, C., Rauch, V., Kirk, J., Hunt, T., & Geley, S. (2009). Loss of the mammalian APC/C activator FZR1 shortens G1 and lengthens S phase but has little effect on exit from mitosis. *Journal of Cell Science*, *122*(22), 4208–4217. https://doi.org/10.1242/jcs.054197

Sigrist, S. J., & Lehner, C. F. (1997). Mitotic Cyclins and Is Required for Cell Proliferation Arrest and Entry into Endocycles. *Cell*, *90*, 671–681.

Singh, A. M., Chappell, J., Trost, R., Lin, L., Wang, T., Tang, J., Wu, H., Zhao, S., Jin, P., & Dalton, S. (2013). Cell-cycle control of developmentally regulated transcription factors accounts for heterogeneity in human pluripotent cells. *Stem Cell Reports*, *1*(6), 532–544. https://doi.org/10.1016/j.stemcr.2013.10.009

Singh, A. M., Sun, Y., Li, L., Zhang, W., Wu, T., Zhao, S., Qin, Z., & Dalton, S. (2015). Cell-Cycle Control of Bivalent Epigenetic Domains Regulates the Exit from Pluripotency. *Stem Cell Reports*, *5*(3), 323–336. https://doi.org/10.1016/j.stemcr.2015.07.005

Song, L., & Rape, M. (2011). Substrate-specific regulation of ubiquitination by the anaphase-promoting complex. *Cell Cycle*, *10*(1), 52–56. https://doi.org/10.4161/cc.10.1.14387

Stegmüller, J., Konishi, Y., Huynh, M. A., Yuan, Z., DiBacco, S., & Bonni, A. (2006). Cell-Intrinsic Regulation of Axonal Morphogenesis by the Cdh1-APC Target SnoN. *Neuron*, *50*(3), 389–400. https://doi.org/10.1016/j.neuron.2006.03.034

Suh, N., Crittenden, S. L., Goldstrohm, A., Hook, B., Thompson, B., Wickens, M., & Kimble, J. (2009). FBF and its dual control of gld-1 expression in the Caenorhabditis elegans germline. *Genetics*, *181*(4), 1249–1260. https://doi.org/10.1534/genetics.108.099440

Suh, N., Jedamzik, B., Eckmann, C. R., Wickens, M., & Kimble, J. (2006). The GLD-2 poly(A) polymerase activates gld-1 mRNA in the Caenorhabditis elegans germ line. *Proceedings of the National Academy of Sciences of the United States of America*, *103*(41), 15108–15112. https://doi.org/10.1073/pnas.0607050103

Sulston, J. E., & Horvitz, H. R. (1977). Post-embryonic cell lineages of the nematode, Caenorhabditis elegans. *Developmental Biology*, *56*(1), 110–156. https://doi.org/10.1016/0012-1606(77)90158-0

Swaffer, M. P., Jones, A. W., Flynn, H. R., Snijders, A. P., & Nurse, P. (2016). CDK Substrate Phosphorylation and Ordering the Cell Cycle. *Cell*, *167*(7), 1750-1761.e16. https://doi.org/10.1016/j.cell.2016.11.034

Tabuchi, T. M., Rechtsteiner, A., Strome, S., & Hagstrom, K. A. (2014). Opposing activities of DRM and MES-4 tune gene expression and x-chromosome repression in aenorhabditis elegans germ cells. *G3: Genes, Genomes, Genetics*, *4*(1), 143–153. https://doi.org/10.1534/g3.113.007849

ter Huurne, M., & Stunnenberg, H. G. (2021). G1-phase progression in pluripotent stem cells. *Cellular and Molecular Life Sciences*, *78*(10), 4507–4519. https://doi.org/10.1007/s00018-021-03797-8

The, I., Ruijtenberg, S., Bouchet, B. P., Cristobal, A., Prinsen, M. B. W., Van Mourik, T., Koreth, J., Xu, H., Heck, A. J. R., Akhmanova, A., Cuppen, E., Boxem, M., Muñoz, J., & Van Den Heuvel, S. (2015). Rb and FZR1/Cdh1 determine CDK4/6-cyclin D requirement in C. elegans and human cancer cells. *Nature Communications*, *6*. https://doi.org/10.1038/ncomms6906

Thornton, B. R., & Toczyski, D. P. (2003). Securin and B-cyclin/CDK are the only essential targets of the APC. *Nature Cell Biology*, *5*(12), 1090–1094. https://doi.org/10.1038/ncb1066

Timmons, L., & Fire, A. (1998). Specific interference by ingested dsRNA. In *Nature* (Vol. 395, Issue October).

Trimarchi, J. M., & Lees, J. A. (2002). Sibling rivalry in the E2F family. *Nature Reviews Molecular Cell Biology*, *3*(1), 11–20. https://doi.org/10.1038/nrm714

Wade Harper, J., Adami, G. R., Wei, N., Keyomarsi, K., & Elledge, S. J. (1993). The p21 Cdk-interacting protein Cip1 is a potent inhibitor of G1 cyclin-dependent kinases. *Cell*, *75*(4), 805–816. https://doi.org/10.1016/0092-8674(93)90499-G

Wan, L., Chen, M., Cao, J., Dai, X., Yin, Q., Zhang, J., Song, S. J., Lu, Y., Liu, J., Inuzuka, H., Katon, J. M., Berry, K., Fung, J., Ng, C., Liu, P., Song, M. S., Xue, L., Bronson, R. T., Kirschner, M. W., … Wei, W. (2017). The APC/C E3 ligase complex activator fzr1 restricts braf oncogenic function. *Cancer Discovery*, *7*(4), 424–441. https://doi.org/10.1158/2159-8290.CD-16-0647

Wan, Y., Liu, X., & Kirschner, M. W. (2001). The anaphase-promoting complex mediates TGF-β signaling by targeting SnoN for destruction. *Molecular Cell*, *8*(5), 1027–1039. https://doi.org/10.1016/S1097-2765(01)00382-3

Wang, L., Eckmann, C. R., Kadyk, L. C., Wickens, M., & Kimble, J. (2002). A regulatory cytoplasmic poly(A) polymerase in Caenorhabditis elegans. *Nature*, *419*(6904), 312–316. https://doi.org/10.1038/nature01039

Wang, W., Nacusi, L., Sheaff, R. J., & Liu, X. (2005). Ubiquitination of p21Cip1/WAF1 by SCFSkp2: Substrate requirement and ubiquitination site selection. *Biochemistry*, *44*(44), 14553–14564. https://doi.org/10.1021/bi051071j

Wang, X., Ellenbecker, M., Hickey, B., Day, N. J., Osterli, E., Terzo, M., & Voronina, E. (2020). Antagonistic control of caenorhabditis elegans germline stem cell proliferation and differentiation by puf proteins fbf-1 and fbf-2. *ELife*, *9*, 1–36. https://doi.org/10.7554/ELIFE.52788

Weber, U., & Mlodzik, M. (2017). APC/CFzr/Cdh1-Dependent Regulation of Planar Cell Polarity Establishment via Nek2 Kinase Acting on Dishevelled. *Developmental Cell*, *40*(1), 53–66. https://doi.org/10.1016/j.devcel.2016.12.006

Wurzenberger, C., & Gerlich, D. W. (2011). Phosphatases: Providing safe passage through mitotic exit. *Nature Reviews Molecular Cell Biology*, *12*(8), 469–482. https://doi.org/10.1038/nrm3149

Xu, L., Fong, Y., & Strome, S. (2001). The Caenorhabditis elegans maternal-effect sterile proteins, MES-2, MES-3, and MES-6, are associated in a complex in embryos. *Proceedings of the National Academy of Sciences of the United States of America*, *98*(9), 5061–5066. https://doi.org/10.1073/pnas.081016198

Xu, L., Paulsen, J., Yoo, Y., Goodwin, E. B., & Strome, S. (2001). Caenorhabditis elegans MES-3 is a target of GLD-1 and functions epigenetically in germline development. *Genetics*, *159*(3), 1007–1017. https://doi.org/10.1093/genetics/159.3.1007

Yang Hong, Richard Roy, & Victor Ambros. (1998). Developmental regulation of a cyclin-dependent kinase inhibitor controls postembryonic cell cycle progression in Caenorhabditis elegans. *Development*, *125*, 3585–3597.

Ye, Y., Li, M., Gu, L., Chen, X., Shi, J., Zhang, X., & Jiang, C. (2017). Chromatin

remodeling during in vivo neural stem cells differentiating to neurons in early Drosophila embryos. *Cell Death and Differentiation*, *24*(3), 409–420. https://doi.org/10.1038/cdd.2016.135

Zachariae, W., Schwab, M., Nasmyth, K., & Seufert, W. (1998). Control of cyclin ubiquitination by CDK-regulated binding of Hct1 to the anaphase promoting complex. *Science*, *282*(5394), 1721–1724. https://doi.org/10.1126/science.282.5394.1721